Sheffield Hallam University

A Sheffield Hallam University thesis

STUDIES OF SEGREGATION LEADING TO

BLOWHOLE FORMATION IN

STEEL INGOTS

by

B. Harkness

Swinden Laboratories   November 1969

<u>Studies of Segregation Leading to</u>

<u>Blowhole Formation in</u>

<u>Steel Ingots</u>

This dissertation is submitted to the Council for National Academic Awards for the degree of Doctor of Philosophy.

The work was carried out at Swinden Laboratories of the British Steel Corporation during the period July 1966 to November 1969, under the supervision of Dr. A. Nicholson and Dr. E. R. Petty.   During this period, a number of post-graduate courses were attended at Sheffield Polytechnic (in conjunction with which the work was carried out).   The courses were as follows:-

1.   Mathematics of Diffusion

2.   Validity of Data and Design of Experiments

3.   Computer Techniques

In addition, the ISI conference 'The Solidification of metals', held in Brighton, December 1967 was attended.

The results obtained in this programme of work and the theories developed are, to the best of my knowledge, original except where reference is made to other authors.   No part of this dissertation has been submitted for degrees at any other college or university

B. Harkness

B. HARKNESS

November 1969

British Steel Corporation
Swinden Laboratories
Moorgate
Rotherham

ABSTRACT

The theoretical model of another author, dealing with gas reactions, producing CO, H_2 and N_2 within an interdendritic cell during solidification, has been developed to the extent that it can be applied to steels containing up to 0.5% carbon, deoxidised with silicon and manganese. The total gas pressures $(= P_{CO} + P_{H_2} + P_{N_2})$ developed in a number of steels, all on the borderline between being porous and solid, and containing various amounts of CO, H_2 and N_2, have been computed. It has been shown that the gas pressures in steels of borderline porosity fall within discrete ranges, which can be used to predict other borderline compositions. The model has been applied to the production of ladle balanced steels. Good agreement has been found between plant data and predicted results from the model. An attempt has also been made to account for blowhole nucleation and growth in terms of the computed gas pressures developed during solidification. The model has the advantage over others so far described in the literature in that it deals comprehensively with the effect of hydrogen and nitrogen in promoting blowholes in steel ingots.

CONTENTS

FIGURES (A1 - A26)

1. INTRODUCTION

A problem of seaminess or sponginess on wrought material from free cutting, low-carbon, and rail steel qualities has led to an intensive study of the factors associated with blowhole formation in steel ingots.

It is well known that sub-surface blowholes, when exposed by oxidation during soaking, tend not to weld up on rolling and leave the surface of the finished product covered in numerous shallow grooves or striations, known as seams. Blowholes form when the solubility of gases dissolved in the liquid steel becomes exceeded locally and there exists a thermodynamic driving force tending to reduce the gas content. The amount of gas in solution may decrease either by escape at the free surface, providing one is accessible, or by the formation of a gas bubble in the liquid[1]. Gas bubble formation is considered most likely to occur at a solid/liquid interface during solidification since it is here that gaseous elements are rejected from the solid and concentrate in the liquid in the same way as other impurity elements for which the distribution coefficient between solid and liquid steel is less than unity. Chalmers[1] observes that gas bubbles are in fact found to nucleate at the solid/liquid interface.

The main gases contributing to blowhole formation in steels are CO, H_2 and N_2, although their relative contributions may vary somewhat. For instance, at the time the present investigation was begun seaminess problems were occurring on:

(i) free cutting and killed basic electric arc steels in which hydrogen pick-up was a problem; and

(ii) rail steels, made by the acid bessemer process, in which nitrogen levels were running high (up to 0.025%).

While there has been much work published, on various types of steels, establishing the maximum gas levels to avoid sub-surface porosity, the results have been mainly qualitative in nature. At the time the present work was instigated, a theoretical treatment became available which made it possible to calculate the partial pressures of CO, H_2 and N_2 in liquid steel during cooling and solidification by considering suitable thermodynamic and segregation data. The method, however, was originally applied only to steels containing small amounts of carbon (0.10% maximum). It was decided, therefore, to modify the model in order that it could be applied to the wide range of compositions upon which porosity studies had to be performed at the time. In conjunction with the theoretical work, the limits, to which CO, H_2 and N_2 must be controlled in order to avoid sub-surface porosity in steel ingots, were determined on an experimental basis. In this dissertation it will be shown that, by applying the theoretical model to the experimental results, a means is available for predicting the limits to which the various gas forming elements must be controlled to avoid porosity in steel ingots. Application of the results to tonnage steels, and balanced steel in particular, is also considered.

2. LITERATURE SURVEY

2.1 General

Detailed work on the formation of blowholes in steel ingots has, not surprisingly, been carried out in most cases on steels in which blowholes are present by design i.e., rimming

or balanced (semi-killed steels). Though the present work is concerned primarily with sub-surface blowholes which occur more by accident than design, many of the principles applying to rimming and balanced steels also apply to the general problem of blowhole formation in steels.

Most of the early available literature on gas reactions in steels dealt with rimming steels, and much of this work was comprehensively reviewed by Hultgren and Phragmen in 1939[2]. Between the latter part of the 19th century and the middle 1930's there had been much controversy regarding the composition of the gases in the blowholes produced in rimming steels. Results of Muller in 1879[3], indicating that hydrogen was the major constituent in blowholes, were widely accepted for half a century in spite of later work which showed that his deductions were incorrect. Muller immersed ingots in water and oil, drilled into the holes and collected the gas evolved when the drill penetrated into the hole. He found that the gas contained 65-90% hydrogen, 10-30% nitrogen and less than $2\frac{1}{2}$% carbon monoxide. After Muller, a number of workers[4-7] carried out similar investigations on blowholes in rimming steel ingots and concluded that carbon monoxide was the major constituent gas, with hydrogen and nitrogen comprising less than 10% of the total amount. There were suggestions that carbon monoxide and hydrogen evolved seperately during blowhole formation in rimming steels, but calculations of Chipman and Samarin[8] showed that this was not possible. Thus even at this early stage it became evident that a mixture of gases must be considered during gas evolution in rimming ingots.

By the time that the two classic works of Hayes and Chipman[9] and Hultgren and Phragmen[2] were published in 1939, it had been firmly established that gas evolution in rimming steels was due mainly to carbon monoxide. It had also been generally agreed that gas evolution occurred at the interface between the solid and liquid steel as a result of solute concentration causing supersaturation of carbon and oxygen in this region. Hayes and Chipman described the mechanism of segregation in rimming steels. They considered that the basic cause of segregation lay in the fact that impurities were less soluble in solid than in liquid iron and that the solid that formed from the impure liquid was purer than the liquid itself. Solidification was assumed to occur slowly so that an equilibrium was set up between the solid and liquid phases which could be represented by a phase diagram. In this way it was possible to define segregating tendencies of various elements by the concept of a "distribution ratio", k, which was the ratio of the concentrations of an element in solid and liquid phases in equilibrium. The smaller the value of k, the greater the tendency to segregate. Hence the quantity $(1 - k)$ was used to measure the tendency to segregate, and so the term "segregation coefficient" originated. The equations used by Hayes and Chipman, though perhaps considered elementary by present day standards made it possible to describe satisfactorily segregation phenomena in rimming steels. An enriched film ahead of the solid interface was considered and in calculating the carbon and oxygen distribution it was assumed that these elements were lost due to CO evolution.

It was found that the concentration of solute in the solid, first decreased from the surface, along with the freezing rate for approximately 3 in. of solid. Subsequently the solute concentration increased rapidly to a thickness of about $4\frac{1}{2}$ in., at about the point where deep-seated secondary blowholes appear.

Hultgren and Phragmen confirmed that CO (and to a lesser extent CO_2) were given off during solidification and explained the evolution of these gases and blowhole formation qualitatively by reference to the Fe-C-O phase diagram. They superimposed the Vacher Hamilton C-O equilibrium curve on the liquidus and solidus surfaces and introduced the concept of a "balanced alloy composition" which would solidify without change in composition. In an alloy with a higher carbon content than the balanced composition the carbon content of the steel would increase during solidification while the oxygen content would decrease. In an alloy with a lower carbon content than the balanced composition the converse would apply. The balanced composition was first considered to lie at 0.05% carbon but later shown[10] to occur nearer 0.10% carbon. It was also deduced by Hultgren and Phragmen that the amount of gas evolved by various alloys was proportional to the size of the solidus-liquidus gap. This meant that only small quantities of gas should be evolved at either low carbon or oxygen contents with respect to the balanced composition and that most gas would be evolved at the balanced composition. It was also predicted that the rimming action would be subdued by an increased manganese level, in particular when the carbon content was below the balanced composition.

These two papers[2,9] took the theory of rimming steels as far as it was possible to go at the time bearing in mind the available thermodynamic data on gas reactions and the early stage of development of segregation theory. The works are still regarded as standard references for studies on rimming steels, and until recent quantitative accounts of gas reactions (see later) formed the basis of the understanding of rimming steel.

Amidst all the work on rimming steels in the 1930's Swinden and Stevenson[11] investigated the effects of various gases on the soundness of small experimental ingots. It was found that bubbling hydrogen into the steel caused unsoundness in steels which would otherwise have been killed due to aluminium additions. However nitrogen appeared to have no effect on soundness, excepting where it was bubbled in after hydrogen, in which case it had a scavenging effect and reduced the effectiveness of hydrogen in promoting unsoundness. It was concluded at the time that while the solubility of hydrogen was less in solid iron than in liquid iron, explaining the unsoundness effects, the solubilities of nitrogen in solid and liquid iron were practically the same. Since then, this conclusion has been shown to be incorrect and there have been numerous[12-25] publications on deoxidised carbon steels and both low and high alloy steels, in which the contribution of CO to the total gas pressure must be vary low, showing how both hydrogen and nitrogen can promote unsoundness. Barraclough[12] listed approximate hydrogen contents in liquid steel to produce wildness in fully killed basic electric arc steel as shown in Table I. Turton[17,19] found that the

amount of hydrogen required to promote porosity in steel castings was governed by the extent to which the steel had been deoxidised. Turton also found that in fully killed steels, containing 3-4 ml. H_2/100g, nitrogen contents above 0.013-0.014% would cause porosity[19]. Similar results to these were reported by Morgan[24] in his paper on rail steels produced in the acid bessemer converter. However, Saito et al[20] showed that aluminium-silicon carbon steel containing 0.04% aluminium could absorb 0.017% nitrogen and remain free from porosity on solidification. In the more highly alloyed steels it was found that the amounts of hydrogen and nitrogen required to promote porosity depended not so much on the degree of deoxidation as on the steel composition especially with regard to chromium, nickel and manganese contents[15,16,23,25]. These elements influence the solubility of nitrogen in liquid iron. Such effects are very relevant when considering blowhole formation and will be mentioned at a later stage of this dissertation.

The hydrogen and nitrogen contents of steel vary according to steelmaking practice and typical levels in low carbon steels are shown in Tables II and III. Much of the information was gathered by Gill[26] who also summarised possible sources of the two gases during steelmaking. The major source of nitrogen is the atmosphere with some pick-up from ferroalloys, scrap, special high nitrogen additions and some slag making additions. Since the major source of nitrogen is the atmosphere, its control depends to a large extent on the contact between the liquid metal and air. This fact is illustrated in Table II. Hydrogen pick-up in liquid steel arises mainly from sources of water, either from the atmosphere or combined with charge

materials, particularly those employed for slag making. Hydrogen pick-up may also occur in the ladle when anthracite additions are made[28] and during uphill teeming from damp runnerware.

In recent work on rimming steels[29] the large contribution made by CO to the gas volume given off during solidification has been confirmed. Most publications dealing with gas reactions in rimming steels tend, therefore, to be written in terms only of the CO reaction, though Johnston et al[30] point out that hydrogen dissolved in the steel may exert an influence on the rimming intensity. It is considered by the present author that unless the gases hydrogen and nitrogen are present in large quantities their effects on blowhole formation in rimming steels are likely to be swamped by a vigorous CO reaction. On the other hand, hydrogen and nitrogen could stimulate a sluggish rimming reaction.

Focus on the CO reaction also seems to apply in the case of balanced (or semi-killed) steels in which gas evolution is generally far less than in a rimming steel. Over the past 20 years papers dealing with this type of steel, of which those by Tenenbaum[31], Wogin and Goodall[32] and more recently, Nilles and Scimar[33] are notable, have restricted consideration of blowhole structures to the formation of CO gas bubbles. However Bauer et al[34] found that increasing the nitrogen content of balanced steel made in the Bessemer Converter increased the incidence of gassy ingots and sub-standard products. They found a similar effect when the hydrogen content of the steel was increased. According to King[13] the manufacture of rimming steel precludes large hydrogen contents because of the high state of oxidation within the bath. Balanced steels of

higher carbon content would be expected to evolve gas containing more hydrogen.

The information summarised in the preceding paragraphs indicates that it is probably not unreasonable to neglect the effects of hydrogen and nitrogen on blowhole formation in rimming steels. However, when dealing with more heavily deoxidised steels, the effects of these gases in promoting and affecting the extent of sub-surface porosity must be regarded as a real threat to product surface quality.

Hence it is desirable to know the limits within which the respective gases CO, H_2 and N_2 must be controlled to avoid trouble due to sub-surface porosity. Advances in the thermodynamics of deoxidation and gas reactions and in the theories of segregation over the last 10-20 years have made it possible to deal with the problem more quantitatively than in the period in which Hultgren and Phragmen and Hayes and Chipman published their works. A number of relevant recent papers have been published dealing quantitatively with gas reactions at a solid/liquid interface. However before these are considered in detail it is pertinent to consider briefly the present position regarding the theories of solute segregation during solidification.

2.2 Segregation Theory

In describing the redistribution of solute elements during solidification it is convenient to define the distribution coefficient, k. As pointed out by Chalmers[1] two distinct meanings have arisen regarding this term. The EQUILIBRIUM distribution coefficient, k_o, is defined as the ratio of concentrations of the solid, C_s, and of the liquid in

equilibrium with it, C_L.   Or, referring to fig. 1:-

$$k_o = \frac{C_S}{C_L} \quad \dots\dots\dots\dots\dots\dots\dots\dots\dots\dots\dots \quad (1)$$

Fig. 1 shows an idealised binary equilibrium diagram for dilute alloys in which the liquidus and solidus lines are both assumed to be straight.

The EFFECTIVE distribution coefficient is given by

$$k_E = \frac{C_S}{C_O} \quad \dots\dots\dots\dots\dots\dots\dots\dots\dots\dots\dots \quad (2)$$

where C_S is the concentration of the solid formed at some instant during solidification of a liquid of initial concentration C_O. k_E depends on the conditions under which solidification takes place but k_o is a characteristic of a particular system. For the purpose of the following discussions it will be assumed that k_o is constant, although in practice this might not necessarily be the case.   It will also be assumed that the solid/liquid interface is planar and that the system undergoing solidification is such that the transport of solute is parallel to the direction of motion of the interface, see fig. 2.

The first case to be considered is one in which complete mixing occurs in both the solid and liquid phases, and that equilibrium conditions described in fig. 1 apply at all times i.e., during solidification the entire liquid composition follows the liquidus line and the solid composition the solidus line.   Under such conditions, the equilibrium distribution coefficient, k_o applies, and the relative amounts of solid and liquid are given at any particular stage of solidification, temperature T, by the ratio $^{CE}/_{BE}$ or $^{C_L-C_O}/_{C_O-C_S}$.   Furthermore, if g represents the fraction of the original volume of liquid

solidified,

$$\frac{C_L - C_0}{C_0 - C_S} = \frac{\varepsilon}{1 - \varepsilon} \quad \dots\dots\dots\dots\dots\dots\dots\dots\dots \quad (3)$$

hence $\quad C_L = \dfrac{C_0}{1 - (1 - k_0)\varepsilon} \quad \dots\dots\dots\dots\dots\dots\dots\dots \quad (4)$

Hence, knowing C_0, k_0, C_L can be calculated at each stage of the solidification process. The assumption that the whole of the solid is at all times in equilibrium with the liquid implies no concentration gradient in the solid and requires that the diffusion rates of solute elements are fast compared with the solidification rate. It is unlikely that these conditions are fully satisfied in practice, but the elements most likely to come nearest to fulfilling the conditions in steel are carbon, hydrogen and nitrogen which are interstitial solutes and diffuse much faster than substitutional solutes.

At the opposite extreme to the above is the condition in which no mixing of solute atoms occurs in the solid and mixing occurs in the liquid only by diffusion away from the interface. The situation which arises was first described by Tiller et al[35] and is shown schematically in fig. 2. The solid/liquid interface is assumed to move from left to right at a finite rate, say R cm/sec.

When solidification begins, solute builds up ahead of the interface and a diffusion profile is set up as shown in fig. 2. Under conditions where D, the diffusion coefficient of a solute element in the liquid metal, is slow compared with R, solute concentration at the interface increases to the stage where it equals C_0/k_0, fig. 2(c), C_0 again being the initial uniform solute concentration in the liquid. Thus solid

concentration at the interface, $C_S = C_0$ and the amount of solute taking part in the diffusion process remains constant as the interface moves further to the right. This is termed the 'steady-state condition' and it has be shown [35] that the liquid concentration at any distance, x, ahead of the interface is given by

$$C_L = C_0 \left[1 + \frac{1 - k_0}{k_0} \exp. \left(- \frac{R}{D} x \right) \right] \quad \dots\dots\dots\dots (5)$$

The ratio D/R is termed the 'characteristic distance' and is the distance over which C_L falls to $1/e$ of its initial value. Assuming a value of $D = 5 \times 10^{-5}$ cm^2. sec^{-1} or 5 cm^2. day^{-1}, Tiller et al[35] have expressed D/R in terms of R, the solidification rate, see fig. 3. It is evident that for fast solidification rates, as would be obtained at the surface of a chill cast ingot, $D/R \simeq 0.05$ mm.

In the stage preceding the 'steady-state condition' solid of composition $k_0 C_0$ is formed first and then increases in concentration to C_0 see fig. 2(b-d). This stage is termed the 'initial transient' and according to Tiller et al[35] the concentration of solute in the solid is given by

$$C_S = C_0 \left\{ (1 - k_0) \left[1 - \exp. \left(-k_0 \frac{R}{D} x \right) \right] + k_0 \right\} \dots\dots\dots (6)$$

The distance over which the 'initial transient' exists is given by $x = D/k_0 R$.

The steady state condition can exist so long as there is sufficient liquid ahead of the interface for the diffusion of the solute to proceed without interference. This is no longer the case when the limit of the liquid space is approached and a 'terminal transient condition' exists. At this stage

the concentration of the solid begins to exceed C_0 in order
to accomodate the excess solute, fig. 2(d) and large
concentrations of solute may build-up within the last liquid
to solidify.

It is unlikely that liquid mixing by diffusion only would
be fully realised in practice and it is pertinent to consider
cases where mixing by other means e.g., convection, occurs in
the liquid ahead of the interface.

For a situation where there is no mixing in the solid but
mixing in the liquid, Scheil[36] and Pfann[37] derived the
following expression for the concentration in the solid.

$$C_S = k_E C_0 (1 - g)^{k_o - 1} \quad \dots\dots\dots\dots\dots\dots\dots\dots (7)$$

where g is the fraction of liquid system solidified see fig. 2.
When the solidification rate is slow and complete mixing in
the liquid can occur, $k_E = k_o$ and the following expression
may be used:-

$$C_S = k_o C_0 (1 - g)^{k_o - 1} \quad \dots\dots\dots\dots\dots\dots\dots\dots (8)$$

In this case the composition of the solid at any moment is
given by $k_o C_I$ where C_I is the composition at the interface
at that particular time. With a fast solidification rate,
k_E approaches unity, and a situation exists similar to that
of steady state growth during "diffusion controlled" solidification
described earlier. The above conditions are represented
schematically in fig. 4.

Equation (7) does not include a term representing the
solidification rate, since this is expressed indirectly by
a fluctuating value of k_E. However, Burton et al[38] have
treated the problem in more general terms. They define d,
in fig. 4, as the thickness of the boundary layer through which
solute must diffuse. The value of d is limited by the

velocity of the liquid parallel to the interface and depends on the viscosity of the liquid. It is reported as varying from 10^{-3} cm. for very vigourous stirring (e.g., rimming steels) to about 10^{-1} cm. for natural convection (e.g. killed steels). The expression derived was as follows:

$$k_E = \frac{k_o}{k_o + (1 - k_o) \exp. (- \frac{Rd}{D})} \quad \dots\dots\dots\dots\dots \quad (9)$$

where all the terms have been defined previously. Alternatively this may be expressed as follows:

$$C_I = \frac{C_S}{k_o} = \frac{C_L}{k_o + (1 - k_o) \exp. (- \frac{Rd}{D})} \quad \dots\dots\dots\dots\dots \quad (10)$$

where C_I has been defined earlier. The condition described by equation (8) of complete mixing in the liquid, when $k_E = k_o$, is obtained when the term $(\frac{Rd}{D})$ is small i.e., when R and d are low and D is high. Conversely, a diffusion controlled condition exists when $(\frac{Rd}{D})$ is high.

The expressions in equations (9) and (10) are probably the most versatile of the ones considered, when applying segregation theory to conditions encountered during ingot solidification in practice. However all the cases considered have referred to unidirectional, plane front solidification, though it is well known that the solid/liquid interfaces in alloys such as steel have a more complex morphology, being cellular or dendritic. The conditions of solute enrichment under these conditions are more complex than in the case of plane-front solidification. However, Brody and Flemings[39] have claimed that equation (8) can apply to solute redistribution between dendrite arms provided diffusion in the solid is negligible. To account for the effect of

diffusion in the solid an analytical expression similar to equation (8) applies.

Recent quantitative studies of gas reactions occurring at the solid/liquid interface have made use of equations (1) to (10) as will be described in the following section.

2.3 Recent Quantitative Work on Gas Reactions

Probably the first significant step taken since the work of Hayes and Chipman[9] and Hultgren and Phragmen[2] to explain the gas reactions at a solid/liquid interface in rimming steels was that outlined by Nilles[40] in 1964. The relationship developed by Burton et al (equations 9 and 10) was used and Nilles was able to predict segregation patterns in the rim zone and the rimming intensity. The term, d, the distance through which solute must diffuse from the interface to reach the concentration of the bulk liquid, was determined in two ways. The first was a direct method, simply involving equation (10). Of the terms in equation (10) D, R, and k_o were obtained from other literature and C_L and C_S from measurements of the concentration of an element, assumed not to undergo reaction at the interface (sulphur in this case), both in the bulk liquid and solid phases at various stages of the rimming period in 500 Kg experimental ingots. The values of d obtained varied from about 0.008 to 0.040 cm. The second method was more indirect, and involved the elements undergoing reaction at the solid/liquid interface, which were assumed to be carbon manganese and oxygen. (It was assumed that silicon took no part in the reaction). d was obtained by means of a mass balance equation for oxygen:

$$O_{Mn} + O_C + O_S = O_L \quad \ldots\ldots\ldots\ldots\ldots\ldots\ldots \quad (11)$$

i.e., for one mass unit of liquid steel which solidifies, the sum of the oxygen reacting with manganese, O_{Mn}, with carbon, O_C, and of the oxygen incorporated into the solidified steel, O_S, is equal to the oxygen present in the liquid steel, O_L. This means that all the oxygen rejected at the interface either reacts to form a new phase or is dissolved in the solid iron, so that no dissolved oxygen diffuses back into the melt. It was also assumed that enrichment without chemical reaction was the same as with reaction.

O_{Mn} was obtained from a set of equations describing the enrichment of manganese and oxygen at the interface (equation 10) and the equilibrium relationships between manganese, iron and oxygen and the appropriate oxides at 1530°C. O_{Mn} is given by $(O' - O_o)$ where O' is the interface concentration from equation (10) and O_o the oxygen concentration in equilibrium with iron and manganese at 1530°C.

The quantity of oxygen reacting with carbon, O_C, was assumed, consistent with other literature, to be proportional to the divergence from equilibrium $(O_o - O_{eq}^P)$, O_{eq}^P being the oxygen in equilibrium with carbon C_o, for the pressure, P, under which the steel solidifies. O_o was determined as mentioned in the previous paragraph. (It will be noted that reaction of oxygen with manganese to give oxides governs the equilibrium oxygen concentration at the interface). O_{eq}^P was obtained from appropriate carbon-oxygen relationships at the interface. With a solidification speed, R, O_C is given by:

$$O_C = \frac{K (O_o - O_{eq}^P)}{R} \quad \ldots\ldots\ldots\ldots\ldots\ldots\ldots\ldots \quad (12)$$

for which K was found to be 3×10^{-3} cm. sec^{-1}. This expression no longer holds when carbon levels are low, since diffusion of carbon and not oxygen then governs decarburisation speed.

O_S, the oxygen incorporated in the solid steel was given by $0.184 O_o$; 0.184 was the assumed equilibrium distribution coefficient of oxygen.

Hence, equation (11) becomes

$$(O' - O_o) + 3 \times 10^{-3} . \frac{O_o - O^P_{eq}}{R} + 0.184 O_o = O_L \quad \ldots \ldots (13)$$

O', O_o and O^P_{eq} all depend only on d, therefore the value of d for which equation (13) is satisfied is the actual thickness of the impure layer at the solid/liquid interface. It was assumed that d was the same for all the solutes.

The values of d obtained by this second method agreed closely with those employing sulphur alone. It was then possible to predict the concentration of the various elements in the solidified steel and this was reasonably successful for carbon, sulphur and phosphorus distribution in the 500 Kg experimental ingots, see fig. 5. However, the results did not explain the steep rise in concentration near the secondary blowholes found by Hayes and Chipman[9]. Johnston et al[30] suggest that this may be because equation (10) does not apply to a non-planar interface, which is likely to be present in commercial steel ingots. In the case of manganese and oxygen the situation was complicated by the occlusion of oxides in the solid. The results indicated that at the start of solidification most of the oxides were trapped in the solid. As the solidification rate decreased more oxides escaped.

The results were used further by Nilles to predict the rate of gas evolution during rimming, termed the 'rimming intensity' and given by $O_C.R$.

By calculating $O_C.R$ for various concentrations of carbon manganese and oxygen, Nilles predicted that the oxygen concentration of the steel had a small influence on rimming intensity compared with carbon and manganese, see fig. 6. This was later confirmed by work carried out on $5\frac{1}{2}$ and $8\frac{1}{2}$ ton ingots[41]. However it was found that the oxygen concentration of the air could greatly influence the final composition of the rimmed ingots. The type of ingot top varied with calculated rimming intensity:

    (i) $O_C.R$ less than 10×10^{-5}, rising ingots

    (ii) between 10 and 11×10^{-5}, level rimmers

   (iii) above 11×10^{-5}, falling rimmers

Nilles also finds that the rimming intensity decreases as the external pressure increases and the solidification rate decreases.

The method employed by Nilles was repeated by Masui et al[42] and in 1968 they reported work carried out on 14 ton ingots. Phosphorus and sulphur concentrations were measured during rimming in order to calculate d, and, though in some cases, slightly different data from those of Nilles were used, values of d were similar to those obtained by Nilles and fell in the range 0.002 to 0.05 cm. It was further found that d depended, for the most part, solely on the solidification rate and not on the extent agitation during rimming. The predicted

sulphur and phosphorus concentrations in the rim zone agreed closely with those analysed.

Masui et al also used a similar method to Nilles to calculate the extent of CO evolution and reaction between manganese and oxygen at the interface, and investigated the effect of steel composition on rimming intensity. The results were for the most part similar to Nilles's but contrary to Nilles they found that while oxygen had little influence on rimming intensity at low carbon levels, there was a stronger influence as the carbon content increased, see fig. 6(b).

Nilles and Scimar[33] extended the principles applied to rimming steel to balanced (or semi-killed) steels, for which they assumed that mixing ahead of the solid/liquid interface was negligible compared with rimming steels, and therefore that the concentrations of solute elements at the interface prior to reacting no longer depended on d, the impure layer thickness. In other words they effectively assumed the 'steady state condition' shown in fig. 2(c) where $C_I = {}^{C}O/k_o$. In this case, due to the presence of silicon, deoxidation products were silicates of the type $(MnO.FeO)SiO_2$ and the oxygen balance of Nilles in equation (11) now became

$$O_{MnSi} + O_C + O_S = O_L \hspace{1cm} \text{.............................. 11(a)}$$

where the symbols are as outlined after equation (11).

It was assumed that O_C was identical in all parts of a balanced ingot and a representative point was chosen 1 cm. away from the ingot skin at the top of the ingot. The requisite carbon, manganese and silicon analyses were carried out on a 6 ton ingot which had a convex ingot top, typical of a steel correctly balanced by silicon and manganese additions in the ladle. A value of O_C = 0.0008 was obtained, which was about 10 times lower than a value calculated for a rimming ingot. Various combinations of carbon, manganese and silicon to give O_C = 0.0008 were then calculated and these are shown in fig. 7, i.e., a balanced steel is characterised by the carbon, manganese and silicon contents rather than by carbon and oxygen. In accepting these compositions it must be borne in mind that the silicon content quoted is "dissolved". If silicon combined as silicates are included in the analysis, then the silicon levels shown in fig. 7 must be increased. Calculated curves were compared with compositions of balanced steels quoted in other literature and fairly good agreement obtained.

The effect of silicon on O_C was demonstrated by Nilles and Scimar, see fig. 8, for a steel containing 0.08% carbon and 0.30% manganese. The detrimental effect of small silicon additions on the gas evolution in rimming steels is obvious.

Deoxidation control in balanced steels using aluminium was not considered feasible by Nilles and Scimar, since very small amounts of aluminium would be required to produce the correct oxygen level. Small errors in additions could lead either to badly worked or piped ingots.

The above work at CNRM[33,40] has been developed further by Oeters et al who have published work[43,44] within the last year. The segregation equation of Burton et al[38] first used by Nilles[40], was employed in the theory and an attempt was made to involve kinetic factors in the calculations. In considering reactions occurring at the solid/liquid interface, allowance was made for a certain amount of reacting solute, e.g., oxide, remaining in the solid. Under these circumstances at the interface it holds that

$$R \left(C_S + C_{Ph} \right) = R C_I - j_0 \quad \dots\dots\dots\dots\dots\dots \quad (14)$$

where R = rate of advance of interface

C_S = composition of solid at interface

C_I = composition of liquid at interface

$j_0 = R \left(C_I - C_S \right)$

C_{Ph} = concentration of a solute precipitated as

a new phase

In order to determine the amount of new phase, the rate of
a first order chemical reaction was considered. Hence

$$C_{Ph} \cdot R = \beta (C_I - C_{eq}) \quad \dots\dots\dots\dots\dots\dots\dots\dots\dots (15)$$

where β is the reaction constant and C_{eq} the equilibrium
concentration. From these basic ideas the following equation
was obtained

$$C_{Ph} = \frac{1}{1 - \exp\left(\frac{-Rd}{D}\right) + \frac{R}{\beta} \cdot \frac{k_o}{k_E}} \left[C_L - \frac{k_o}{k_E} \cdot C_{eq} \right] \quad \dots\dots (16)$$

For solidification without convection (i.e., mixing by
diffusion only) d was taken to approach infinity. Hence:

$$C_{Ph} = \frac{C_L - k_o C_{eq}}{1 + \frac{R}{\beta} \cdot k_o} \quad \dots\dots\dots\dots\dots\dots\dots\dots\dots\dots\dots (17)$$

This equation was applied to the case of a balanced steel.
First of all only reaction between carbon and oxygen was
considered and it was shown that for a given carbon content
the amount of oxygen required to produce sufficient CO for
blowhole formation should decrease with decreasing solidification
rate. (Earlier work by Knuppel and Eberhard[45] was used to
obtain the criteria for the amount of CO for blowhole formation).

On the premise that large ingots solidify slower than
smaller ones, the oxygen content required for balanced steels
should decrease with ingot weight. Alternatively the silicon
content should increase, as is shown in fig. 9.

The more complicated cases of reactions involving carbon,
manganese and silicon were subsequently considered. By
substitution of suitable thermodynamic data into equation (17)
and using additionalequations to describe equilibrium relationships
between carbon, manganese, silicon and oxygen, boundary compositions
were established which gave steel compositions in which the
various oxides (i.e., CO, $MnO.SiO_2$, SiO_2, MnO) were capable of
formation during the solidification process. Fig. 10 shows
the situation in a carbon-oxygen diagram with a silicon content
of 0.10%. With the inclusion of manganese the calculation
becomes more complicated and a three-dimensional space diagram
is required to describe the formation of the various phases, see
fig. 11. A constant oxygen content of 0.010% was assumed in
this case, but it is claimed that the calculated curves change
only slightly with varying oxygen provided the silicon content
exceeds 0.03%. The vertical planes in the diagram are drawn
so that their upper edges indicate the compositions above which
no carbon monoxide bubbles form and below which carbon monoxide
evolution occurs. For example, the line EBHL gives the limit
for CO formation at 0.17% carbon, depending on the manganese
and silicon contents. The plane DEFONB indicates the limit
of CO formation in the case of SiO_2 precipitation, and plane

GHIONG the limit of CO formation when MnO precipitates.

The predicted compositions for CO bubble formation in fig. 11 were applied to the results from a large number of production casts of balanced steels (11-22 ton ingots). The compositions of ingots with convex tops were computed and compared with the compositions predicted from fig. 11. There was shown to be good agreement between theory and practice, see fig. 12. Apparently there was little difference between the predicted composition obtained from the more complex treatment of Oeters et al and those obtained from the earlier work of Scimar and Nilles.

In the first instance little consideration had been given in the work carried out in Europe to the effects of hydrogen and nitrogen on blowhole formation. These elements however were considered briefly in the more recent paper of Oeters et al[44], and the levels of hydrogen and nitrogen necessary to produce blowholes in fully killed ingots were outlined, see fig. 13. These results assume a negligible oxygen concentration in the steel. If a residual oxygen content was assumed the amounts of hydrogen and nitrogen individually required to produce porosity were reduced. No details were given as to how fig. 13 was derived. While the foregoing theories were being developed, mainly in Europe, Turkdogan[46] in the USA in 1965 outlined a

method of assessing the contribution of CO, hydrogen and nitrogen to blowhole formation by calculating their actual partial pressures during the solidification process. Turkdogan's prime concern was with castings and he assumed that a dendritic structure had developed at the time blowholes form. The main dendrite stems grow in the direction of heat flow and side arms then grow laterally such that impure liquid becomes trapped between them. According to Flemings[47] both main dendrite arms and their side branches can be considered as platelets. Reactions involving the various elements leading to blowhole formation were considered to occur in a discrete volume of liquid trapped between the dendrite platelets. All the solute elements were assumed to be completely mixed in the interdendritic liquid and to build up progressively during solidification. The oxygen available for reaction with carbon to produce CO was assumed to be controlled by the amount of deoxidants (silicon and manganese in this case) in the liquid steel. The amount of CO_2 produced was assumed to be negligible above 0.02% carbon.

Since the diffusivities of carbon, oxygen, hydrogen and nitrogen are high in δ-iron and liquid steel at high temperatures it was assumed that these elements were completely mixed in both the solid and liquid phases during solidification. This means that at any stage of solidification, the equilibrium

distribution coefficient, k_o, see equation (1), applies, and assuming linearity of liquidus and solidus lines, the concentrations of the above elements can be calculated from equation (4). The diffusivities of manganese and silicon in liquid iron at 1500 to 1600°C are in the range 10^{-5} to 10^{-4} $cm^2 sec^{-1}$. In solid iron, near the melting point, these diffusivities are lower by about two orders of magnitude. Thus it was assumed, by Turkdogan, that there would be complete mixing of manganese and silicon in the liquid phase but negligible mixing in the solid. For this situation, equation (8) was chosen. This means that the effect of solidification rate was neglected by Turkdogan and the equilibrium distribution coefficient applied at all times.

Deoxidation by manganese and silicon in combination was considered to produce pure manganese silicates, and by employing suitable thermodynamic data, the dissolved oxygen content, and hence P_{CO} the partial pressure of carbon monoxide, were determined. These latter quantities changed progressively during solidification of the small interdendritic cell as the various solute elements became concentrated, and equilibrium relationships became displaced. At each stage of solidification allowance was made for the manganese, silicon and oxygen combining as silicates

and suitable adjustments made to the concentrations before proceeding to the next stage. In doing this it was assumed that nucleation of both inclusions and CO gas bubbles was overcome easily with little supersaturation and that equilibrium conditions prevailed, i.e., no kinetic factors were involved. No allowance was made for the loss of carbon and oxygen, as carbon monoxide, to the system. The condition for blowhole formation to occur was that $P_{CO} + P_{H_2} + P_{N_2}$, the sum of the partial pressures of the gases, exceeded one atmosphere. Consistent with the earlier work of Nilles and Scimar[33] and Oeters et al[43,44], Turkdogan predicted that blowhole formation could be discouraged by

(i) increasing silicon and manganese contents

(ii) decreasing carbon and oxygen contents

(iii) decreasing hydrogen and nitrogen contents

It was also found that increasing the pressure and decreasing the temperature of the system discouraged blowhole formation.

Fig. 14 shows the predicted effect of manganese on the critical initial silicon and carbon contents for blowhole formation at 0.010% oxygen, one atmosphere CO pressure, and freezing temperature 1525°C (with no hydrogen or nitrogen). Turkdogan later[48] carried out experimental work to show that

these predictions were reasonable.   Included in fig. 14 are

the silicon compositions predicted by Nilles and Scimar (see

fig. 7) to give balanced ingots at 0.5% and 1.0% manganese

and 0.06 and 0.08% carbon.   There is extremely good agreement

between the two sets of predictions over the range of compositions

considered by Turkdogan in spite of the differences in approach

to the problem.   However when the effects of adding hydrogen

and nitrogen, in amounts common to many steelmaking practices,

see Tables II and III, are considered, there is marked disagree-

ment between the two sets of results, see fig. 15.   This

demonstrates the important effect that hydrogen and nitrogen

may have on blowhole formation in deoxidised steels.

The theoretical treatment of Turkdogan became available

at the time the present work was instigated and it was decided

to adopt the model to try and predict steel compositions to avoid

sub-surface porosity.   A more detailed description of the

model, together with modifications made to enable the model to

be applied to a wider range of compositions than was originally

treated by Turkdogan, is given in Section 3 and the Appendix

of this dissertation.

2.4   Other Factors influencing Blowhole formation in steel

So far it has been assumed that blowholes are produced

during solidification solely by the solute elements, dissolved

in the steel as it enters the mould cavity, being rejected into the liquid ahead of the solidifying interface. However other factors which result in localised high concentrations of gases in the liquid steel can contribute to blowhole formation in steels. Hydrogen pick-up from mould moisture has been reported by Turton[19] who observed increases of up to 7 ml/100g after running steel over green sand. Porosity, resulting from localised carbon-oxygen reactions due to oxygen pick-up at the mould wall, has also been reported by a number of authors[18, 19,50,51]. Damp green sand moulds are thought to be one source of oxygen[19,49], but Seastone[50] in considering balanced and killed ingots found that iron oxide and lime present on mould walls could give rise to porosity. The oxide tended to build up progressively and stick to the mould wall. Seastone found the problem could be alleviated by cleaning the moulds or by coating with either aluminium paint or a gilsonite base material. Cleaning moulds will obviously help remove existing dirt, and a mould coating helps repel splash, caused during teeming, which would otherwise stick to the mould wall and oxidise rapidly, providing an ideal site for a carbon-oxygen reaction. A volatile mould dressing could, on the other hand, cause sub-surface porosity, if the rate of metal

rise in the mould is sufficiently rapid to cover the coating before all the volatiles have been driven off.

Volker[51] suggested that localised sub-surface porosity occurred as a result of bubble nucleation on foreign nuclei on the mould wall and that there must be a slag skin, preferably a reactive silicate, to prevent the porosity. He postulated that sub-surface blowholes occur to a severe degree in plain carbon steels since they contain insufficient silicon to form a suitable skin through its selective oxidation. He considered that a rusty mould wall did not cause porosity by local oxidation, but that the roughness of the mould wall in the vicinity of the rust rips off the ingot skin, leaving it bare and accessible to the foreign nuclei. On this issue, Volker's theory seems a little incredible.

Bergh and Josefsson[18], together with Volker[51], found slag droplets associated with blowholes in some cases. Though it was by no means proved conclusively, Bergh and Josefsson assumed that the blowholes could have been caused by reaction between the carbon in the steel and iron oxide in the slag particle. They also considered that the slag particles could aid blowhole nucleation by lowering surface tension.

The steels most likely to be susceptible to localised carbon-oxygen reactions are those with high carbon levels. This is because, all other things being equal (e.g., degree of deoxidation), the carbon-oxygen equilibrium relationship will be more easily exceeded by a given increase in oxygen concentration in high carbon steels than in low carbon steels. In fact Pribyl[49] observes that in the case of carbon-oxygen reaction resulting from oxygen pick up in the mould, the reaction

occurs more easily with high carbon levels.

A final example of effects, over and above those produced by solute rejection during solidification, which can affect the final blowhole structure, is the case of rimming steels. Nilles's[40] initial treatment of rimming steels did not take into account atmospheric oxidation while the steel is in the mould. The later study of Oeters et al[43] took this factor into account and showed it could influence the loss of carbon from the ingot, i.e., stimulate the rimming action. In fact results of a study carried out at IRSID[52] suggest that without atmospheric oxidation, a satisfactory rimming action would not be obtained, tending to confirm earlier work by Ward and Widdowson[53] who showed that the rimming intensity could be reduced markedly by casting under an inert atmosphere.

In this section an attempt has been made to show that, while a great deal of care may be taken to develop models which can successfully account for processes occurring during solidification, other effects obtained in practice, but difficult to consider on a theoretical basis, must not be completely ignored.

2.5 Blowhole Nucleation and Growth

The condition for a stable gas bubble to exist in a liquid melt is given by the well known formula:-

$$P_{Total} \geqslant P_A + P_F + \frac{2\sigma}{r} \quad \dots \dots \dots \dots \dots \dots (18)$$

where P_{Total} = total pressure of gases supporting the bubble (assumed = $P_{CO} + P_{H_2} + P_{N_2}$, the sum of the separate gas partial pressures)

P_A = Atmospheric pressure or pressure applied above the surface of the liquid steel

$$P_F = \text{Ferrostatic pressure}$$

$$r = \text{gas bubble radius}$$

$$\sigma = \text{surface tension of the molten steel}$$
in contact with the gas bubble

$$\frac{2\sigma}{r} = \text{pressure required to maintain a bubble,}$$
radius r, in molten steel of surface

tension σ.

All pressures are in atmospheres, except $\frac{2\sigma}{r}$ where a factor of 10^6 is required in the denominator to convert the term to atmospheres.

Homogeneous nucleation of bubbles within a steel melt can virtually be discounted after the work of Körber and Oelsen[54], who showed it was possible to build up a large supersaturation of carbon and oxygen, in an iron melt contained in a glazed silica crucible, without CO evolution taking place. Considered quantitatively, a bubble nucleus of molecular dimensions $(r \sim 6\text{Å})$ would have an internal pressure of 5×10^4 atmospheres[55]. This would involve impossibly large supersaturation of gas forming elements.

Heterogeneous nucleation must therefore be considered. Blowholes are in fact observed to nucleate at the solid/liquid interface[1,56]. This is a logical location since (i) gas concentrations will be highest in this region due to solute rejection and (ii) the surface tension of iron should be lower in this region due to build-up of various elements, and sulphur in particular. From surface energy considerations, Chalmers[1] shows that a cap type of nucleus should not be obtained. While conditions are slightly more favourable for a near spherical

nucleus, a planar interface is not an ideal spot for nucleation to occur. Small crevices or irregularities on the interface increase the chances of nucleation, since, for given surface energy conditions and contact angle between the nucleus and the solid, a smaller nucleus volume is required to become stable in a crevice than at a planar interface[1]. A typical example of a crevice in the solid/liquid interface would be a cell wall or an interdendritic space. Such a region is considered by Chalmer's to become highly enriched in solute elements due to lateral segregation which causes a situation similar to the 'terminal transient' condition, see fig. 2, to exist. Under such circumstances conditions for blowhole nucleation could be satisfied but it is unlikely that any of the models described earlier[33,40,43,44], used to establish critical amounts of gas forming elements in steels, would satisfactorily account for such conditions. However by employing the model of Turkdogan[46] it should be possible to substitute gas pressures, calculated during solidification, directly into equation[18] in order to assess the extent to which solute build up in a completely mixed interdendritic volume of liquid meets the gas pressure requirements for nucleation.

It is possible that a situation postulated by Campbell[57] may apply to blowhole nucleation. Campbell calculated that conditions for heterogeneous bubble nucleation would not be met by solute concentration alone, but would need an additional driving force. He suggested that minute air pockets trapped in certain exogeneous inclusions appear to be capable of stable existance for a period of time in a melt and able to provide

bubbles as nuclei for blowholes.   This hypothesis does not seem unreasonable, especially in view of the observations of Bergh and Josefsson[18] and Volker[51] who on occasion found slag inclusions associated with blowholes.   The mechanism would, however, be very difficult to verify in practice.

A vital stage in the appearance of blowholes is the initial growth of bubbles from atomic proportions to a stable size. A bubble of radius 0.05 mm would require a supporting gas pressure of only 0.2 atmospheres if the surface tension, σ, can be reduced to about 500 dynes/cm by solute enrichment. At $\sigma = 1000$ dynes/cm, the supporting pressure needed would be 0.4 atmospheres.   These pressures are in more reasonable proportions than those quoted earlier for atomic-sized bubbles, and providing there is sufficient flow of gas atoms to a bubble nucleus, early in its development, the pressure of gases required to maintain the bubble drops rapidly with increasing bubble size.   The ability of a bubble to become stable and its subsequent growth into a blowhole depend on:

    (i)   quantity of gas atoms being supplied per unit time to the blowhole

    (ii)   rate of advance of the surrounding solid/liquid interface

  (iii)   liquid flow ahead of the interface

    (iv)   external pressure being applied (i.e., atmospheric and ferrostatic).

If there are insufficient gas atoms being transferred to a bubble during its early stages of growth, then the bubble may collapse.   However, once a bubble begins growing into a

blowhole, it becomes a 'sink' for gas atoms from the surrounding enriched liquid, thus discouraging further blowholes forming in the immediate vicinity. Willes[40] in setting up his oxygen balance equation, see equation (11), assumed that the concentration gradient between the enriched liquid and blowhole was greater than between the enriched liquid and the bulk liquid. Hence for his particular case, oxygen diffused to the blowhole to form CO rather than to the bulk liquid. For carbon contents exceeding 0.04%, diffusion of oxygen to the blowhole was considered rate controlling. Below 0.04% carbon, the diffusion of carbon became the rate controlling factor.

The diffusion rate of nitrogen in liquid steel is reputedly 1-2 orders of magnitude slower than that of hydrogen[58-60]. Thus it might be anticipated that blowhole growth would exhibit different features in high nitrogen steels to those in high hydrogen steels. Sulphur has been shown[61,62] to reduce the flow of nitrogen atoms across gas/liquid interfaces. The effect reaches a maximum at 0.3% sulphur[61], above which the rate of transfer remains steady. Sulphur concentrates to approximately 20 times its original amount during solidification [9]. Assuming no reaction with other elements, it seems unlikely that increasing the initial sulphur concentration above about 0.015% will have much effect on the transfer of gas atoms to blowholes during solidification, but that from nil to 0.015% sulphur an effect may be observed.

While a bubble grows, the solid/liquid interface continues to advance and the relative growth rates of the solid and gas phases, together with flow ahead of the interface, determine the final blowhole shape, as was lucidly outlined by Hultgren and Phragmen[2]. They considered first, the type of blowhole

obtained when the gas quantity is small and the bubble grows at the same rate as the surrounding interface. In this case no gas is dislodged from the interface and the bubble grows into an elongated blowhole with a tapered shape, as shown in fig. 16 a-c, due to the advance rate of the solid/liquid interface lessening slightly. If the quantity of gas atoms being supplied to the bubble is such that it grows more rapidly than the interface, part of the bubble begins to protrude into the liquid steel. When this protrusion reaches a critical size, part of it may be dislodged, the amount depending on the turbulence ahead of the interface, and form a rising bubble which in turn will increase the turbulence. If the movement ahead of the interface is slow, enough gas will be left to maintain a protruding bubble, see fig. $16d_1$. The next layer of steel which solidifies causes the bubble to contract slightly, fig. $16e_1$, but further gas evolution causes expansion, fig. $16g_1$. With more turbulence ahead of the interface, more gas is flushed out from the bubble. This situation applies in a rimming steel, where in the first place, bubbles grow so quickly that they escape completely from the solid/liquid interface to create turbulence which gathers in momentum towards the top of the ingot. If the movement ahead of the interface is slower, such as at the bottom of a rimming ingot, where ferrostatic pressure starts to retard gas evolution, not all the gas escapes from the interface and liquid steel can enter the bubble cavity, fig. $16d_2$. Further growth of the bubble tends to force the liquid outwards again, fig. $16e_2$, until gas is again removed ahead of the interface, fig. $16f_2$.

The procedure repeated results in a worm-hole type blowhole.

For a given amount of gas evolution per unit time solidification rate can affect the resulting blowhole structure, particularly in large ingots, where ferrostatic pressure plays a large part in controlling blowhole growth. With a slow solidification rate, less gas will have been evolved by the time a critical pressure builds up to suppress blowhole growth, than with a fast solidification rate. Clark[63] and Binnie[64] reported a decrease of skin thickness of mould balanced and rimming ingots when the teeming temperatures were high. This effect was probably due to changes in solidification speed. When gas evolution is only slight and very small blowholes are formed just below the ingot surface, it is unlikely that the above effects will be observed.

The external pressure applied to the region in which gas is evolving in an ingot can greatly affect blowhole growth. The effect of ferrostatic pressure, P_F, was mentioned above. Morikawa et al[65] demonstrated the effect of increasing P_A, (see equation 18) in preventing porosity occurring in sand castings while Hultgren et al[66] showed that blowhole formation could be largely suppressed in rimming ingots by increasing the external pressure from 1 to 15 atmospheres.

Once the ingot top has solidified over, atmospheric pressure is eliminated, and one of two things may happen. Firstly, a back pressure can be set up which curtails blowhole growth. Secondly, if a pipe cavity begins to form, a shrinkage (or negative) pressure may stimulate blowhole growth particularly near the top of the ingot where the pipe occurs. This is a

mechanism thought to operate to some extent in ladle balanced ingots, to give the characteristic cone of blowholes just below the top surface.

3. DEVELOPMENT OF THEORY

As pointed out by Turkdogan[46] his method of calculating gas pressures in steel became less accurate as the concentrations of impurity elements increased. In attempting to apply this method to a wider range of compositions than was originally considered, the literature has been examined for evidence of likely effects of increasing the concentrations of the solute elements on the accuracy of the calculations. It became apparent that increasing the carbon concentration would lead to a major source of errors unless its effect was offset by suitable modifications to the original method. However, the effects of other elements in the steel (manganese and silicon) could by no means be neglected.

In modifying the original method, the following factors were considered:

    (i)   solute interaction coefficients

   (ii)   change of primary solidification phase (i.e., first phase to precipitate) from δ to γ.

 (iii)   varying solidification (liquidus) temperature and hence the temperature at which thermodynamic reactions occur. (It must be emphasised that solidification of a small interdendritic volume of liquid is being considered at all times in this theoretical treatment).

For the purpose of the present work, the parts of Turkdogan's work applicable to combined deoxidation by manganese and silicon were considered. A computer programme has been written which includes original equations necessary to calculate gas pressures under these conditions, together with suitable modifications

to account for factors (i) to (iii) above. Equations upon which the computer programme was based are given in section A.1 of the Appendix, which also includes a number of examples of the effects of the modifications introduced into the method, section A.2. A summary of the modifications is, however, considered appropriate at this stage.

3.1 Solute Interaction Effects

3.1.1 Carbon Monoxide

For the reaction

$$\underline{C} + \underline{O} \rightleftharpoons CO(g) \quad \dotfill \quad (19)$$

the equilibrium constant K_{CO} was expressed as follows:-

$$K_{CO} = \frac{P_{CO}}{[\%C][\%O]} \quad \dotfill \quad (20)$$

where P_{CO} is in atmospheres and the carbon and oxygen concentrations in liquid iron in weight per cent. Equation (20) is satisfactory providing these concentrations are small. However in steels of commercial composition it is more correct to express K_{CO} as follows:

$$K_{CO} = \frac{P_{CO}}{[f_c \cdot wt.\%C][f_o \cdot wt.\%O]} \quad \dotfill \quad (21)$$

where f_c and f_o are the henrian activity coefficients of carbon and oxygen respectively in liquid steel. These coefficients allow for the effects of interaction of other solute elements present in the liquid steel on carbon and oxygen in solution. f_c and f_o can be expressed as follows:-

$$\log_{10} f_c = \sum e_c^x [wt.\%X] \quad \dotfill \quad (22)$$

and $\quad \log_{10} f_o = \sum e_o^x [wt.\%X] \quad \dotfill \quad (23)$

where $\sum$ represents the sum of a number of terms and e_c^x, e_o^x are interaction coefficients, expressing the effect of a solute

element, X, on carbon and oxygen respectively in the ternary solutions Fe-C-X and Fe-O-X. For the purpose of the present work, interaction was considered to occur between carbon, oxygen, silicon and manganese. Hence f_c and f_o are expressed as follows:-

$$\log_{10} f_c = e_c^c \left[\text{wt.\%C}\right] + e_c^O \left[\text{wt.\%O}\right] + e_c^{Mn}\left[\text{wt.\%Mn}\right] + e_c^{Si}\left[\text{wt.\%Si}\right] \text{..(24)}$$

$$\log_{10} f_o = e_o^c \left[\text{wt.\%C}\right] + \text{etc.} \quad \dots\dots\dots\dots\dots\dots\dots\dots \text{ (25)}$$

Selected values of e_c^x and e_o^x are given in Tables IV and V together with other published data[67-84]. Second order interaction effects are ignored. In choosing e_c^x and e_o^x attempts were made to use data about which there seemed most agreement in the literature. When this was not possible the tendency was to use the more recently published data.

The oxygen available for reaction with carbon to produce CO is determined by the silicon and manganese levels in the liquid steel at each incremental stage of solidification, in a similar manner to that adopted by Turkdogan, and no modifications (e.g., interaction parameters for manganese and silicon, e_{Mn}^x and e_{Si}^x) have been made to the equations used to calculate the dissolved oxygen content. P_{CO} is now calculated, at each stage of solidification, from equations 21, 24 and 25, and the computer programme takes into account the changes in f_c and f_o that must occur as the concentrations of solute elements vary during solidification.

3.1.2 Hydrogen and Nitrogen

Solution of hydrogen and nitrogen in molten iron can be expressed as:

$$\tfrac{1}{2} H_2(g) = \underline{H} \quad \dots\dots\dots\dots\dots\dots\dots\dots \text{ (26)}$$

$$\tfrac{1}{2} N_2(g) = \underline{N} \quad \dots\dots\dots\dots\dots\dots\dots\dots \text{ (27)}$$

For binary Fe-H and Fe-N systems, the equilibrium constants for these reactions are given by Sievert's Law:-

$$K_H = \frac{[ppm \; H]}{\left(P_{H_2}\right)^{\frac{1}{2}}} \qquad \dots\dots\dots\dots\dots\dots\dots\dots\dots\dots (28)$$

$$K_N = \frac{[wt.\%N]}{\left(P_{N_2}\right)^{\frac{1}{2}}} \qquad \dots\dots\dots\dots\dots\dots\dots\dots\dots\dots (29)$$

where P_{H_2} and P_{N_2} are in atmospheres.

The above expressions for K_H, K_N were used in the initial work of Turkdogan. However, in a complex alloy system, such as commercial steels, other elements influence the behaviour of hydrogen and nitrogen in solution. These effects are expressed by the introduction of activity coefficients as in equation 21. Thus equations 28 and 29 become:-

$$K_H = \frac{f_H \cdot [ppm \; H]}{\left(P_{H_2}\right)^{\frac{1}{2}}} \qquad \dots\dots\dots\dots\dots\dots\dots\dots\dots\dots (30)$$

$$K_N = \frac{f_N \cdot [wt.\%N]}{\left(P_{H_2}\right)^{\frac{1}{2}}} \qquad \dots\dots\dots\dots\dots\dots\dots\dots\dots\dots (31)$$

where f_H and f_N are the respective henrian activity coefficients of hydrogen and nitrogen, given at low concentrations, by the following equations:

$$\log_{10} f_H = \sum e_H^x \; [wt.\%X] \qquad \dots\dots\dots\dots\dots\dots\dots\dots (32)$$

$$\log_{10} f_N = \sum e_N^x \; [wt.\%X] \qquad \dots\dots\dots\dots\dots\dots\dots\dots (33)$$

where e_H^x, e_N^x are the interaction coefficients, expressing the effect of solute element, X, on hydrogen and nitrogen respectively in the ternery systems Fe-H-X, and Fe-N-X.

In the present work, the interaction of carbon, manganese and silicon with hydrogen and nitrogen has been considered. Consequently, f_H and f_N are given as follows:-

$$\log_{10} f_H = e_H^C \left[\text{wt.\%C}\right] + e_H^{Mn} \left[\text{wt.\%Mn}\right] + e_H^{Si} \left[\text{wt.\%Si}\right] \quad \ldots\ldots \quad (34)$$

$$\text{and } \log_{10} f_N = e_N^C \left[\text{wt.\%C}\right] + \text{etc.} \quad \ldots\ldots\ldots\ldots\ldots\ldots\ldots\ldots \quad (35)$$

e_H^H and e_N^N are not included in the equations as both of these interaction parameters have been shown to be zero[87,95]. The values of e_H^X and e_N^X in the present work are listed, together with other published data[85-100] in Tables VI and VII. Values of e_N^X used were those selected by Chipman and Corrigan[101] from the literature. Values obtained by Weinstein and Elliott[87] were used for e_H^C and e_H^{Mn}. These are the more recent values and fall within the range of data obtained from other literature. For e_H^{Si} the value obtained by Laing et al[89] was used as this fell in the middle of the published range. In calculating f_H and f_N it was assumed that second order effects do not affect the result.

The concentrations of carbon, manganese and silicon in the interdendritic liquid change during solidification. Hence f_H and f_N change accordingly. These changes are computed in a similar manner to f_C and f_O, and P_{H_2} and P_{N_2} are calculated from equations 30, 31, 34 and 35.

3.2 Influence of Primary Solidification Phase

It was apparent, when dealing with higher carbon levels than those considered by Turkdogan, that at some stage of the solidification process, the carbon concentration in the enriched interdendritic liquid would exceed the limit of the peritectic

line in the Fe-C phase diagram, point D in fig. 17, i.e., the first phase to solidify would change from δ to γ. It is known that many elements, including most of those involved in the present work, have greater solubility in γ-iron than in δ-iron at a particular temperature. This means that their equilibrium distribution coefficients, k_o, will be greater for solidification to γ than for solidification to δ, neglecting any possible secondary effects of other solute elements. Selected data for k_o^δ and k_o^γ are given in Tables VIII and IX together with other published data[9,33,40,46,48,55,67,95,103-117].

For δ-solidification the k_o values used were those suggested by Turkdogan. Data on distribution coefficients between liquid and γ-iron are scarce and that available is mainly from one source[67].

Allowance for change in phase during solidification was taken into account when the computer programme was written. As shown in fig. 17, the limit of the peritectic line occurs at approximately 0.5% carbon. (The effects of other elements on this composition are neglected). The computer was programmed to make it possible to switch from values of k_o for δ-iron to k_o for γ-iron when the carbon content in the interdendritic liquid exceeded this level of carbon. The equations employed for calculating solute enrichment during solidification to δ-iron (see equations 4 and 8) and the assumptions made in choosing these equations (i.e., regarding diffusivities) were assumed to hold for solidification to γ-iron. Only values of k_o were programmed to change at the appropriate point.

3.3 Effect of varying the Solidification (ie. liquidus) Temperature

Equilibrium constants for the reactions involved in calculating gas pressures are temperature dependant. Turkdogan considered steels containing up to 0.1% carbon and assumed a constant solidification temperature of 1525°C. Any change in solidification temperature by solute enrichment was neglected. However, Turkdogan pointed out the shortcomings of this procedure when dealing with higher carbon concentrations. Changes in solidification temperature resulting from increased carbon concentration in the interdendritic liquid can give rise to large changes in the equilibrium constants, particularly those involved in the deoxidation reactions, when initial carbon levels in the range 0.1 to 0.5% are considered. Hence, large errors, in P_{CO} can occur.

In the present work steps have been taken to allow for changes in solidification temperature, which is assumed to be determined solely by the carbon content of the liquid steel. If the liquidus curves in the Fe-C phase diagram, fig. 17, are assumed linear then it is possible to compute the solidification temperature in terms of carbon content as follows:-

(i) Solidification to δ-iron ($\leqslant$ 0.5% carbon)

$$T°K = 1810 - 73(\%C) \quad \ldots\ldots\ldots\ldots\ldots\ldots\ldots (36)$$

(ii) Solidification to γ-iron ($>$ 0.5% carbon)

$$T°K = 1819 - 91.3(\%C) \quad \ldots\ldots\ldots\ldots\ldots\ldots (37)$$

The initial solidification temperature, and hence the temperature at which the thermodynamic reactions first take place, is determined by the initial uniform carbon concentration

when $g = 0$. The temperature then changes progressively with carbon content between $g = 0$ and 1. Should the first phase to solidify change from δ to γ during solidification, then equation (36) is replaced by equation (37). The computer is programmed to alter course at 0.5% carbon.

It is possible to operate the programme in two ways:-

(i) the solidification temperature is determined by the initial carbon level (at nil % solidified) and remains the same throughout solidification.

(ii) the solidification temperature changes with carbon concentration during solidification.

These two methods have been compared, see the sections A2.1.3 and A2.2.3 of Appendix.

The equations from which the equilibrium constants can be calculated were given, by Turkdogan, only for the deoxidation reactions. However, K_H and K_N (see equations 30 and 31), are also temperature dependant, and are expressed in the computer programme as follows:-

$$\log_{10}K_H = \frac{-1637}{T} + 2.316 \quad \dots\dots\dots\dots\dots\dots\dots \quad (38)$$

$$\log_{10}K_N = \frac{-188.1}{T} - 1.246 \quad \dots\dots\dots\dots\dots\dots\dots \quad (39)$$

T is in degrees absolute and K_H and K_N are expressed in ppm hydrogen and weight per cent nitrogen respectively. Equations are taken from data of Geller and Sun[109] and Weinstein and Elliott[87].

3.4 Results of Modifications

It is shown in section A2 of the Appendix that the modifications outlined in sections 3.1 to 3.3 can have marked

effects on the calculated gas pressures.   Three carbon levels have been considered for demonstration purposes, 0.10, 0.20 and 0.50%.   These are examples of steels in which the primary solidification phase is

 (i) wholly δ (0.10% carbon)

 (ii) primarily δ, but changes to γ during solidification (0.2% carbon)

 (iii) wholly γ (0.50% carbon)

Manganese and silicon levels considered at each carbon level were 1.0% and 0.10% respectively.   In addition, two further silicon levels, 0.03 and 0.25% were considered for the calculations of P_{CO} in 0.10% carbon steels.   The hydrogen and nitrogen levels considered were 7 ppm and 0.016% respectively.

The three carbon levels examined cover much of the commercial plain carbon range.   The manganese level of 1.0% is approximately in the middle of the range found in commercial carbon steels and the three silicon levels should cover a range of ingot conditions from "blown" to fully killed (depending of course on the hydrogen and nitrogen contents of the steel). The hydrogen and nitrogen levels chosen are to the top side of those normally found in modern steelmaking practices, but demonstrate effects of the computer programme modifications the most clearly on the scale chosen.

Given below is a summary of the effects:

(a) The interaction terms for carbon tend to be dominant particularly at the higher carbon levels considered and during the later stages of solidification. Terms involving silicon and manganese cannot however be neglected, especially at low carbon contents.

Terms involving oxygen tend to be very small
and could be neglected.

(b) The net effect of interaction is to reduce P_{CO}
but increase P_{H_2} and (for the most part) P_{N_2}, the
changes being most marked at the higher carbon
levels and towards the end of solidification.

(c) Changing from δ to γ during solidification reduces
all the gas partial pressures by virtue of the
fact that distribution coefficients of elements
in γ are greater than in δ, thus resulting in a
slower build-up of gases in front of a solid γ
interface.

(d) Programming the liquidus temperature to decrease
as the carbon content of the steel increases
results in a drop in P_{CO} but increases (fairly
small) in P_{H_2} and P_{N_2}. These effects also
become more pronounced as the carbon content
increases and solidification proceeds.

(e) Combined effect of the modifications is to reduce
P_{CO} and, for the most part, increase P_{H_2} and P_{N_2}.
The exception with the latter two gases arises when
the drop in pressure resulting from the δ to γ change
exceeds the increase in pressure caused by interaction
and varying temperature effects.

(f) P_{Total}, the total pressure of gases in the liquid steel
($= P_{CO} + P_{H_2} + P_{N_2}$) is lowered as a result of pressure
changes described in (e). Increasing the carbon
content of the steel enlarges this pressure drop, which
also generally increases during solidification.

EXPERIMENTAL WORK

4.1 Procedure

4.1.1 Steels Investigated

A list of steels investigated, together with variables studied is given in Table X. Variation of hydrogen in the free cutting steels and nitrogen in the rail steel compositions was consistent with the problems being encountered on the steelplant at the time the present work was instigated. The work was extended to plain carbon steels, containing 0.1 and 0.2% carbon, in order to obtain a comprehensive picture of blowhole formation over a fairly wide range of steel qualities.

4.1.2 Steelmaking and Casting

Laboratory melts, weighing 28 lb., were made up in a high frequency melting furnace with a magnesite lining. Air melting was employed and the melting procedure was as follows:-

(i) Swedish iron (see Table XI) was melted down to give a bath of metal containing approximately 0.2% oxygen.

(ii) Where appropriate, hydrogen was bubbled into the bath at this stage through a silica tube, held just under the surface of the molten metal. The apparatus was fitted with a safety value since, occasionally, the tube blocked, causing steel to splash when the pressure was released.

(iii) A bath temperature of 1580°C was attained and ferrosilicon, see Table XI, added. The bath was then left for a period of 5 minutes, during which, experience in the steelmaking section at Swinden Laboratories had shown, the silicon reacted with the oxygen in the

steel to form oxides which, aided by the eddy currents created by the coil, floated to the surface and were removed as slag. After the 5 minute period theoxygen had been reduced ostensibly to an equilibrium value and sufficient silicon remained to meet final analysis requirements.

(iv) Finishing additions were made. These consisted of warner iron, high or low-carbon ferromanganese and, where appropriate, nitrogen-manganese metal. Average analyses for these alloys are given in Table XI. Low-carbon ferromanganese additions were restricted to cases where the specified carbon content was less than about 0.10%. Nitrogen-manganese metal was used to boost the nitrogen content of the steel. The respective amounts of gases in the steel were varied by varying the amounts of carbon, silicon, hydrogen and nitrogen added to the steel. In the free cutting steels, sulphur was added in the form of ferrous sulphide.

(v) After the finishing additions had been allowed to melt, the bath temperature was checked. Casting temperatures were standardised in the range 1580 to 1610°C. The 0.5% carbon steels were cast at temperatures towards the lower end of this range (1580-1590°C), while the low carbon steels tended to be cast towards the top end of the range (1600-1610°C).

(vi) The melts were cast into cast iron moulds, about 16 in high, with square cross section, tapering

from 2 in at the bottom to 3 in at the top. The ingots were left open-top, with no feeder head or exothermic powder additions.

4.1.3 Sampling

Pot samples for chemical analysis (including nitrogen) were taken immediately prior to casting. Samples for hydrogen analysis were taken, first from the furnace, prior to casting by means of 'gravity filling' silica tubes, and then from the mould, on completion of casting, by means of evacuated pyrex tubes. Details of the sampling tubes are given in fig. 18. For the furnace samples, the silica tubes were dipped into the molten steel so that the filler hole, see fig. 18(a) was just below the surface. Steel then flowed into the tube. The ends of the evacuated tubes were thinned down so that, on contact with the molten steel in the mould, the glass melted and steel was sucked into the tube.

The silica tubes were preferred to split moulds for the furnace samples since preliminary experiments had indicated that it would be difficult to avoid slag contamination when teeming the split mould samples. On the other hand, slag-free silica tube samples could be ensured by first freeing the liquid metal surface from slag and then keeping the furnace power on during sampling, (once the power was switched off and the eddy currents removed, the top surface of the steel slagged over). It was impractical to obtain 'gravity filled' samples from the metal in the mould and hence the evacuated tubes were used for this purpose, having first confirmed that comparable results were obtained from the two methods.

The furnace and mould samples were plunged into cold water and the glass surrounding the samples shattered so that the steel was quenched to room temperature in a matter of seconds, (5 seconds maximum). The samples were then transferred to cardice where they remained until analysed by the hot extraction method (at 650°C). Furnace samples were also utilised, in certain cases and when suitable, for oxygen analysis by the vacuum fusion method. Mould samples were initially used in the same way, but extremely high oxygen contents were obtained. This was attributed to glass being sucked up into the tube along with the steel. Oxygen analysis, therefore, was subsequently restricted to furnace samples.

4.1.4 Study of Ingot Blowhole Structures

Ingot blowhole structure was studied visually after sectioning the ingots longitudinally. A selection of blowhole structures obtained during the experiments is shown in fig. 19. For simplicity, ingots were classed either as 'porous' or 'solid'. Thus, only ingot 'A' in fig. 19 would fall into the latter category.

4.1.5 Metallographic Examination of Samples

4.1.5.1 Blowholes

After undergoing preliminary examination, suitable ingots were sectioned further, and blowholes studied in more detail metallographically. During the preparation of samples, surfaces were ground down in stages, and the distances of the blowhole tips from the ingot surface measured at each stage. In so doing it was possible to obtain some specimens for examination with blowholes at, or near, their minimum distance from the surface.

4.1.5.2 Inclusion Examination

Specimens for inclusion examination were also taken from furnace
hydrogen samples.

This was in an attempt to:-

(i)   estimate by inclusion counting the extent to which
        oxides contributed to the total analysed oxygen.

(ii)   assess the validity of assuming an equilibrium
        deoxidation product of pure $MnO.SiO_2$.

For (i) above, the Quantitative Television Microscope was
employed.   When representative inclusions had been selected,
they were analysed on the Electron Probe Microanalyser for (ii)
above.

4.2 Experimental Results

4.2.1 Chemical Analysis

Since about 450 casts were involved in the present work,
it is not practical to account for each chemical analysis here.
Elements varied by design (i.e., silicon, hydrogen and nitrogen)
are accounted for in the following sections.   When hydrogen
and nitrogen were not boosted artificially, the levels of these
elements in the steel were found to be 3-4 mls/100g and 0.007-
0.009% respectively, see Table X.   The sulphur and phosphorus
ranges obtained are also given in Table X.

For a given steel quality, attempts were made to maintain
constant carbon and manganese levels.   This was not always
possible, and hence steels inside the following analysis ranges
were used in assessing the results.

(i)   0.04 - 0.06% carbon (Av. .05%), 0.9 - 1.15%
        manganese (Av. 1.0%)

(ii) 0.09 - 0.11% carbon (Av. .10%), 0.9 - 1.15%
        manganese (Av. 1.0%)

(iii) 0.18 - 0.22% carbon (Av. .20%), 0.9 - 1.15%
        manganese (Av. 1.0%)

(iv) 0.45 - 0.55% carbon (Av. .48%), 1.0 - 1.3%
        manganese (Av. 1.2%)

4.2.2 Establishing Porous/Solid Borderlines

As indicated in Table X, for a particular steel base
composition, silicon and either nitrogen or hydrogen were varied
so as to vary the gas content. Hence, results were divided
into a number of discrete silicon ranges, and within these
ranges, the effects of increasing nitrogen or hydrogen were
studied. Results for 0.10% carbon free cutting steels are
shown in fig. 20. Here the ingots were classed as 'porous'
or 'solid' according to the scheme outlined in fig. 19. The
manganese and nitrogen were held constant at 1.0% and 0.008%
respectively and the silicon ranges were chosen as follows:
nil-0.02%; 0.02-0.05%; 0.05-0.10%; 0.10-0.20%; 0.20-0.30%.
The ranges were wider for the higher silicon steels since the
effect of silicon on the oxygen content of the steel diminishes
with increasing amount of deoxidant[46]. To make it possible
to divide up the silicon levels into the smaller discrete
ranges, e.g. nil-0.02%, with confidence, it was necessary to
employ colorimetric silicon analysis (accurate to ±0.005% silicon)
in place of the more routine gravimetric analysis, accurate
to ±0.02% silicon.

The hydrogen content plotted in fig. 20 is that of the
liquid in the mould at the end of casting. The evacuated tubes
used to obtain mould samples for hydrogen analysis did not
always operate satisfactorily, but it was always possible to

obtain good furnace samples.   For this reason, a relationship
was established between the hydrogen content in the furnace
and that in the mould on casts where both samples were
satisfactory.   This made it possible to obtain a good estimate
of the hydrogen content of steel in the mould from the furnace
value when a poor mould sample was obtained.   Relationships
between furnace and mould hydrogen contents are given in fig. 21
for free cutting steel (0.05 and 0.10% carbon) and plain low
carbon steels (0.1 and 0.2% carbon).   It will be noted in
both cases, that there was a certain hydrogen level above which
hydrogen was lost between furnace and mould and below which
hydrogen was picked up.   For free cutting steels this value
was 3.6 ml/100g;   for plain carbon steels the value was 5.8 ml/100g.

In fig. 20, the upper limit of the porous/solid borderline
scatter band was taken as the highest hydrogen level at which
a solid ingot was obtained.   The lower limit was taken to be
the lowest hydrogen level to produce a porous ingot.   In the
silicon range nil-0.02% no lower limit to the borderline could
be established at the minimum levels of hydrogen and nitrogen
attainable on the air melting furnaces.   The point demonstrated
in fig. 20 is that the hydrogen content at the porous/solid
borderline increased with increasing silicon content, although
above about 0.10% silicon, very little change in the position
of the borderline was detected.   The effect is shown more
clearly in fig. 22.   Here the scatter bands were re-drawn
with the silicon content increasing continuously, rather than
in a series of discrete steps.   The best curve was drawn
through the bands to depict the best estimate of the porous/
solid borderline over the range of compositions studied.

Ideally the results should have been divided into a large number of discrete silicon ranges between nil and 0.30%, but this would have involved a prohibitive number of casts.

Similar exercises, involving about 450 experimental casts, were carried out for the compositions listed in Table X, and the results are presented in fig. 23. In this figure, the points on the curves are the mid-points of scatter bands, similar to those shown in fig. 22. Results from the free cutting steel experiments in fig. 23(a) show that the porous/solid borderline hydrogen content was higher in the 0.05% carbon than in the 0.10% carbon steels over the full range of silicon levels studied. A similar pattern emerges from fig. 23(c), where the nitrogen content at the porous/solid borderline is higher in the 0.1% plain carbon than in the 0.48% plain carbon steels, over the full silicon range, in spite of the manganese level being slightly higher in the 0.48% carbon steels. However, this trend is reversed in fig. 23(b), in which borderlines in 0.1 and 0.2% plain carbon steels are compared. Though the curves are close together up to approximately 0.15% silicon, the porous/solid borderline is higher in the 0.2% than in the 0.1% carbon steels. Comparing 0.1% carbon free cutting with plain carbon (or low-sulphur) steel, figs. 23(a) and (b) it is seen that for a given silicon level, more hydrogen is required to produce porous ingots in the high-sulphur ingots than in the low sulphur ones. A general feature of the results was a sharper change in the porous/solid border-lines at low silicon levels compared with the silicon levels exceeding 0.1%

In only one of the series of experimental steels, the 0.05% carbon FCS, was it found possible to obtain solid ingots (and therefore a porous/solid borderline) below about 0.03% silicon, even when the hydrogen and nitrogen contents were not boosted.

In the rail steels (0.48% carbon), solid ingots could not be obtained below about 0.075% silicon.

From the curves in fig. 23, it was possible to read off porous/solid borderline hydrogen or nitrogen levels for a number of silicon levels, see Table XII, and this data was fed into the computer for gas pressure calculations (see Section 5).

4.2.3   Silicon-Oxygen Relationships in Experimental Steels

Since air melting was employed, and the experiments were not being carried out under ideal circumstances as far as equilibrium for the deoxidation and gas reactions was concerned, it was decided to compare the oxygen levels obtained in the experimental steels with those predicted by work carried out under controlled conditions and utilised by Turkdogan[46]. Also, in view of the apparent effect of sulphur in causing an increase in the porous/solid borderline, the oxygen levels in 0.1% carbon free cutting and plain carbon steels were compared, see fig. 24.   Normally, at least 2-3 oxygen determinations were carried out on each silica tube sample, and the average value taken.   If the values from these determinations disagreed markedly (by more than about 10%), extra determinations were performed until a reasonable average value was obtained.

The theoretical silicon-oxygen curve in fig. 24 was calculated from the data given in Turkdogan's paper.   A manganese level of 1.0% was assumed.   In general, the experimental points, as expected, fell above the theoretical line.   However, a number of points from the high sulphur steel experiments fell on or below the theoretical curve, and in the range nil to 0.10% silicon in particular, the oxygen levels in the high-sulphur

steels were generally lower than in the plain carbon steels.
Average oxygen levels for the following silicon ranges: nil-
0.05%; 0.05-0.10%; 0.10-0.20% and 0.20-0.30% in the low and
high sulphur steels are given in Table XIII. For each silicon
range the oxygen content of high sulphur steels was lower than
that of the low-sulphur steels.

The technique employed for oxygen analysis measures the
total oxygen content of the steel (i.e. not only dissolved
oxygen, but also oxygen in the steel combined as oxides).
Unless all these inclusions are eliminated from the liquid steel,
it is obvious that a true silicon-oxygen relationship cannot be
established. Thus, as mentioned earlier, an attempt was made
to assess the effect of inclusion content on the total oxygen
content in the steel. In addition, suitable inclusions were
analysed on the electron probe microanalyser to establish
whether the assumptions made in the theoretical treatment,
regarding silicate analysis (i.e. that the silicates were of
composition $MnO.SiO_2$), were reasonable.

4.2.4 Inclusion Examination

Specimens for metallographic examination were selected so
that a number of samples having the same silicon content but
varying total oxygen contents were examined. Work was carried
out by a quantitative television microscope and results for
a number of plain carbon steel specimens are shown in Table XIV.
It was possible, using the QTM, to measure total area per cent
of oxides and the number of oxides in various size ranges, but
not the area per cent oxides in each size range.

Preliminary metallographic examination revealed three
fairly well defined size ranges of oxides (see fig. 25):

(i)   a large number of very small inclusions,
     $<4\mu$ in diameter,

(ii)   a smaller number of inclusions $4-10\mu$,

(iii)   a few inclusions, $>10\mu$ in size.

The inclusions in the range $4-10\mu$ and $>10\mu$ in size were considered unlikely to have formed during solidification and cooling of the steel samples, which had been quenched rapidly, giving inclusions very little time to grow or coagulate. It was inferred, therefore, that these inclusions were present in the liquid steel prior to solidification and the oxygen combined in these inclusions could not be classed as 'dissolved' at casting temperatures. On the other hand, the large numbers of very small inclusions, by virtue of their more general distribution and size, probably precipitated as a result of manganese, silicon and oxygen enrichment during solidification and the oxygen combined in these inclusions could be classed as 'dissolved' prior to solidification.

The results presented in Table XIV show that the above inferences were reasonable. For a particular silicon content, increasing the numbers of the larger inclusions, particularly those above 10μ, led to an increase in the total oxygen content. This effect was apparent, but not as marked, for the inclusion size range $4 - 10\mu$ and there was little trend of total oxygen content with the number of inclusions $<4\mu$ in size.

Analysis of a number of oxides is given in Table XV. Only the larger oxides (i.e. those formed prior to solidification) were of suitable size for probe analysis. These oxides were found to be silicates containing mainly MnO and SiO_2 but with small amounts of FeO and TiO_2. The TiO_2 was thought to have

originated from residual titanium in the steelmaking additions
or furnace lining contamination from previous casts.   The
information given in Table XV indicates that the inclusion analysis
varied between $(MnO.FeO)SiO_2$ and $(MnO.FeO)_{1.5}.SiO_2$.   Excluding
the small amount of FeO, the composition can be said to vary
between $MnO.SiO_2$ and $(MnO)_{1.5}.SiO_2$.   There appeared to be
a trend from the former to the latter composition with increasing
Si/Mn ratio.   This information suggests that an assumed silicate
composition of $MnO.SiO_2$ in the theoretical model was not
unreasonable.

Area per cent oxide figures are included in Table XIV.
From these figures weight per cent silicon and oxygen combined
as oxides, assumed to be of composition $Mn.SiO_3$ were calculated.
Fig. 26 shows a reasonable relationship between vacuum oxygen
results and the calculated oxygen figures, and indicates that
most of the oxygen in the steel was combined as oxides after
solidification.

4.2.5 Blowhole Examination

There was a trend in the type of blowhole produced from
an acicular type in the very low carbon steels (up to 0.1%)
to a more lenticular or bulbous type in the higher, 0.48% carbon
steels.   Examples of the different types of blowhole are
given in figs. 27-29.

Irrespective of the type of blowhole, those in ingots
of borderline porosity, or on the slightly gassy side (see
fig. 19(b), were trapped very close to the ingot surface,
although in many cases this was not immediately apparent due
to sectioning effects.

Using the technique of grinding the specimens in stages, surface-to-blowhole distances of as low as 0.06 mm were measured. The close proximity of a blowhole tip to the ingot surface is demonstrated in fig. 30. Note the protuberance at the surface adjacent to the tip of the blowhole in fig. 30(a) suggesting, perhaps, that the pressure of gases in the blowhole has forced the surface skin outwards.

It is apparent in fig. 29 that there is a very fine dendrite spacing in the region of the base of the blowholes. The structure was in fact so indistinct at this point that it was not possible to obtain a reasonable estimate of the spacings. Measurements made about 10 mm from the ingot surface showed the spacing at this position was approximately 0.05 mm.

5. USE OF THEORY TO CALCULATE GAS PRESSURE IN STEELS
    OF POROUS/SOLID BORDERLINE COMPOSITION

The theory, outlined earlier in the dissertation and in
the Appendix, was applied to the calculation of gas pressures
in steels of porous/solid borderline composition shown in
Table XII. All the modifications outlined in section 3
(i.e., interaction, varying temperature, $\delta - \gamma$ change)
were included in the calculations. Examples of how P_{CO},
P_{H_2} and P_{N_2} can contribute to P_{Total} are given in fig. 31.
It is apparent that the relative contributions of the three
component gases change during solidification. In the early
stages of solidification, P_{CO} tends to dominate, but towards
the end of the solidification, the combination of P_{H_2} and P_{N_2}
makes the larger contribution to P_{Total}. Note the difference
in P_{Total} between the 0.10 and 0.48% carbon steels at nil%
solidified. P_{Total} in the 0.48% carbon steel is much higher
than in the 0.10% carbon steel initially, but during the
solidification process the values of P_{Total} for the two carbon
levels gradually merge, and, at some stage, reach a common
value. This agreement in P_{Total} during the later stages of
solidification is a very important factor in determining how
the theory can be applied successfully to practice, as will
be described in more detail in the discussion.

P_{Total} curves for the porous/solid borderline compositions,
given in Table XII, are presented in figs. 32-34. The
general pattern is for P_{Total} to increase during the solidifica-
tion process, although in some cases, this is followed by a
decrease in the later stages of solidification.

In interpreting the pressure curves, two assumptions were made. The first was that for blowholes to form, P_{Total} must exceed at least one atmosphere. The reason for this assumption was that metallographic examination had indicated that blowholes nucleate very close to the ingot surface, almost certainly before a significant ferrostatic pressure had built up, and before the ingot top had solidified over, removing the influence of atmospheric pressure. For the moment, nucleation problems were neglected. The second assumption was that blowhole formation, and hence the porous/solid borderline, should occur for all compositions, at a particular pressure or within a small pressure range. Furthermore, a certain value of P_{Total} should correspond to a certain blowhole structure. Hence, for a particular set of porous/solid borderline P_{Total} curves, there should be close agreement at some stage of solidification and particularly in the region of one atmosphere and above. The first curves to be obtained were those for free cutting steels, fig. 32(a) and (b). Scatter bands for these two series of curves are drawn in fig. 35(a). Closest agreement in P_{Total} between the two sets of steels occurred at approximately 90% solidified, the pressure range at this point being 1.2 to 1.45 atmospheres.

A similar agreement in pressure at 90% solidified was obtained for the 0.1% carbon steels, containing 0.008% nitrogen, fig. 33(a). However, in this case the pressure range was 0.9 to 1.0 atmospheres (see also scatter band in

fig. 35(b)). At this stage, therefore, it seemed reasonable to use the discrete pressure range at 90% solidified as the criterion for predicting porous/solid borderlines in steels.

Such close agreement in P_{Total} obtained for the low-carbon steels with varying hydrogen, was not repeated when the nitrogen content was varied, see fig. 33(b). The porous/solid borderline P_{Total} values for the high-nitrogen ($> 0.014\%$) steels deviated from those for low-nitrogen ($< .014\%$) during the later stages of solidification. The pressure range at 90% solidified for the high-nitrogen steels was 1.10 to 1.25 atmospheres, while for the low-nitrogen steels it was 0.85 to 1.10 atmospheres. A similar trend of a higher P_{Total} at 90% solidified with increasing nitrogen content for porous/solid borderline compositions was observed with the 0.48% carbon steels, fig. 34(b). In this case, for steels containing up to 0.013% nitrogen, P_{Total} at 90% solidified was 1.0-1.1 atmospheres, in good agreement with the low-nitrogen 0.1% carbon steels (see scatter bands, fig. 35(b)). Above 0.013% nitrogen, P_{Total} (90%) was 1.1 to 1.2 atmospheres, again in excellent agreement with the results from the 0.1% carbon steels, see fig. 35(c). The results from the 0.2% carbon steels, fig. 34(a) did not fall into the above pattern. However if curves for steels containing up to 0.15% silicon are considered, it is evident that closest agreement in P_{Total} occurs at about 90% solidified in the range 1.1 to 1.2 atmospheres. The curve for the 0.25% silicon steels containing 7.6 ppm hydrogen does not give such good agreement, and pressures approaching 1.4/1.5 atmospheres are attained at 90-95% solidified.

Further features of the P_{Total} curves in figs. 31 - 35, possible implications of which will be discussed later, were the fairly high initial gas pressures in 0.2 and 0.48% carbon steels compared with those in 0.05 and 0.10% carbon steels. Also, the P_{Total} curves for the higher carbon steels tended to approach one atmosphere at an earlier stage of solidification than the curves for the low carbon steels.

The relative contributions that CO, H_2 and N_2 make to the final mixture of gas is demonstrated in Table XVI, in which the gas pressures at 90% solidified, for the porous/solid borderline compositions obtained in the present work, are listed. The increasing importance of P_{H_2} and P_{N_2}, as the degree of deoxidation in the steel increases, is evident.

6. DISCUSSION

6.1 Limitations of Theory

6.1.1 Equilibrium Data

In calculating the partial pressures of carbon monoxide, hydrogen and nitrogen, it was assumed, consistant with Turkdogan's original work, that all deoxidation and gas forming reactions occurred under equilibrium conditions, that there was no problem of oxide nucleation, and that no kinetic factors were involved, either during cooling or the subsequent solidification process. Furthermore, in considering deoxidation reactions, it was assumed that only manganese and silicon determined the amount of dissolved oxygen available to react with carbon to produce carbon monoxide. The oxides involved in the deoxidation process were assumed to be pure liquid manganese silicates.

In the first stage of the experimental procedure, melting was carried out under atmospheric conditions. Thus, unlike the conditions under which the thermodynamic data were obtained, there was a continuous supply of air to the molten steel, making the attainment of complete equilibrium unlikely. In spite of this, analysis of oxides present in the steel prior to solidification, showed that silicates, similar in composition to those predicted from the theory, were obtained. The silicon - oxygen relationship (for 1.0% manganese) in the experimental steels at tap lay above the equilibrium line calculated from theory, see fig. 24. However, quantitative metallography revealed that much of the oxygen in the steel was combined as oxides which had not escaped from the system. Therefore, the true experimental

silicon - oxygen relationship lay nearer the equilibrium
line than was first suspected.

Sulphur, not included in the theoretical deoxidation
equations, had a significant effect on the oxygen content
of the steels. Though sulphur is reputedly a weak deoxidant
(the negative free energy of formation of SO_2 is less than
half those of MnO and SiO_2 at 1600°C[118]) and should,
therefore, have little effect on the oxygen content of the
steel, evidence from the present work indicated that the
oxygen content of resulphurised steels was lower than that
of the plain carbon steels over the silicon range examined.
The difference was most marked at the lower silicon levels.
It is possible that sulphur indirectly affects the deoxidation
reactions by influencing the activities of the other deoxidants,
manganese for instance. This apparent 'killing' action of
sulphur has been noted elsewhere in other investigations[119-123]
but apparently without explanation, until Yeo[124] suggested
that the function of this element might be to impair the
transfer of carbon and oxygen atoms across the gas/liquid
metal interface in the same way it is reputed to slow down
nitrogen transfer[61,62]. Clearly, there is scope for
further work to be done to study the true deoxidation effects
of sulphur.

During casting, the contact of the molten steel with
the atmosphere is another factor which can upset equilibrium
conditions. For instance, Pribyl[49] noted oxygen pick-up
in steel during teeming. Oxidation effects during casting
were not examined in the present work, but, as shown in

fig. 21, note was taken of the change in hydrogen content of the steel as it passed from the furnace to the mould. The results from this part of the experiments showed that there was a certain level of hydrogen in the liquid steel, as it left the furnace, above which hydrogen was lost between furnace and mould and below which it was picked up. This suggests a kinetic effect and an equilibrium hydrogen content of the liquid steel. Hence there will be a driving force trying to either increase or reduce the hydrogen content of the steel, and this force will be particularly active when there is sufficient free surface available for transfer of gas atoms to occur. Sulphur was observed to have an effect on the change in hydrogen content of the steel between furnace and mould (fig. 21). A tenfold increase in the sulphur content apparently reduced the equilibrium hydrogen content of the steel mentioned earlier. This suggests that the solubility of hydrogen in the steel may be lowered by sulphur, an observation verified by the results of Weinstein and Elliott[87]. Furthermore, the slope of the line for the high sulphur steels in fig. 21 is less than that for the low sulphur steels, suggesting that sulphur slows down the transfer of hydrogen gas atoms from the liquid steel to the atmosphere in a similar fashion to the nitrogen transfer effects[61,62]. Possible implications of these observations, with regard to blowhole nucleation and growth, will be discussed later.

While it was possible to examine the larger inclusions (> 10μ) in the steel present prior to solidification, the

smaller inclusions, and, in particular, those formed
during solidification of the samples, were unsuitable for
probe analysis. The composition of these smaller inclusions
was consequently not established. It can only be stated
that they appeared siliceous on visual examination. In view
of the extremely rapid solidification rates at the surface
of the chill cast ingots, which must result in quite variable
localised conditions, due, in part, to changes in solute
concentrations, it is unlikely that equilibrium conditions
can exist. The assumption of equilibrium at this stage
of the process is therefore one of the most obvious limitations
of the theory.

6.1.2 Solidification Model

The assumptions made regarding solute mixing during
solidification are questionable, particularly in view of the
rapid solidification rates obtained in the chill cast
experimental ingots. The use of equation (8) implicitly
assumes that the liquid is completely mixed at all times,
that there is no diffusion in the solid, and that k_o,
the equilibrium distribution coefficient, applies at all
times. While Brody and Flemings[39] showed that equation (8)
satisfactorily describes the solute distribution between
dendrite arms, Pfann[37] demonstrated that the use of
equation (8), in place of equation (7), i.e. k_o in place
of k_E, the effective distribution coefficient, was valid
only when solidification rates were very low. With finite
solidification rates, of cm/min, such as would be obtained
in chill cast ingots, k_E was greater than k_o and approached

unity at fast rates. A diffusion controlled situation had then to be considered. In other words a condition of partial mixing with some diffusion control in the liquid would be more appropriate to the fast solidification rates found in chill cast ingots, the degree of mixing depending on the solidification rate.

Under these circumstances, it seems more appropriate to use the equation of Burton et al[38], see equation (9), which was employed by Cetere et al[43,44] and Delmar and Miller[53]. These authors, in considering solidification and blowhole formation at the surface of killed and balanced steels, assumed that there was negligible mixing in the liquid and that the solute ahead of a planar interface was diffusion controlled. Effectively, they assumed the 'steady state' condition described in section 2.2, with $k_0 \simeq 1$, and the liquid concentration at the interface $\simeq c_0/k_0$. Under such circumstances, an "initial transient" must exist before the steady state can be established, see fig. 2. The distance over which the initial transient exists is given by $x = D/k_0 R$ (where all the terms were defined in section 2.2). For rapid solidification rates, $D/R \simeq 0.05$ mm, see fig. 3, and hence x, can vary between 0.05 mm if $k_0 = 1$, and about 0.25 mm if $k_0 = 0.2$, as in the case of carbon for solidification to δ-iron. It has been found in the present work that blowholes nucleate within 0.06 mm of the surface. Hence, under conditions of plane-front solidification, blowholes could nucleate within the initial transient,

i.e. when the interface liquid concentration lies between C_o and C_o/k_o. (This was not taken into account by the above workers[33,43,44].) These are almost exactly the conditions found when employing the completely mixed liquid model used in the present work. A liquid concentration of C_o/k_o in the plane-front model virtually corresponds to the later stages (i.e. 90-95% solidified) of solidification in the completely mixed liquid model. Hence, it is not unreasonable to expect the two models to produce similar results with regard to the prediction of porous/solid borderlines, assuming of course that similar data are used.

In the above paragraphs, the two solidification models considered have been one of complete liquid mixing between dendrites and one of mixing by diffusion only ahead of a planar interface. The occurence of a completely planar interface is very unlikely in a complex alloy such as steel, even in the very early stages of solidification. Similarly, it also is unlikely that a dendritic structure will have time to develop fully in the time it takes a blowhole to appear. An intermediate situation of an interface, made up of protrusions, shown in fig. 36, is more likely to exist. The completely mixed liquid model could still be applied to the localised regions between the protrusions into which liquid is being rejected laterally. In this case, the calculations of solute enrichment and gas pressures will be no different to those performed in the present work. At the other extreme, if the solidification rate is fast enough to set up a diffusion profile, the thickness of the diffusion

layer, d, must be considered. Burton et al found values of d of approximately 1 mm for conditions of natural convection in killed or balanced steels. This figure was also quoted by Scimar and Hilles[33]. Interdendritic spacings (this term is used loosely in the present context to describe the spacings between the protrusions) near the surface of chill cast ingots have been found in the present work, and also by Poirer and Flemings[125], to be less than 0.05 mm, i.e. nearly two orders of magnitude less than the reported thickness of the diffusion layer, d. This means that diffusion profiles from neighbouring protrusions, both rejecting solute laterally into the liquid, will overlap as shown in fig. 37. Furthermore, it is probable that the individual profiles will be similar to those existing under 'initial transient' conditions described earlier, since the distance over which the initial transient exists is generally greater than the diffusion layer (or characteristic distance), and hence much greater than the interdendritic spacing. Under such conditions, the liquid concentration at the solid protrusion/liquid interface will be less than C_0/k_0, see fig. 2 and 37. The overlapping of the diffusion profiles will result in a levelling-out of solute concentrations in the interdendritic liquid and create a situation not unlike one of complete mixing. Thus, the solidification model used in the present work is probably not so unreasonable as was first imagined. However, since diffusion will be restricted to a certain extent within the liquid regions between protrusions, a 'terminal transient' condition, see section 2.2, may exist on a very small scale near the

end of the solidification process. Under these circumstances extremely high concentrations of solute elements could be found, as pointed out by Chalmers[1]. These concentrations would be higher than those calculated either by the model employed in the present work or by the one used by Oeters et al[43,44], but would be difficult to estimate in practice. However, as mentioned in section 2.5 fairly high concentrations would probably be required to aid the formation of a stable blowhole nucleus at the solid/liquid interface. A fuller discussion on blowhole nucleation and growth is given later.

6.1.3 Modifications

It is evident from Tables IV to IX that there can, in some cases, be marked disagreement between the reported interaction and distribution coefficients. The interaction terms $e^x[wt.\% \; x]$ will obviously be influenced by the choice of data, and hence P_{CO}, P_{H_2} and P_{N_2} will be affected. The effect of varying the input data has not yet been studied. It would appear, however, from Tables IV to VII that changing the interaction parameters would not, in the majority of cases, alter the general trend in results outlined in section 3 and the Appendix. Exceptions seem to be in the choice of e_N^{Mn}. If the value of -0.094 was used for e_N^{Mn}, then f_N could be less than unity over a wide range of carbon and silicon levels, depending of course on the manganese content of the steel.

Available data on the distribution coefficients, see Tables VIII and IX, indicate that those for carbon, hydrogen

and nitrogen (k_C, k_H and k_N) increase on changing from
δ to γ, thus tending to decrease the amount of these
elements rejected into the interdendritic liquid and hence
reduce P_{CO}, P_{H_2} and P_{N_2}. The information on k_{Si} in γ
indicates that it is less than in δ. Thus more silicon
will be rejected from the solid once solidification to γ
occurs, and this will also tend to reduce P_{CO}. Reported
values for k_{Mn} in δ and γ indicate that k_{Mn} increases from
δ to γ, thus tending to increase P_{CO}. For oxygen, values of
k in δ and γ overlap slightly, but the weight of evidence
suggests that k decreases from δ to γ increasing the amount
of oxygen in the liquid and hence increasing P_{CO}. As
observed earlier, the net effect of these changes in k, is
to lower P_{CO}, P_{H_2} and P_{N_2}. Altering the values of k
from those used at present in the programme would alter
the magnitude of the pressure changes, on moving from
δ to γ, but not the general trend in results. Of course,
changing the values of k will in any event change the rate
at which the elements concentrate in the interdendritic
liquid during solidification, and hence the gas pressures.

The k values used in this work have been determined
on binary Fe - X alloys. Doherty and Melford[126] showed
that the presence of carbon in Fe - C - Cr alloys influenced
the value of k_{Cr} in the steel. Work at Swinden Laboratories
has indicated that increasing the carbon content increases
the segregation tendencies of both chromium and manganese,
but detailed information on values of k for elements of
interest in the present work has not been found.

The conditions under which the δ to γ phase change takes place during solidification have been simplified for the purpose of the computer programme. It has been assumed that when the interdendritic liquid contained up to 0.5% carbon, the primary solidification is δ, and that above 0.5% carbon, the primary phase simply changes to γ, without complex reactions occurring.

Reference to the Fe - C phase diagram, see fig. 17, shows that steels solidifying to between 0.11 and 0.52% carbon undergo peritectic transformation during solidification. Steels whose initial carbon contents lie between points B and C in fig. 17 will first precipitate δ during solidification. Under the conditions assumed in the solidification model in this work (i.e. complete diffusion of carbon in liquid and solid), the composition of the solid will follow the solidus line AB as the temperature drops and solidification proceeds. Similarly, the liquid composition follows the liquidus line AD. When the temperature falls to 1,499°C, solid δ of composition 0.11% carbon (point B) is in equilibrium with liquid of composition 0.52% carbon (point D). At this stage, under equilibrium conditions all the solid δ and the remaining liquid react to produce a mixture of δ and γ, which then continue to precipitate simultaneously. During this joint precipitation the liquidus carbon content remains at a constant value, viz. 0.52%, and the compositions of δ and γ being precipitated are 0.11% and 0.16% carbon respectively. On these considerations

alone it might be anticipated that the value of P_{CO} in the liquid should remain fairly constant once peritectic transformation had begun. However the other impurity elements (i.e. manganese, silicon, etc.) in the steel should prevent this. For example, with the addition of a third element to the Fe - C system, e.g. silicon, the binary $\delta + \gamma$ phase field will become a ternary region containing $L + \delta + \gamma$. Hence solidification will continue along with the precipitation of $\delta + \gamma$. Under these conditions it is difficult to decide what values should be assigned to the distribution coefficients, since a mixture of two solid phases, with different solubilities for the impurity elements, are being formed.

In steels where the initial carbon content lies between C and D in fig. 17, the first phase to solidify is δ, but this time when the temperature falls to the peritectic line, δ (containing 0.11% carbon) and the remaining liquid react to produce liquid and γ, containing 0.52 and 0.16% carbon respectively. At equilibrium all the δ is consumed and solidification then proceeds with the precipitation of γ. The composition of the liquid will then follow the line DG. Similarly the solid composition follows CF. The simple approach employed in the programme for δ to γ transformation would appear to be more suitable for steels solidifying under these conditions, than for the case described earlier where δ and γ precipitate jointly.

All the carbon levels considered in this work are
either close to or within the composition range in
which peritectic reaction occurs. According to fig. 17,
the 0.05 and 0.10% carbon steels lie just to the left of point
B on the peritectic line and should, under ideal conditions,
solidify as δ. The 0.48% carbon steels lie just within
the peritectic region, to the left of point D, but should
solidify substantially as γ. The 0.20% carbon steels lie between
C and D and should undergo δ to γ transformation during solidi-
fication. None of the alloys chosen lies between B and C.
The positions of B, C and D will probably be shifted in the
presence of other impurity elements, nitrogen in particular
which is a strong austenite former. Therefore the phase
relationships just described for the three carbon levels could
change to some extent.

The limitations of the approach employed for δ to γ
transformation also apply to the equations used to
calculate the liquidus temperatures during solidification.
Any further modifications made to the model with
respect to the phase relationships during solidification
should also apply to these equations. However, at this
stage of the work, emphasis has been placed more on applying
the model in its present form to results from laboratory
and plant work than to experimenting with the various
theoretical data. It is however appreciated that at some later
stage it may be necessary to alter, and possibly add to, the
theoretical data fed into the programme as more information
becomes available. In particular a study of solidification

through the peritectic reaction warrants detailed study.

6.2 Implication of the Theory

In spite of limitations in the theoretical approach, the gas pressures calculated for ingots of porous/solid borderline composition have been shown to agree quite well over a fairly wide range of carbon contents, see figs. 31-35. The present work has highlighted the varying roles that CO, H_2 and N_2 can play in the formation of blowholes in steel ingots. When the state of oxidation is high in the steel, then only small amounts of hydrogen and nitrogen are required to produce blowholes and the contribution of P_{CO} to the total gas pressure, P_{Total}, is large. However, as the amount of deoxidants in the steel is increased, and P_{CO} decreases, blowholes can still occur when the hydrogen and/or nitrogen levels are high enough and P_{H_2} and P_{N_2} make the major contribution to P_{Total}. This was demonstrated in Table XVI.

It is the object of this section of the discussion to describe ways in which the results can be applied usefully in practice to compositions other than were examined in the present work, but within similar limits of carbon, manganese, silicon, hydrogen and nitrogen.

6.2.1 Prediction of Porous/Solid Borderlines in Practice

It was shown in section 5, when considering the total gas pressures, P_{Total}, developed during solidification of steels of porous/solid borderline composition, that P_{Total} (90% solidified) provided a suitable criterion for measuring the tendency of blowholes to form in an ingot.

There were two reasons for this:-

(i) P_{Total} approached or exceeded one atmosphere pressure at this stage of solidification. (Metallographic examination showed that blowholes probably form under atmospheric conditions when ferrostatic pressure is very low.)

(ii) There seemed to be closest agreement between the P_{Total} curves for the various porous/solid borderline compositions during the later stages of solidification (i.e. at about 90% solidified).

Point (ii) arose from the assumption that blowhole nucleation, and hence the porous/solid borderline, should occur at a certain pressure or within a discrete pressure range. In addition, a particular type of blowhole structure should be produced by a given total gas content in the steel.

The criterion of P_{Total} (90%) is equivalent to the term, O_C, used by Scimar and Nilles[33] to describe the amount of carbon monoxide produced in steels, and can be used in a similar way to predict ranges of composition which will be solid, gassy, or porous/solid borderline. P_{Total} (90%) should, however, be more versatile than O_C since it takes into account, not only CO, but also H_2 and N_2.

For the free cutting steels, P_{Total} (90%) for the various porous/solid borderline compositions fell within the range 1.20 to 1.45 atmospheres, irrespective of the carbon, hydrogen and silicon levels of the steel (constant manganese and nitrogen). Thus, this discrete pressure range was used to predict porous/solid borderlines in steels of other compositions than those examined in the present work. This was done by feeding a whole complex of compositions into the computer and calculating P_{Total} at 90% solidified for each composition.

When analysing the results it was convenient to choose particular carbon, hydrogen and nitrogen levels and consider variations in manganese and silicon. It was then possible to construct porosity charts such as those shown in fig. 38. Values of P_{Total} (90%) were plotted for each manganese and silicon combination and then isobars drawn for the appropriate porous/solid borderline pressures. This gives composition ranges in which solid, gassy or borderline ingots will be obtained. In fig. 38, the charts show the effect of increasing the hydrogen content of the steel from 4 to 8 ppm at constant carbon (0.1%) and nitrogen (0.004%) levels. As the hydrogen increases more silicon and manganese are required to ensure freedom from porosity. It is also evident that the width of the porous/solid borderline range increases as the manganese content decreases, and the hydrogen content increases. In fact at hydrogen levels such as 8 ppm it would be very difficult to ensure freedom from porosity in 0.1% carbon FCS, no matter how high the silicon and manganese.

By considering various permutations of the carbon, hydrogen and nitrogen contents of the steel, a whole series of charts such as those shown in fig. 38 can be constructed.

For the plain carbon steels it was found that practically all values of P_{Total} (90%), for the various steels considered, fell within the range 0.9 to 1.25 atmospheres. These are lower pressures than were obtained for the free cutting steels and again demonstrate the 'killing' effect of sulphur in steels.

While the width of the range 0.9 to 1.25 atmospheres for

plain carbon steels is similar to that obtained for the free

cutting steels, it was found that it could be sub-divided

into smaller discrete pressure ranges for particular steels.

In considering the 0.1 and 0.48% carbon steels there seemed

to be no effect of carbon content on the value of P_{Total}

(90%). However P_{Total} (90%) increased as the nitrogen

content,needed to promote porosity,increased. For low

nitrogen ($\leqslant$0.013/0.014% nitrogen) levels the range of P_{Total}

(90%) was 0.9 to 1.1 atmospheres irrespective of the hydrogen

content. For nitrogen levels above 0.013/0.014%, the critical

pressure range was 1.1 to 1.25 atmospheres. It may be

significant that the low nitrogen levels also corresponded

to low silicon levels. It was shown in Table XIV that part

of the analysed silicon could be tied up as silicates, and

therefore be ineffective as a deoxidant. Mostly, the amount

of silicon combined in this way was very small, but it is

shown in section A.2 of the Appendix that below about 0.03%

silicon, small changes in the silicon actively deoxidising,

can lead to fairly large increases in P_{CO}. Allowing for combined

silicon in this way could bring the pressures in the low nitrogen-

low silicon steels more into line with the high nitrogen-high

silicon steels, where a small amount of combined silicon would

make little difference to the calculated pressure.

However, allowing for such adjustments in P_{Total} (90%)

would not account for the differences in pressure observed

between high silicon-high hydrogen and high silicon-high

nitrogen steels shown in fig. 33. Experimental errors and

the wrong choice of data might account for these differences,

but on the other hand, the effect might be real, and due to kinetic factors, since the diffusivity of nitrogen is reported as being lower by 1-2 orders of magnitude lower than that of hydrogen[56-60]. A lower diffusivity should restrict the supply of gas atoms to the gas bubble nucleus and, in so doing, possibly affect the porous/solid borderline. At the moment, however, this is still supposition.

P_{Total} (90%) for the 0.2% carbon steels for the most part fell within a discrete range (1.1 to 1.2 atmospheres) and showed little trend with varying hydrogen, consistent with the above results. However, the pressures obtained were similar to those for the high nitrogen versions of the 0.1 and 0.45% carbon steels, and in this respect were inconsistent with the pressures obtained for the low-nitrogen versions of these steels.

In the case of the 0.1% carbon steels, the computed carbon concentration did not build up sufficiently for the δ to γ change to occur, while in the 0.45% carbon steels, the phase change occurred almost immediately solidification had begun. Thus, in both cases, solidification occurred substantially to a single phase. However in the 0.2% carbon steels, the δ to γ change occurred during the solidification process, at about 70% solidified. It is possible that the that the simple treatment of the phase change, discussed in 6.1.2 accounted for the above pressure discrepancies. It must be emphasised that, if no allowance had been made for the phase change, the pressures in the 0.2% carbon steels would have been much higher and the disagreement in results more marked.

At this stage of the work, no further attempt has been made to modify the model to try and remove these slight anomalies. Instead, when attempting to predict porous/solid compositions for plain carbon steels, different pressure ranges for P_{Total} (90%) are specified for low and high nitrogen steels. For low nitrogen steels ($\leq 0.013/0.014$), a pressure range of 0.9 to 1.1 atmospheres is specified, while for high nitrogen steels ($> 0.013/0.014$), 1.1 to 1.25 atmospheres are specified. Porosity charts were drawn in exactly the same way as for the free cutting steels and examples are given in fig. 39, for 0.1 and 0.5% carbon and 0.004 and 0.016% nitrogen for a constant hydrogen level of 3.0 ppm. Here it is seen that the composition ranges of porous/solid borderline ingots increase with increasing carbon and nitrogen levels, and decreasing manganese. The results are compared with those of Scimar and Nilles[33] for plain carbon balanced steels. It is evident that, at low levels of hydrogen and nitrogen, agreement between the two sets of results is good. However, when larger quantities of hydrogen and nitrogen are taken into account, the present results differ markedly from those of Scimar and Nilles, who did not allow for these two gases. Oeters et al[43,44] did, later, account for hydrogen and nitrogen, but their model for these gases was not explained in any detail, and it is difficult to obtain a direct comparison with the results from the present work.

While steps can be taken, on the basis of the present results, to control the gas contents of the steel in the ladle, to ensure freedom from porosity, gas pick up during teeming

may still cause trouble. For instance, gas pick-up may
occur from moist runnerware during uphill teeming, or from
mould coatings containing excessive amounts of hydrogen.
Oxidised splash particles on the mould wall may lead to localised
high concentrations of oxygen in the liquid steel, and cause a
CO reaction to occur, if the deoxidants present in the steel
are insufficient to combine with the extra oxygen.

6.2.2 Application to Balanced Steel Production

The work of Scimar and Milles and Octers et al refers
particularly to the production of balanced steels. Results
from the present study have also been applied to this
problem. In trying to predict compositions for balanced
steels a slightly different approach was used to that
outlined in 6.2.1 of establishing porous/solid borderlines.
The final results, however, have proved to be very similar.

Experimental ingots of the type shown in fig. 19(b)
have a blowhole structure which just compensates for shrinkage
cavity, to produce a flat or convex ingot top surface.
These ingots may be regarded as "balanced" and it was decided
that this type of structure in an experimental ingot
probably corresponded to a properly ladle balanced ingot on
a tonnage scale.(A ladle balanced ingot is regarded as
one in which, as a result of correct deoxidation in the
ladle by silicon and manganese, the blowholes just
compensate for shrinkage to produce a flat or convex top
surface). It does not seem unreasonable to make this
comparison, since on both scales, blowholes should originate
first of all near to a chill mould surface where freezing

rates and dendritic spacings will be very similar.

The value of P_{Total} (90%) was calculated for a large
number of experimental plain carbon steel ingots which
exhibited a blowhole structure similar to that shown in
fig. 19(b). The results applied mainly to the low nitrogen
group of steels (≤0.013/0.014% nitrogen) and gave an average
value of 1.02 atmospheres with a standard deviation of 0.145
atmospheres. Strictly, P_{Total} (90%) should have been
calculated for all the experimental ingots whether piped,
balanced or gassy, since it was obvious from the experiments
that, occasionally, ingots having undesirable structures
(i.e. piped or gassy) could be obtained having values of
P_{Total} (90%) close to 1.02 atmospheres. In this way some
idea of the proportions of ingots which would not be balanced
within the specified ranges could then be obtained. However,
the excessive demands of this approach on the computer and
the urgency of works trials at the time necessitated a more
expedient approach. This was to assume that, provided P_{Total}
(90%) was within $\pm$ one standard deviation of the mean
(i.e. 1.02 $\pm$ 0.145 atmospheres on low nitrogen steels), there
would be reasonable certainty of producing an acceptable
ladle balanced ingot.

Preliminary pilot plant trials on $3\frac{1}{2}$ ton ingots indicated
that this approach was reasonable and a balanced ingot obtained
from these trials is shown in fig. 40, together with the
steel analysis and calculated P_{Total} (90%). Subsequently,
extensive plant trials on 15 ton ingots, at a plant within
the BSC Midland Group, have confirmed the validity of this
approach. Fig. 41 shows how a series of production casts

fit in with the theoretical predictions. The shaded area shows the predicted composition range for balanced steels of 0.2/0.25% carbon, 0.004% nitrogen and 5 ppm hydrogen (The effect of carbon on P_{Total} (90%) has proved negligible within the specification range). The production casts fell within the composition range 0.2/0.25% carbon, 0.0035/0.0045% nitrogen and 4.5/5.5 ppm hydrogen, except for the cast of gassy ingots shown at 0.075% silicon; 0.54% manganese. This had an above average hydrogen content of 6.2 ppm and was outside the specified manganese range.

It would appear, from fig. 41, that the above approach has provided a reasonable basis for establishing analysis ranges for the production of balanced steels, although, perhaps slight changes in composition range may be found necessary as more production data is accumulated.

The results of Scimar and Nilles[33] are also included in fig. 41. Here it is seen that by ignoring the hydrogen and nitrogen in the steel, their approach could lead to gassy ingots being produced. Their predictions should apply more successfully to steelmaking practices in which both hydrogen and nitrogen are very low (say 3 ppm and 0.004% respectively), for instance the LD practice. The model is, however, much less versatile than the one used in the present work, which should be applicable to most steelmaking practices.

Ceters et al.[43,44] reported an effect of ingot size on the degree of deoxidation required to ladle balance steels of low carbon content. The effect virtually disappeared above 0.1% carbon. The present work has indicated good agreement, in terms of blowhole structure, between small

laboratory melts and commercial ingots of up to 15 tons.
It should, however, be noted that most of the present work
has been on plain carbon steels of greater than 0.1% carbon.
Nevertheless, it can be argued that ingot size should have
little or no effect on the formation of sub-surface blowholes,
since these are formed almost instantaneously when the liquid
comes into contact with the mould surface. In the first few
millimetres of ingot skin development, there can be little
difference in the solidification rate over a wide range of
ingot sizes. Since blowholes of the type found in ladle
balanced ingots form in this region, ingot size should not
be a significant factor in their formation.

It will be recalled that the original basis for choosing
P_{Total} (90%) was partly on the assumption that a value of
at least one atmosphere would be necessary to enable blowholes
to form. It has subsequently been found that P_{Total} (90%)
could be below one atmosphere for a balanced steel. It could
be argued that blowholes can form at less than one atmosphere
pressure once the ingot top has frozen over and shrinkage
has reduced the pressure of the system.

6.2.3 Blowhole Nucleation and Growth

Equation (18) gave the conditions for a stable gas
bubble in a liquid melt:-

$$P_{Total} \geqslant P_A + P_F + \frac{2\sigma}{r} \quad .. \quad .. \quad .. \quad .. \quad .. \quad .. \quad (18)$$

where all the above terms have been defined previously in
section 2.5. Examination of blowholes during the present work
indicated that they formed very close (within 0.06 mm) to
the ingot surface, and in a very short time after the liquid
metal had come into contact with the chill cast iron mould.

Hence it is assumed that atmospheric conditions exist (i.e. P_A = 1 atmosphere) at the time of blowhole nucleation and that P_F, the ferrostatic pressure can be neglected in the very early stages of blowhole growth to macroscopic dimensions. Hence the above condition can be re-written:-

$$P_{Total} \geqslant 1 + \frac{2\sigma}{r} \qquad \cdots \quad \cdots \quad \cdots \quad \cdots \quad \cdots \quad \cdots \quad ..18(a)$$

Pressure curves in figs. 31-35 indicate that, in ingots of porous/solid borderline composition i.e. in which the conditions for blowhole nucleation and growth have just been satisfied, values of P_{Total} are in the region of 1 atmosphere, and that consequently the term $\frac{2\sigma}{r}$ must be very small.

It has been assumed so far that solute build-up and the consequential blowhole formation during solidification occur within discrete interdendritic spaces at the solid/liquid interface. This being so, it has also been assumed that the spacing of dendrites, between which the solutes are concentrating, controls the size of the initial stable blowhole nucleus. While it has been difficult to obtain an accurate measure of the very fine dendrite spacing at the ingot surface the value is certainly less than 0.05 mm, which was measured at about 10 mm in from the surface.

Since a cap-type nucleus is unlikely to be obtained[1], the nucleus is assumed to be near spherical with a radius of curvature, r, equal to ½ the dendrite spacing. As the liquid in the interdendritic space solidifies, dendrite arms thicken and the maximum permissible value of r must correspondingly decrease. Hence, from equation (18), the pressure to maintain a bubble radius 0.025 mm in the solute rich liquid is 0.4

atmospheres. (This assumes that σ, the surface tension of the liquid has been reduced to 500 dynes/cm by the combined effects of enriched solute elements, sulphur in particular, present in steel[127]). The situation is represented schematically in fig. 42 in which the increase in $(1 + \frac{2\sigma}{r})$ atmospheres is compared with P_{Total} during solidification. It is obvious that P_{Total} never reaches sufficient dimensions to nucleate a blowhole under the set of assumptions made regarding solute enrichment and blowhole nucleation made earlier.

From fig. 30 it is obvious that blowholes can reach diameters greatly in excess of the dendrite spacings within about 0.1 mm of the surface. This suggests a situation soon after initial blowhole growth, represented schematically in fig. 36, in which solute enrichment between a number of dendrites has combined to produce the blowhole. The radius of curvature of the blowhole within a few mm of the surface shown in fig. 30(b) is estimated to be 1 mm giving a value of $\frac{2\sigma}{r}$ of $\frac{1}{100}$ atmosphere. For the blowhole shown in fig. 30(a) $\frac{2\sigma}{r} = \frac{1}{10}$ atmosphere. These results indicate that the values of P_{Total} obtained from the present work and substituted in the expression 18(a) are realistic in proportions and can be used to explain the occurrence of stable blowholes within a short distance from the surface. The results do not however account for nucleation and the initial period of growth prior to that shown in figs. 30 and 36 when bubble radii must be very small. For reasons mentioned in section 6.1.2, for high solute concentrations to be achieved at the solid/liquid interface or between dendrite arms, mixing in

the liquid must be diffusion controlled and "terminal transient" conditions must exist. However, it may be necessary to consider the presence of pre-existing bubble nuclei such as those suggested by Campbell[57]. It will be recalled from section 2.5 that Campbell suggested that exogeneous inclusions present in the steel might contain air pockets capable of providing stable nuclei to which gas atoms could diffuse to produce blowholes.

There is obviously much scope for studying factors leading to bubble nucleation and preliminary work has been carried out on a Stereoscan Instrument at Swinden Laboratories. This instrument probably provides the best means available at present for examining blowholes in detail.

There are a number of factors which can affect the growth and shape of a blowhole in ingots:-

(a) rate of advance of the solid/liquid interface

(b) quantity of gas being supplied per unit time to the blowhole

(c) liquid flow ahead to the solid/liquid interface

(d) external pressure being applied to the blowhole (i.e. atmospheric + ferrostatic)

In the present set of experiments the solidification rates in the small chill cast ingots were very much the same in all cases, and though for a particular ingot the solidification rate will obviously decrease from surface to centre, variation between ingots can be discounted. The experimental ingots were at maximum 15 in. high, and ferrostatic pressure effects have been neglected. The effects of the remaining variables on blowhole shape and distribution in the experimental ingots will be considered.

Various modes of blowhole growth were obtained within the series of experimental ingots examined, with a trend from the acicular type of blowhole to a more bulbous type as the carbon content of the steel increased. The effect is attributed to the higher initial total gas pressure P_{total}, (i.e. at nil % solidified, see figs. 31-35) in the higher carbon steels, which requires less driving force from solute enrichment, and hence gas pressure build up during solidification, to cause the critical pressure for bubble formation to be exceeded. It will be noted in fig. 31 that one atmosphere pressure tends to be exceeded at an earlier stage of solidification process in the 0.48% carbon steels than in the lower carbon steels. Thus for a given solidification rate and stage of interdendritic solidification bubble growth should progress further for the higher carbon steels. Hence the more bulbous growth.

The above development in blowhole structure applies to the stage reached in fig. 16(c), described by Hultgren and Phragmen[2]. There are other factors to be examined when considering subsequent growth. The primary solidification phase in the higher carbon steels is γ while in lower carbon steels it is δ. Reference to the distribution coefficients of the various solute elements between liquid iron and solid δ and γ shows that there is more solute rejection from δ. Thus it is reasonable to assume that, once blowholes have formed in the low carbon steels solidifying to δ, the rate of gas supply to blowholes should be faster than in the steels solidifying to γ, given the same amounts of potential gas forming elements. Hence a fairly rapid rate

of blowhole growth followed by bubble detachment should
lead to the conditions described in fig. 16 d2 to g2 in steels
solidifying to δ. This is in fact demonstrated by figs. 27
and 29(a) and (b) from the present work which show wormhole
type blowholes. A slower rate of blowhole growth and less
severe bubble detachment process in steels solidifying to γ
results in the condition described in fig. 16 d1, e1 and
g1 and demonstrated by blowholes in fig. 28 and 29(c)-(e).

It is anticipated that elements such as sulphur should
affect blowhole growth in some way since they have been shown[61,62]
to affect the flow of gas atoms across gas/liquid interfaces.
In the case of sulphur which slows down nitrogen transfer,
the effect reaches a maximum at 0.3%[61], above which it
seems to have no further effect. Sulphur concentrates to
approximately 20x its original amount during solidification
(the distribution coefficient, k, of sulphur is reputedly[67]
0.05) and, presumably, surrounds the surface of the blowhole.
Hence it is unlikely that increasing the initial concentrations
of sulphur above about 0.015% will have much effect on the
transfer of gas atoms to blowholes during solidification.
In fact increasing sulphur was not found to have a noticable
effect on blowhole size and shape in the experimental
steels.

The diffusion rate of nitrogen atoms in liquid steel is,
as mentioned earlier, reputedly 1-2 orders of magnitude
slower than that of hydrogen[58-60]. Thus it might be
anticipated that blowhole growth would exhibit different
features in high nitrogen steels to those in high hydrogen
steels. There is also the possiblity however, in critical

cases, that the γ-forming properties of nitrogen may affect the solidifying phases and in this way change blowhole characteristics. These affects have not been apparent in practice, although higher porous/solid borderline pressures were observed in the higher nitrogen steels as mentioned in 6.2.2.

Once the experimental ingot top solidifies then a back pressure sets up and blowhole growth is curtailed. This is demonstrated in fig. 29(c)-(e). The same situation would probably not arise on tonnage ingots since, on this scale, ferrostatic pressure tends to influence blowhole growth before the ingot top solidifies. The effect of ferrostatic pressure is to curtail blowhole growth and will be greater in the lower regions of the ingots. Therefore an increase in the length of blowholes is obtained from the bottom to the top of the ingot. This effect is well known in practice.

7. SUMMARY AND CONCLUSIONS

Modifications have been made to a model, devised by Turkdogan[46], which, by computation of suitable thermodynamic and segregation data, permits the calculation of gas partial pressures (P_{CO}, P_{H_2} and P_{N_2}) within an interdendritic volume of completely mixed liquid steel during solidification. In order that the model could be applied to a wider range of compositions than had been considered in the original work, the following factors were taken into account:

(i) Interaction effects between solute elements.

(ii) Changes in primary phase from δ-to γ-iron during solidification, as the interdendritic liquid becomes more impure.

(iii) Changes in liquidus temperature (and hence the temperature at which thermodynamic reactions were assumed to occur) during the solidification process.

It has been shown that these factors can have a large effect on the computed gas pressures, particularly in the higher carbon steels considered (0.2 and 0.5%). The effect on pressure is less pronounced when the modifications are applied to lower carbon levels (0.1%), similar to those originally considered.

The modified model has been used to compute gas pressures in plain carbon and resulphurised steels, all of porous/solid borderline composition, (i.e. composition at which blowholes first appear in the steels), but containing various amounts of the gas forming elements, carbon, oxygen, hydrogen and nitrogen

which were specifically varied. The porosity borderlines were established experimentally and deoxidation was carried out with manganese and silicon.

The varying contributions made by P_{CO}, P_{H_2} and P_{N_2} to the total gas pressure, P_{Total}, both in partially and heavily deoxidised steels of porous/solid borderline composition, have been demonstrated. In particular the detrimental effects of high hydrogen and/or nitrogen contents on ingot soundness, even in heavily deoxidised steels, have been highlighted.

Examination of the computed values of P_{Total} in the experimental porous/solid borderline steels indicated that suitable criteria for predicting borderline compositions, in a wide range of carbon steels, could be obtained by considering discrete P_{Total} ranges near the end of the solidification process in the interdendritic volume of liquid. (90% solidified was chosen as being most suitable). Examples of predicted compositions have been given.

The results have been applied to the problem of ladle balance steel production. Predicted compositions from the theoretical and experimental work have been shown to apply extremely well in steelplant practice to ingots of up to 15 ton.

The predictions have been compared with those from other workers, who employed different solidification models, centred around theories dealing mainly with the CO reaction. Extremely good agreement was obtained when comparing their results with the predictions obtained, from the present work, for low hydrogen ($\sim$3 ppm) and nitrogen ($\sim$0.004%) steels. However when larger amounts of these two gases were present in the steel, predictions differed markedly. The model used in the present

work is therefore considered more versatile than the other models.

An attempt has been made to apply the model to the phenomenon of nucleation of sub-surface blowholes and their subsequent growth characteristics. It would appear that the gas pressures developed, as a result of solute enrichment during solidification, are alone, insufficient to nucleate blowholes at the solid/liquid interface. Alternative means of nucleation are considered. The calculated pressures do, however, appear to satisfactorily explain the radius of blowholes a short distance ($\sim$1mm) away from the ingot surface. Also growth characteristics of blowholes in steels of ranging carbon content are accounted for.

Limitations to the theory, remaining in spite of the modifications, have been discussed. In particular those relating to assumptions of equilibrium, the solidification model employed, and the choice of data have been detailed.

R E F E R E N C E S

1.	B. Chalmers	'Principles of Solidification', John Wiley & Sons, 1964, Chapter 6.
2.	A. Hultgren and G. Phragmen	Trans. AIME, 1939, 135, pp. 133-239
3.	F. C. G. Muller	Ber. Deut. Chem. Gesell, 1879, 12, p.93
4.	P. Klinger	Stahl und Eisen, 1925, 45, p.835
5.	L. F. Reinartz	Trans. AIME, 1926, 73, p.1036
6.	F. B. McKune	Ibid, 1929, 84, p.255
7.	E. Ameen and H. Willners	Jernkont. Annaler, 1928, p. 195
8.	J. Chipman and A. M. Samarin	Trans. AIME, 1937, 125, p.331
9.	A. Hayes and J. Chipman	Ibid, 1939, 135, p.85-125
10.	L. B. Kosterev and G. I. Oiks	Izvest. VUZ Chern. Met., 1960, (11), p.50
11.	T. Swinden and W. W. Stevenson	ISI Seventh Report in the Heterogeneity of Steel Ingots, 1935, p.137
12.	K. C. Barraclough	Murex Review, 1954, 1, (13), p.305
13.	T. B. King	Proc. Electric Furnace Steel Conf., AIME, 1956, p.159
14.	H. Epstein et al	J. Metals, 1957, p.597-608
15.	G. R. Adams et al	Proc. Electric Furnace Steel Conf., AIME, 1957, pp.17-20
16.	F. C. Langenberg and M. J. Day	Ibid, pp. 7-16
17.	J. Turton	BSCRA Annual Conf., 1964, Paper 6,
18.	S. Bergh and A. Josefsson	JISI 1964, 202, pp. 356-366
19.	J. Turton	Brit. Foundryman 1967, 40, pp. 23-32
20.	T. Saito et al	Tetsu-to-Hagane, 1967, 53, (7), pp. 812-814
21.	R. Kupfer et al	Geisserei, 1967, 19, (4), pp. 203-705

22.	B. Lux	Ibid, pp. 197-202
23.	B. R. Nijhawan et al	JISI 1967, 205, p.292
24.	E. L. Morgan	JISI 1968, 206, pp. 39-46
25.	H. Kohl	BHM 1968, (11) p.377
26.	G. M. Gill	BSCRA Annual Conf., 1964, paper 5
27.	Data collected by author from work carried out within BSC Midland Group	
28.	J. Hewitt	ISI Special Report No. 73, 1962, p.15
29.	V. Parma and St. Wildmann	HUTNIK (Prague) 1967, 17, pp. 432-435
30.	K. A. Johnston et al	J. Aust. Inst. Metals, 1966, 11, (3), pp. 204-212
31.	M. Tenenbaum	Metals Technology, 1947, 14, No. 6
32.	R. Wogin and A. Goodall	JISI, 1952, 171, p.154
33.	R. Scimar and P. Nilles	CNRM Report No. 11, 1967, p.17
34.	G. Bauer et al	Stahl und Eisen, 1967, 87, p.1435
35.	W. A. Tiller et al	Acta Met., 1953, 1, p.428
36.	E. Scheil	Z. Metallk., 1942, 34, p.70
37.	W. G. Pfann	J. Metals, 1952, 4, p.747
38.	J. A. Burton et al	J. Chem. Phys. 1953, 21, p.1991
39.	H. D. Brody and M. C. Flemings	Trans. AIME, 1966, 236, p.615
40.	P. Nilles	JISI, 1964, 202, p.601
41.	P. Nilles et al	Stahl und Eisen, 1965, 85, p.1025
42.	Masui et al	Trans. I.S.I.J., 1968, 8, p.195
43.	F. Oeters et al	ISI Conference 'Mathematical Models in Metallurgical Process Development', 1969. Proceedings to be published.
44.	F. Oeters et al	Archiv. Eisen., 1969, 40, p.603

45.	H. Knuppel and F. Eberhard	Archiv. Eisen, 1963, 34, p.325
46.	E. T. Turkdogan	Trans. A.I.M.E, 1965, 233, p.2100
47.	M. C. Flemings	Mod. Castings, 1964, 46, p.353
48.	E. T. Turkdogan	J. Metals, 1967, (1), p.38
49.	J. Pribyl	Geisserei, 1965, 52, p.813
50.	J. E. Seastone	A.I.M.E, O.H, Proc, 1964, p.458
51.	W. Volker	Stahl und Eisen, 1968, 88, p.1455
52.	J. Dieudonne	Private Communication.
53.	M. Ward and R. Widdowson	J.I.S.I, 1965, 203, p.486
54.	F. Korber and W. Oelsen	Mitt. K.-Wilh. Inst. Eisenforsch 1935, 17, p.39
55.	R. G. Ward	'The Physical Chemistry of Iron and Steelmaking', Arnold, 1962, Chapter 9.
56.	D. P. Woodruff	Metals and Materials, 1969, May, p.171
57.	J. Campbell	I.S.I. Publication 110, Proceedings of Conference 'The Solidification of Metals' 1968, p.18
58.	N. M. El-Tayeb and N. A. D. Parlee	Trans. A.I.M.E, 1967, 239, p.2010
59.	N. M. El-Tayeb and N. A. D. Parlee	ibid. 1967, 239, p.1345
60.	K. Schwerdtfeger	ibid. 1967, 239, p.134
61.	R. D. Pehlke and J. F. Elliott	ibid. 1963, 227, p.844
62.	P. Kozakevitch and G. Urbain	Mem. Sci. Rev. Met. 1963, 60 p.143
63.	E. E. Clark	I.S.I.P. 107 'Optimisation of Steel Product Field', 1967, p.36
64.	D. Binnie	J.I.S.I. 1949, 163, p.159
65.	H. Morikawa et al	Trans. I.S.I.J. 1966, 6, p.18

66. Hultgren et al | J. Metals, 1951, 3, p.101

67. J. Chipman | 'Basic O.H. Steelmaking', Ed. Philbrook & Mever, A.I.M.E, New York, 1951, p.621

68. F. D. Richardson and W. E. Dennis | Trans. Farad. Soc. 1953, 49, p.171

69. H. Schenck and H. Hinze | Archiv. Eisen, 1966, 37, p.545

70. E. T. Turkdogan et al | J.I.S.I. 1955, 181, p.123

71. E. T. Turkdogan et al | Acta. Met. 1956, 4, p.396

72. A. Rist and J. Chipman | Rev. Met. 1957, 53, p.796

73. T. Fuwa and J. Chipman | Trans. A.I.M.E. 1960, 218, p.887

74. S. Banya and S. Matoba | Tetsu-to-Hagane, 1958, 44, p.643

75. J. Chipman | J.I.S.I. 1955, 181, p.97

76. H. Schenck and G. H. Gordon | Archiv. Eisen, 1959, 30, p.451

77. H. Ohtani and N. A. Gokcen | Trans. A.I.M.E. 1960, 218, p.534

78. T. P. Floridis and J. Chipman | ibid. 1958, 212, p.549

79. J. F. Elliott | Proceedings of Conference "The Physical Chemistry of Iron and Steelmaking", Massachusetts, 1956, p.37

80. H. Schenck et al | Archiv. Eisen, 1968, 39, p.69

81. J. Pearson and E. T. Turkdogan | J.I.S.I. 1954, 176, p.19

82. D. V. Linchivskii and A. M. Samarin | Izv. Ak. Nauk. Otd. Tekn. 1957, 2, p.9

83. S. Matoba et al | Tetsu-to-Hagane, 1959, 45, p.1328

84. J. Chipman and T.C.M. Pillay | Trans. A.I.M.E, 1961, 221, p.1277

85. M. T. Kurochkin et al | Izv. Akd. Nauk. Otd. Tekn. 1957, 2, p.19 (Brutcher 4031)

86. S. Maekawa and Y. Nakagawa | Reports I & II, Japanese Steel Works Ltd., March 1961 (This reference obtained from ref. 87)

87. M. Weinstein and J. F. Elliott	Trans. A.I.M.E. 1963, 227, p.302
88. T. Bagshaw et al	J.I.S.I. 1965, 203, p.60
89. H. Laing et al	Trans. A.I.M.E. 1946, 167, p.395
90. D. W. Gomersall et al	ibid. 1968, 242, p.1309
91. H. Schenck et al	Archiv Eisen, 1959, 30, p.533
92. T. Kootz	ibid. 1941, 15, p.77
93. T. Saito	Sci. Reps. Res. Inst. Tohoku University, 1950, 2, No.6, p.909
94. S. Maekawa and Y. Nakagawa	Tetsu-to-Hagane, 1959, 45, p.255
95. R. D. Pehlke and J. F. Elliott	Trans. A.I.M.E. 1960, 218, p.1088
96. R. A. Dodd and N. A. Gokcen	ibid. 1961, 221, p.233
97. S. Z. Beer	ibid. 1961, 211, p.2
98. H. Wentrup and O. Rief	Archiv. Eisen, 1949, 20, p.359
99. T. Saito	Sci. Reps. Res. Inst. Tohoku University, 1949, 1, Series A. p.419
100. J. C. Vaughan and J. Chipman	Trans. A.I.M.E. 1940, 140 p.224
101. J. Chipman and D. A. Corrigan	ibid. 1965, 233, p.1249
102. United States Steel	"The Making, Shaping and Treating of Steel" 8th Edition, 1964, p.289
103. B. E. Lindblom	Jernkont. Ann. 1968, 152, p.53
104. M. Hansen	'Constitution of Binary Alloys' 2nd Ed. 1958.
105. W.A. Tiller	"Liquid Metals and Solidification" A.S.M. Seminar, 1958, p.276
106. C. J. Smithells	Metals Reference Book, 1955, 2nd Ed. Vol. I.
107.	A.S.M. Metals Handbook, 1948 Ed.
108. W. A. Fischer et al	Archiv. Eisen, 1960, 31, p.365

109. J. Geller and T. Sun   ibid. 1950, 21, p.423

110. L. S. Darken and
    R. W. Gurry   "Physical Chemistry of Metals"
                      1953, McGraw Hill Publ.

111. P. Grievson and
    E. T. Turkdogan   Trans. A.I.M.E. 1954, 230,
                      p.1604

112. F. Wever et al   Stahl und Eisen, 1954, 74,
                      p.1521

113. M. T. Hepworth et al   Trans. A.I.M.E. 1966, 236, p.1278

114. J. H. Swisher and
    E. T. Turkdogan   ibid. 1967, 239, p.426

115. S. Tankis and N. A. Gokcen   ibid. 1961, 221, p.843

116. C. R. Taylor and
    J. Chipman   ibid. 1943, 154, p.228

117. M. Wahlster and H. Brocker   Technische Mitteilungen Krupp 3,
                      1962, 20, p.73

118. F. D. Richardson and
    J. H. E. Jeffes   J.I.S.I. 1948, 160, p.261

119. R. L. Cain   A.I.M.E. O.H. Proc. 1937, 20, p.104

120.   I.S.I. 2nd Report on Heterogeneity,
                      1928, 1, p.477

121. E. C. Bitzer   Blast Furnace and Steelplant,
                      1931, 19, p.249

122. G. L. Darnforth   ibid. 1936, 24, p.781

123. C. A. Muller et al   Archiv Eisen, 1966, 37, p.27

124. R. B. Yeo   J. Metals, 1967, 19, p.23

125. D. R. Poirier et al   M.I.T. AF33(615)-1030, 1964

126. R. D. Doherty and
    D. A. Melford   J.I.S.I. 1966, 204, p.1131

127. W. D. Kingery   "Physical Chemistry of Steelmaking"
                      Conf. Proc., Mass., U.S.A., 1956, p.33

TABLE I

Approximate Hydrogen Contents in Liquid Steel expected to produce porosity and wildness in fully killed Basic Arc Steel (After Barraclough[12])

Type of Steel	Hydrogen content, ml/100g		
	Sound Ingots	Porous Ingots	Wild Ingots
Carbon steel	Up to 6.5	6.5 - 8.5	Over 8.5
Low-alloy steel	Up to 7.0	7.0 - 9.0	Over 9.0
Chromium stainless	Up to 10.0	10.0 - 12.0	Over 12.0
Austenitic steel	Up to 12.0	12.0 - 14.0	Over 14.0

TABLE II

Nitrogen Contents of Commercial Low-Alloy Steels

Steelmaking Practice	N_2 content % *
Basic Open Hearth	0.005 - 0.007
Ajax	0.004**
Basic Side Blown Converter	0.003 - 0.006
Basic Bessemer Air Blown	0.011 - 0.016
Basic Bessemer Enriched Air	0.0063 - 0.007
Basic Bessemer $O_2 + H_2O$	0.0035 - 0.005
Basic Bessemer $O_2 + CO_2$	0.0035
Basic Electric	0.007
L.D.	0.0065***
O.L.P. (Oxygen lime powder)	0.0015
Acid Open Hearth	0.005 - 0.006
Acid Bessemer	0.01 - 0.02
Acid Side Blown	0.003 - 0.009
Acid Electric	0.008 - 0.010

* Results compiled by Gill (reference[26]) unless indicated otherwise.

** Results obtained during works trials by the present author (27)

*** Evidence obtained by the present author, suggests this value should be nearer 0.003/0.004%

TABLE III

Hydrogen Contents of Commercial Low-Alloy Steels

Steelmaking Practice	Average H$_2$ at tap ppm
Basic Open Hearth	5.0*
Ajax	4.8**
Acid Open Hearth	3.5*
Basic Electric	4.9*
Acid Electric	2.0*
Basic Bessemer	6.5*
Acid Bessemer	3.5**

* Information compiled by Gill (reference[26])

** Results obtained from works trials during the present investigation (27)

Table IV

Interaction coefficients e_C^X at 1600°C

Solute, X	Ref.	e_C^X	Selected Value
Carbon	67	+0.10	+0.22
	68	+0.19	
	69, 70	+0.22	
	71, 72	+0.23	
Oxygen	73	-0.10	-0.31
	74	-0.24	
	75	-0.31	
	69	-0.34	
	71	-0.36	
Manganese	75	-0.002	-0.012
	69	-0.012	
Silicon	76	+0.055	+0.07
	75	+0.088	

Table V

Interaction Coefficients, e_0^X, at 1600°C

Solute, X	Ref.	e_0^X	Selected Values
Oxygen	77	0 to -0.05	-0.20
	78	-0.20	
Carbon	73	-0.13	-0.41
	74	-0.32	
	79	-0.40	
	75	-0.41	
	80	-0.44	
	69	-0.46	
	70	-0.49	
Manganese	75, 81	0	-0.021
	82	-0.036 to +0.009	
	69	-0.021	
Silicon	75	-0.02	-0.16
	76	-0.087	
	83	-0.137	
	84	-0.16	
	81	-0.87	

Table VI

Interaction Coefficients, e_H^X, at 1600°C

Solute, X	Ref.	e_H^X	Selected Value
Carbon	85	+0.045	+0.060
	86	+0.050	
	87	+0.060	
	88	+0.072	
Manganese	87	−0.0014	−0.0014
	77	−0.020	
	86	+0.047	
Silicon	88	+0.022	+0.027
	89	+0.027	
	86	+0.038	

Table VII

Interaction Coefficients, e_N^X, at 1600°C

Solute, X	Ref.	e_N^X	Selected Values
Carbon	90	+0.103	
	91	+0.125	
	92	+0.130	+0.130
	93, 94	+0.135	
	95	+0.250	
Manganese	77	0	
	96	−0.013	
	95, 94	−0.020	−0.023
	97	−0.023	
	98	−0.025	
	99	−0.094	
Silicon	100	+0.032	
	95	+0.047	+0.047
	94	+0.048	
	91	+0.065	

Table VIII

Distribution Coefficients of Carbon,

Manganese and Silicon between Liquid and

Solid iron

Solute, X	Ref.	k_X^δ	Selected k_X^δ	Ref.	k_X^γ	Selected k_X^γ
Carbon	103	0.06				
	75, 9	0.13		67	0.36	0.36
	46,33,104	0.20	0.20			
	105(106,107)	0.25				
	108	0.29				
Manganese	105(106,107)	0.15		104	0.86	
	46	0.68	0.68	67	0.95	0.95
	103	0.73				
	75, 9	0.84				
	33	0.90				
Silicon	46	0.60	0.60	67	0.50	0.50
	103	0.64				
	75, 9	0.66				
	105(106,107)	0.70				
	33	0.83				

( ) numbers inside the brackets refer to
original references mentioned by
another author who is given the
reference number preceding the bracket

Table IX

Distribution Coefficients of Hydrogen, Nitrogen and Oxygen between Liquid and Solid iron

Solute, X	Ref.	k_X^δ	Selected k_X^δ	Ref.	k_X^γ	Selected k_X^γ
Hydrogen	46(109)	0.27	0.27		0.37	
	67	0.32		67	0.45	0.45
Nitrogen	67	0.28		55(95,110)	0.42	
	55(95,110)	0.29		67	0.54	0.54
	46(95,111)	0.38	0.38			
Oxygen	46	~0				
	67, 108	0.02		67	0.02	0.02
	112	0.03				
	48(113,114)	0.054	0.054			
	105(106,107)	0.10				
	40(115,116)	0.184				
	117	0.18/ 0.29				

( ) numbers inside the brackets refer to
original references mentioned by
another author who is given the
reference number preceding the bracket

Table X

RANGE OF EXPERIMENTAL STEELS STUDIED

(Composition in wt.% unless otherwise specified)

Steel Type	C	Mn	S	P	Si	N_2	H_2
Free cutting steel	.04/ .06 and .09/ .11	0.9/ 1.1	.23/ .30	.04/ .06	Varied nil to .30	.007/ .009	Varied up to 12 ml/ 100 g.
Low carbon steel	.09/ .11	0.9/ 1.1	.02/ .03	.03 Max	"	Varied .007 to .024	Varied up to 10 ml/ 100 g.
Low carbon steel	.18/ .22	0.9/ 1.1	"	"	"	.007/ .009	"
Rail Steel	.45/ .55	1.0/ 1.3	"	"	Varied .05 to .30	Varied .006 to .022	3/4 ml/ 100 g.

TABLE XI

Average Composition of Alloys used in steelmaking

Alloy	C	Mn	Si	S	P	N_2	Others	Fe
Swedish Iron	.013	.01	.01	.013	.002	.005	N	Remainder
Warner Iron	4.0	.2	.15	.02	.02	N	N	"
Low-carbon Ferromanganese	.06	90.0	1.0	.02	.08	N	N	"
High-carbon Ferromanganese	6.8	78.0	0.5	.03	.2	N	N	"
Ferrosilicon	N	N	75.0	N	N	N	Up to 2% Al	"
Nitrogen-Manganese	N	95.0	NO	N	N	5.0	N	N

N - Small amounts, not quoted.

TABLE XII

Porous/Solid Borderlines in Experimental Steel Ingots (1.0/1.2% Manganese)

Gas Variable / %Si	Free Cutting Steels		Plain Carbon Steels			
	.05% C .008% N$_2$ H$_2$ (ppm)	.10% C .008% N$_2$ H$_2$ (ppm)	.10% C .008% N$_2$ H$_2$ (ppm)	.10% C 3.5 ppm H$_2$ % N$_2$	.20% C .008% N$_2$ H$_2$ (ppm)	.48% C 3.5 ppm H$_2$ % N$_2$
.03	7.3	6.6	3.4	.007	3.6	N.D.
.05	7.9	7.0	3.9	.009	4.5	N.D.
.08	8.4	7.2	4.5	.012	5.2	.010
.10	8.5	7.3	5.0	.014	5.8	.012
.15	8.8	7.4	5.6	.0165	6.4	.013
.25	9.1	7.5	5.9	.0165	7.6	.015

N.D. = Not Determined

TABLE XIII

Silicon-Oxygen Relationships in Experimental
Steels Containing 0.1% Carbon and 1.0% Manganese

Si range wt.%	Average Oxygen Content wt.%	
	Low-sulphur steel (.02 - .03%S)	Free cutting steel (0.2 - 0.3%S)
NIL/.05	.026	.016
.05/.10	.021	.010
.10/.20	.016	.012
.20/.30	.014	.011

TABLE XIV

Effect of Cleanness on Total Oxygen Content of Experimental Steels Containing 0.1 and 0.2% Carbon, 1.0% Manganese

Cast No.	wt.% Si	wt.% O_2 (vacuum fusion)	No. of oxides in size range:-			Total Area % oxide	wt.% Si in oxide (calc.)*	wt.% O_2 in oxide (calc.)*
			>10μ	4-10μ	<4μ			
7976		.0214	5	70	422	.094	.0094	.0160
7962	.05	.0272	18	167	427	.193	.0193	.0330
7983		.0294	42	78	531	.216	.0216	.0370
7541		.0133	1	128	2444	.266	.0266	.0455
7752		.0155	6	24	588	.069	.0069	.0115
7753	.09/.10	.0215	15	63	1042	.169	.0169	.0290
7960		.0218	1	115	849	.150	.0149	.0255
7967		.0261	7	87	346	.108	.0108	.0185
7853		.0402	35	385	2559	.524	.0524	.0900
7685		.0111	0	13	759	.073	.0074	.0120
7691	.12/.13	.0145	0	52	619	.082	.0082	.0137
7693		.0166	7	46	759	.115	.0115	.0197
7751		.0195	21	57	611	.135	.0135	.0230
7665		.0109	2	18	349	.055	.0055	.0095
7858	.14	.0125	14	17	434	.080	.0080	.0135
7958		.0145	2	24	347	.073	.0073	.0120
7539		.0127	3	25	384	.0515	.0052	.0085
7666	.18/.22	.0138	5	32	294	.0547	.0055	.0090
7860		.0174	7	27	529	.0874	.0088	.0150
7792		.0204	21	31	382	.0949	.0095	.0165

* Assuming silicates of composition $MnO.SiO_2$

<u>TABLE XV</u>

<u>Inclusion Analyses in Low-Carbon Steels (0.1% Carbon, 1.0% Manganese)</u>

Cast No.	Steel analysis, wt.%			Spec. No.	Inclusion analysis				Ratio MnO/SiO_2 in inclusions	Av. ratio MnO/SiO_2
	C	Mn	Si		TiO_2	MnO	FeO	SiO_2		
7961	.10	.89	.035	1	2.0	54.6	9.1	34.8	1.57	1.68
				2	1.2	60.6	4.9	32.5	1.86	
				3	3.0	55.7	2.5	34.4	1.62	
7966	.10	1.07	.07	1	5.5	55.2	2.1	33.5	1.65	1.65
				2	2.1	55.8	3.7	35.8	1.55	
				3	2.5	57.3	2.8	32.6	1.76	
8010	.09	1.02	.30	1	4.3	51.8	2.2	38.4	1.35	1.23
				2	4.3	47.8	2.7	44.8	1.07	
				3	2.9	47.2	5.8	39.7	1.19	
				4	3.5	51.6	2.0	39.1	1.32	

For $MnO.SiO_2$ $\frac{MnO}{SiO_2}$ ratio = 1.18

$(MnO)_{1.5} SiO_2$ $\frac{MnO}{SiO_2}$ ratio = 1.72

TABLE XVI

Relative Contributions of P_{CO}, P_{H_2} and P_{N_2} to

P_{Total} (90% Solidified) in steels of porous/solid

composition (pressures in atmospheres)

(a) 0.05% carbon free cutting steel (1.0% manganese, 0.008% nitrogen)

Composition	P_{CO}	P_{N_2}	P_{H_2}	P_{Total}
.03%Si; 7.3 ppm H_2	.36	.15	.73	1.24
.05%Si; 7.9 ppm H_2	.29	.15	.86	1.30
.10%Si; 8.5 ppm H_2	.23	.15	1.01	1.39
.25%Si; 9.1 ppm H_2	.16	.16	1.11	1.43

(b) 0.10% carbon free cutting steel (1.0% manganese, 0.008% nitrogen)

Composition	P_{CO}	P_{N_2}	P_{H_2}	P_{Total}
.03%Si; 6.6 ppm H_2	.59	.17	.65	1.41
.05%Si; 7.0 ppm H_2	.49	.17	.73	1.29
.10%Si; 7.3 ppm H_2	.38	.17	.81	1.36
.25%Si; 7.5 ppm H_2	.27	.18	.89	1.34

TABLE XVI Contd.

(c) <u>0.10% carbon steels (1.0% manganese. 0.008% nitrogen)</u>

Composition	P_{CO}	P_{N_2}	P_{H_2}	P_{Total}
.03%Si; 3.4 ppm H_2	.59	.17	.17	0.93
.05%Si; 3.9 ppm H_2	.49	.17	.23	0.89
.10%Si; 5.0 ppm H_2	.38	.17	.38	0.93
.25%Si; 5.9 ppm H_2	.27	.18	.55	1.00

(d) <u>0.10% carbon steels (1.0% manganese. 3.5 ppm hydrogen)</u>

Composition	P_{CO}	P_{N_2}	P_{H_2}	P_{Total}
.03%Si; .007% N_2	.59	.13	.17	0.90
.05%Si; .009% N_2	.49	.21	.17	0.87
.10%Si; .014% N_2	.38	.52	.18	1.08
.25%Si; .0165% N_2	.27	.73	.18	1.18

TABLE XVI Contd.

(e) <u>0.20% carbon steels (1.0% manganese, 0.008% nitrogen)</u>

Composition	P_{CO}	P_{N_2}	P_{H_2}	P_{Total}
.03%Si; 3.6 ppm H_2	.84	.17	.17	1.18
.05%Si; 4.5 ppm H_2	.70	.18	.27	1.15
.10%Si; 6.8 ppm H_2	.54	.18	.45	1.17
.25%Si; 7.6 ppm H_2	.38	.20	.81	1.39

(f) <u>0.48% carbon steels (1.2% manganese, 3.5 ppm hydrogen)</u>

Composition	P_{CO}	P_{N_2}	P_{H_2}	P_{Total}
.08%Si; .010% N_2	.59	.28	.13	1.00
.10%Si; .012% N_2	.54	.40	.13	1.07
.25%Si; .015% N_2	.42	.60	.12	1.14

$$k_0 = \frac{C_S}{C_L}$$

g = fraction solidified = AE
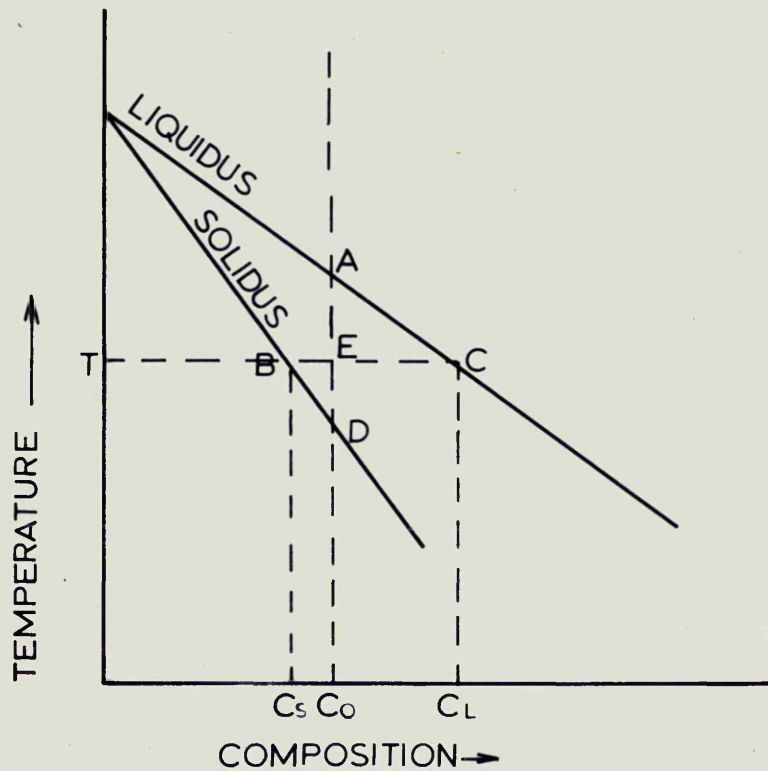
BINARY DIAGRAM SHOWING EQUILIBRIUM
RELATIONSHIP BETWEEN LIQUID AND SOLID
(COMPLETE MIXING IN BOTH SOLID AND
LIQUID)
FIG. 1.
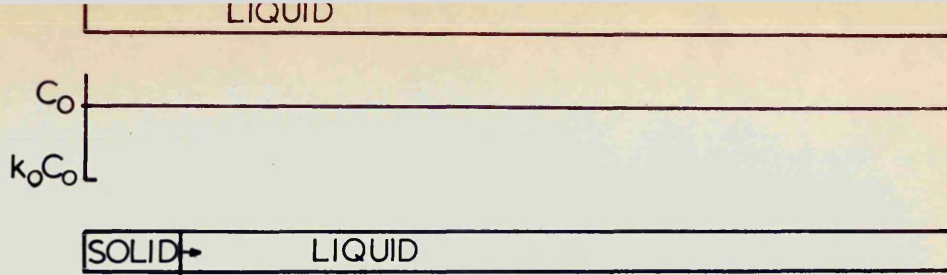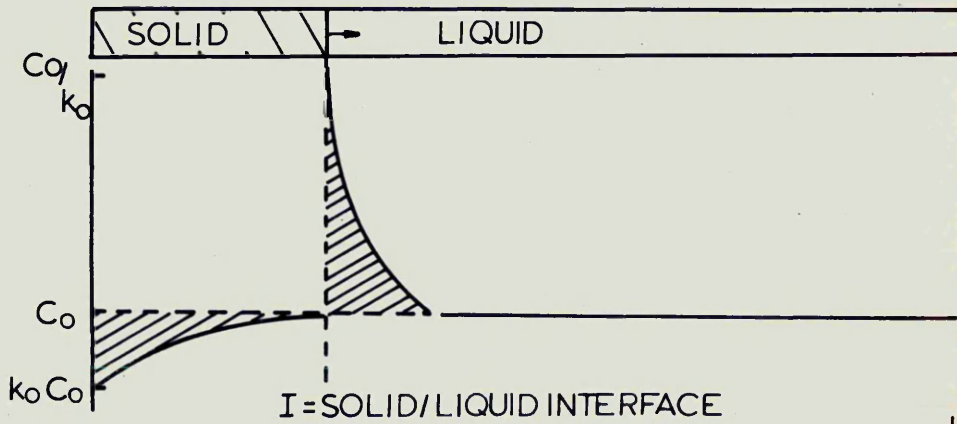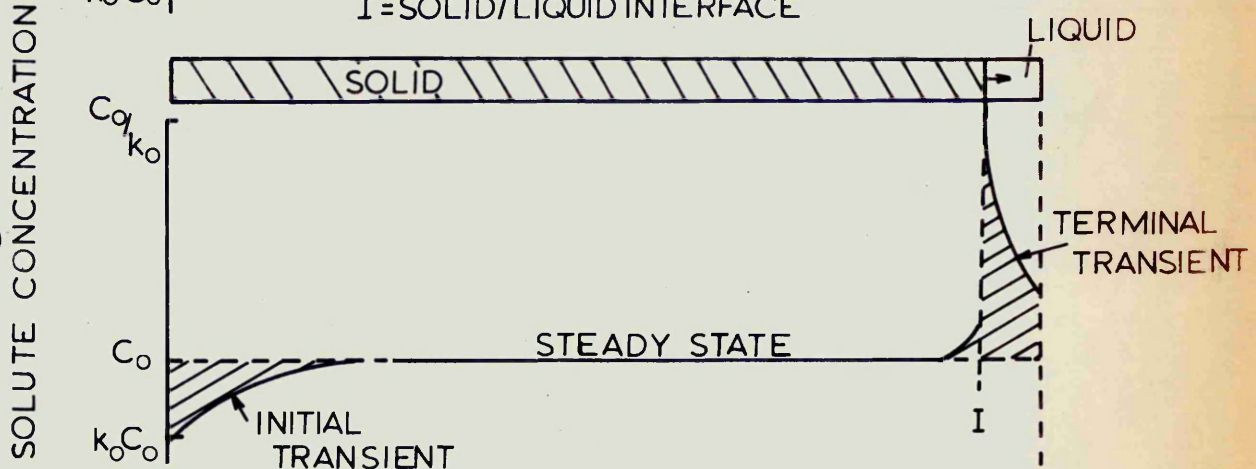
DISTRIBUTION OF SOLUTE DURING VARIOUS STAGES
OF SOLIDIFICATION (ASSUMING NO MIXING IN SOLID
AND MIXING IN LIQUID BY DIFFUSION ONLY)

FIG. 2 .
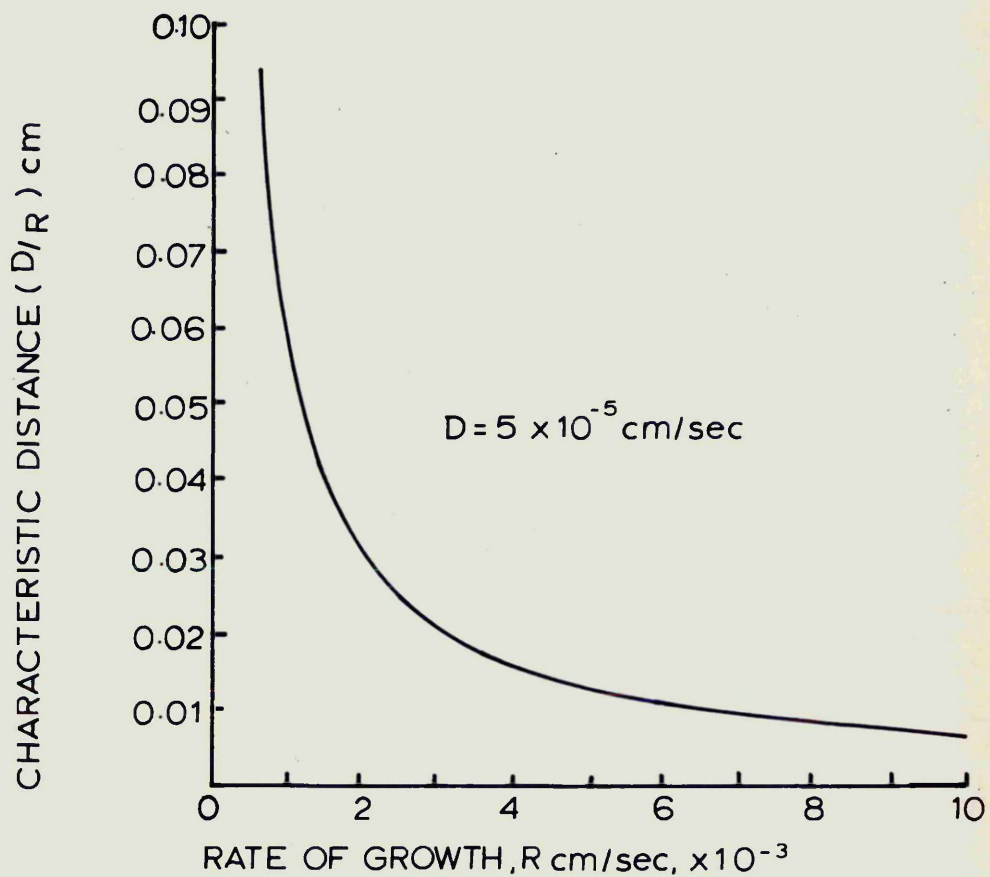
THICKNESS OF DIFFUSION ZONE AS A FUNCTION

OF GROWTH RATE   (AFTER TILLER et al[35])

FIG.3 .

(a) PARTIAL MIXING IN LIQUID

C_I

C_S

C_L

C_O

$\leftarrow d \rightarrow$
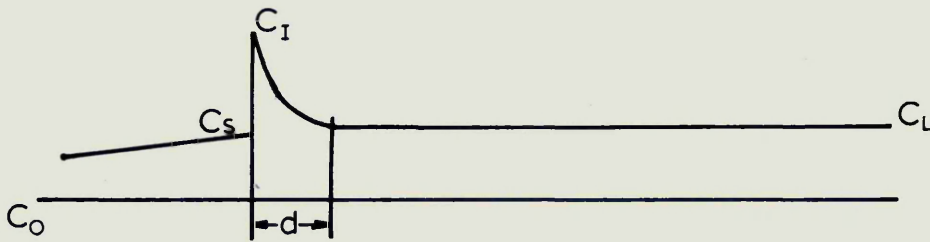
(b) COMPLETE MIXING IN LIQUID

C_I

C_L

C_S

C_O
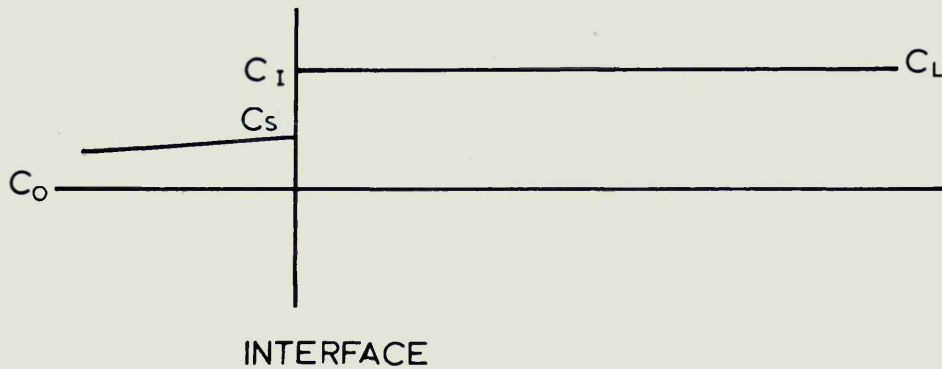
INTERFACE

SOLUTE DISTRIBUTION AT SOLID/LIQUID INTERFACE
IN CASES WHERE NO DIFFUSION OCCURS IN SOLID
BUT MIXING OCCURS IN THE LIQUID

FIG. 4.
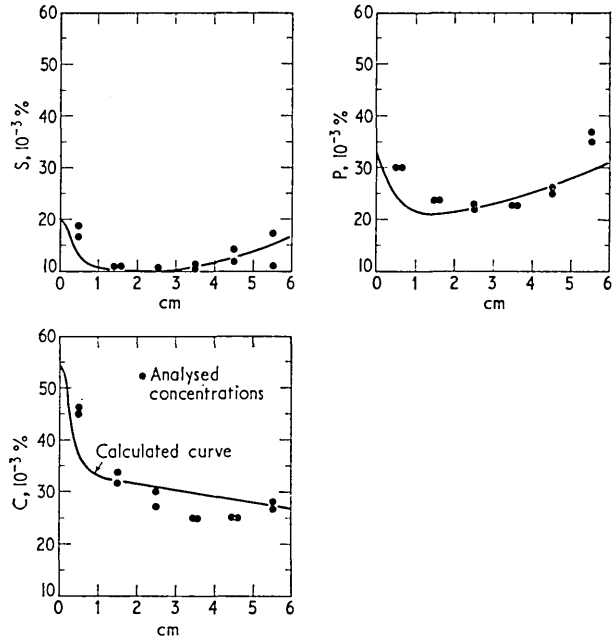
(a)
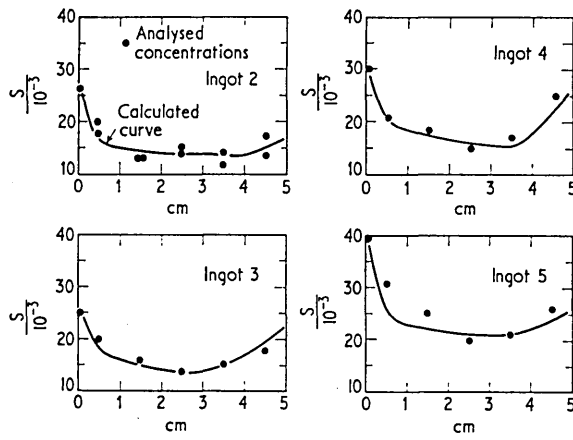
(b)

COMPARISON OF CALCULATED AND ANALYSED IMPURITY CONCENTRATIONS
IN THE RIM OF 500Kg INGOTS (After Nilles[40])

Fig. 5
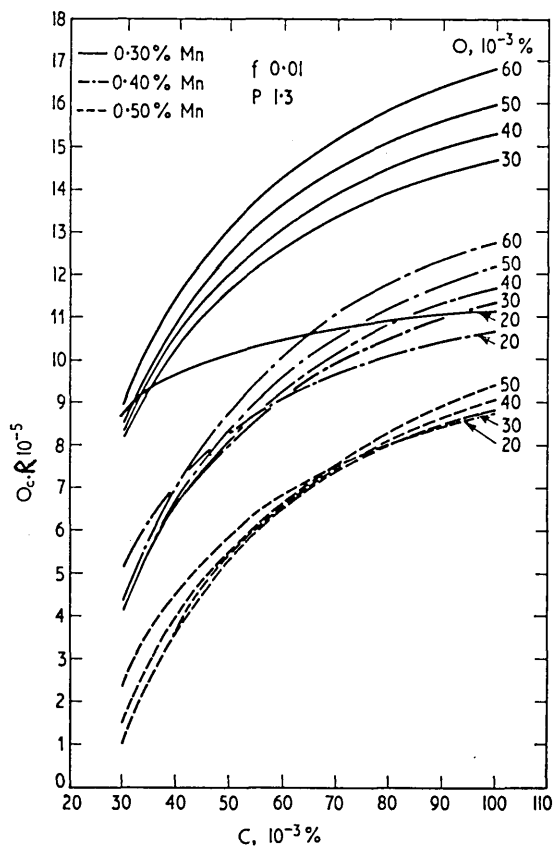
(a) After Nilles[40]
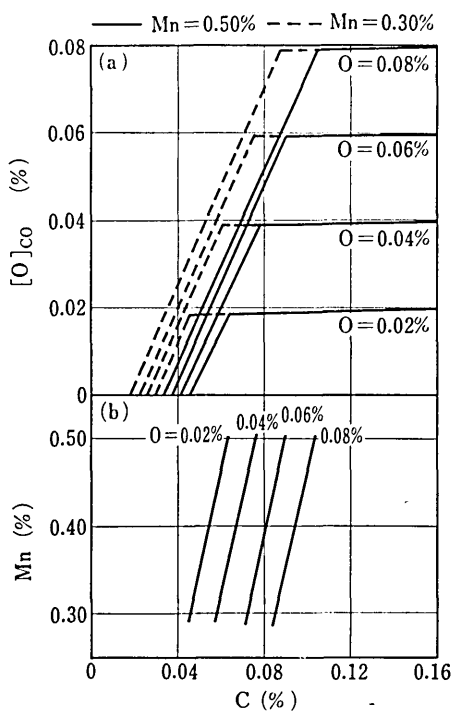
(b) After Masui et. al.[42]

INFLUENCE OF CARBON, MANGANESE AND OXYGEN CONCENTRATIONS

ON THE RIMMING INTENSITY

Fig. 6
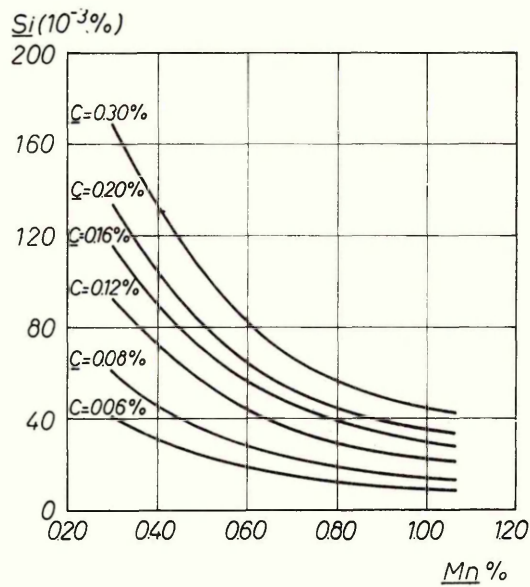
PREDICTED COMPOSITIONS OF CONVEX BALANCED INGOTS

(After Scimar and Nilles[33])

Fig. 7
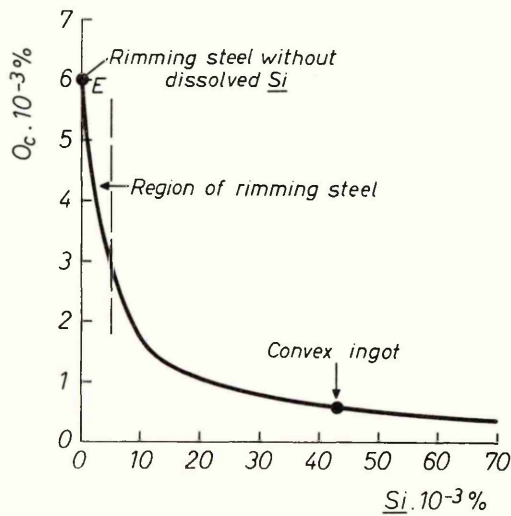
INFLUENCE OF DISSOLVED SILICON ON GAS EVOLUTION AT THE SOLID/LIQUID

INTERFACE (After Scimar and Nilles[33])

Fig. 8
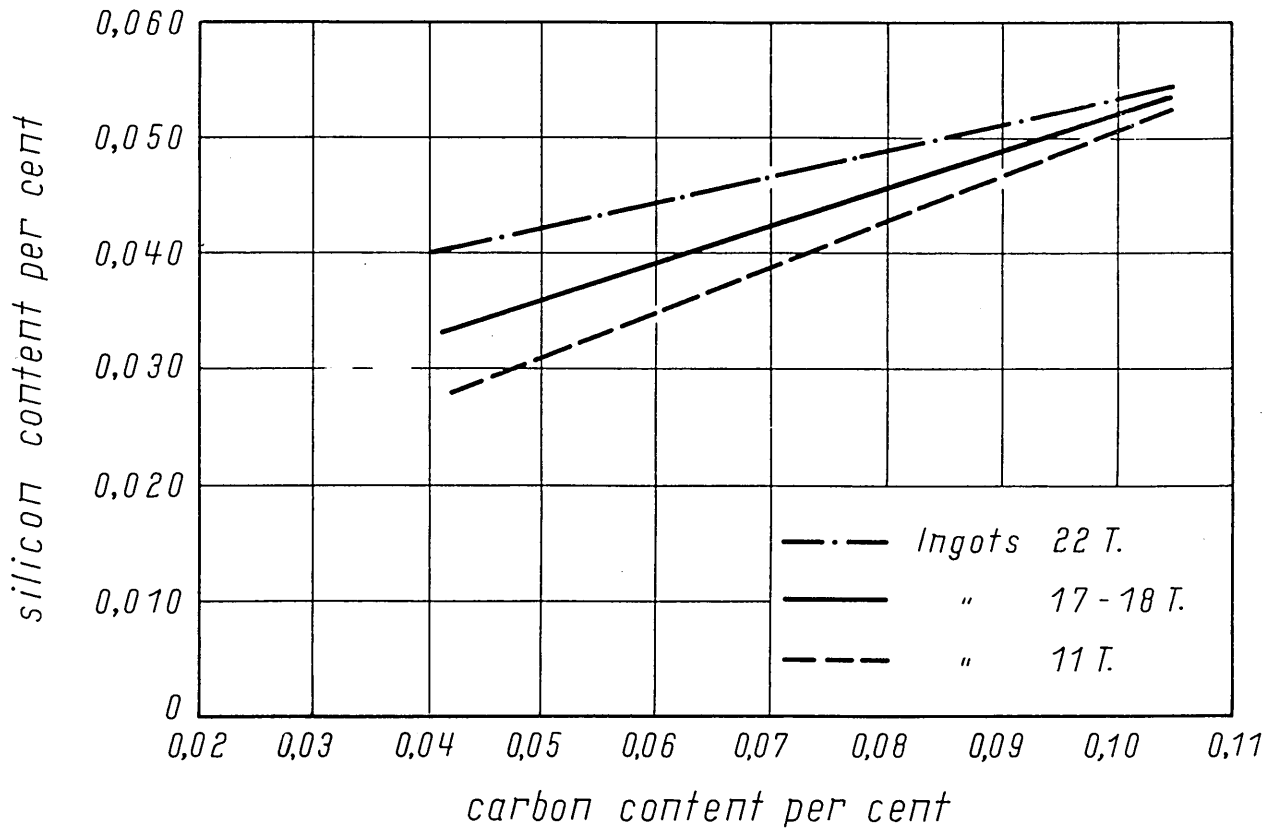
INFLUENCE OF INGOT SIZE ON THE SILICON CONTENT OF A
BALANCED STEEL (After Oeters et. al.[43])

Fig. 9
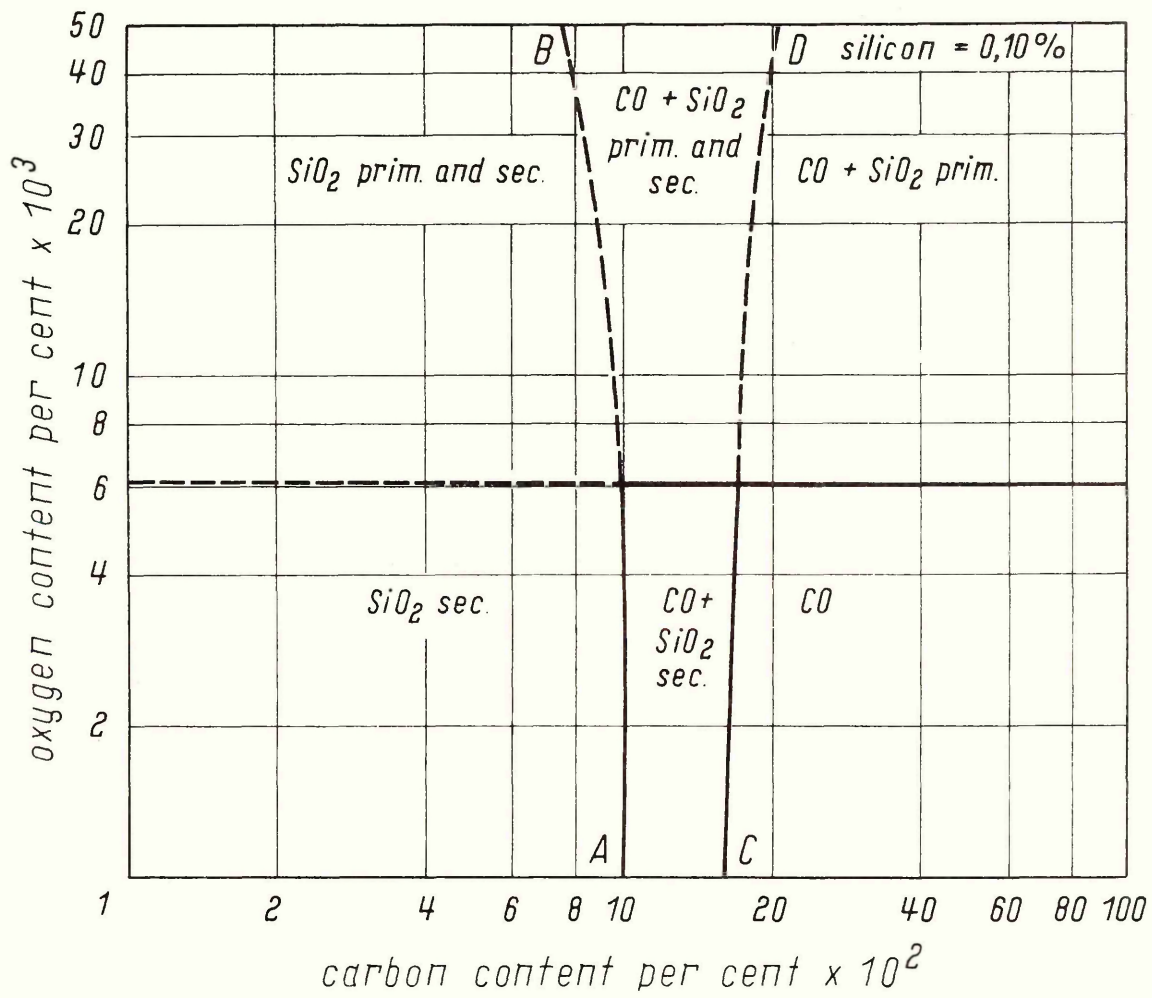
COMPOSITION BOUNDARIES FOR CO FORMATION DURING SOLIDIFICATION

FOR SILICON DEOXIDATION (After Oeters et. al.[43])

Fig. 10
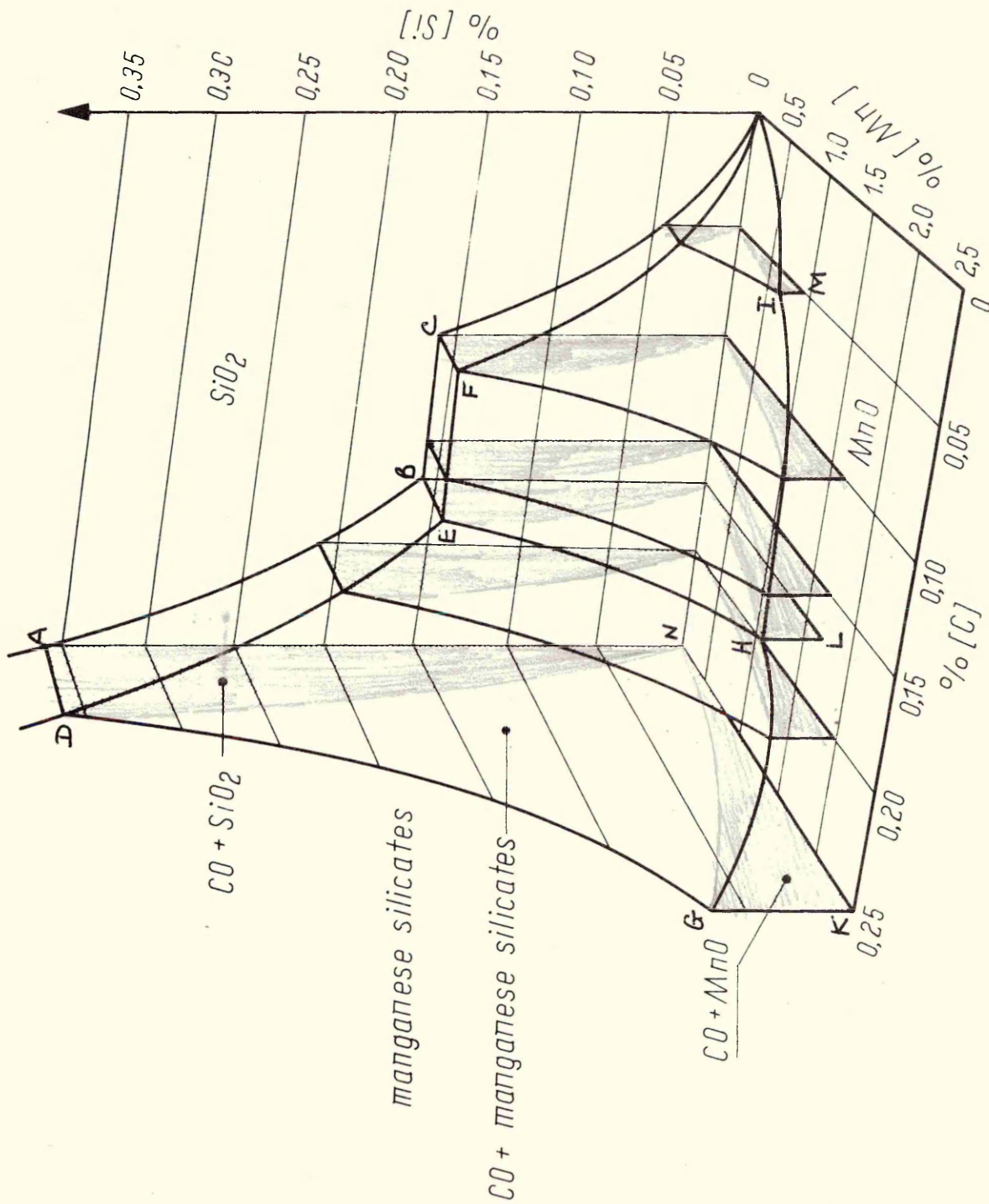
COMPOSITION BOUNDARIES FOR CO FORMATION DURING SOLIDIFICATION
WITH COMBINED MANGANESE AND SILICON DEOXIDATION
(After Oeters et. al.[43])

Fig. 11
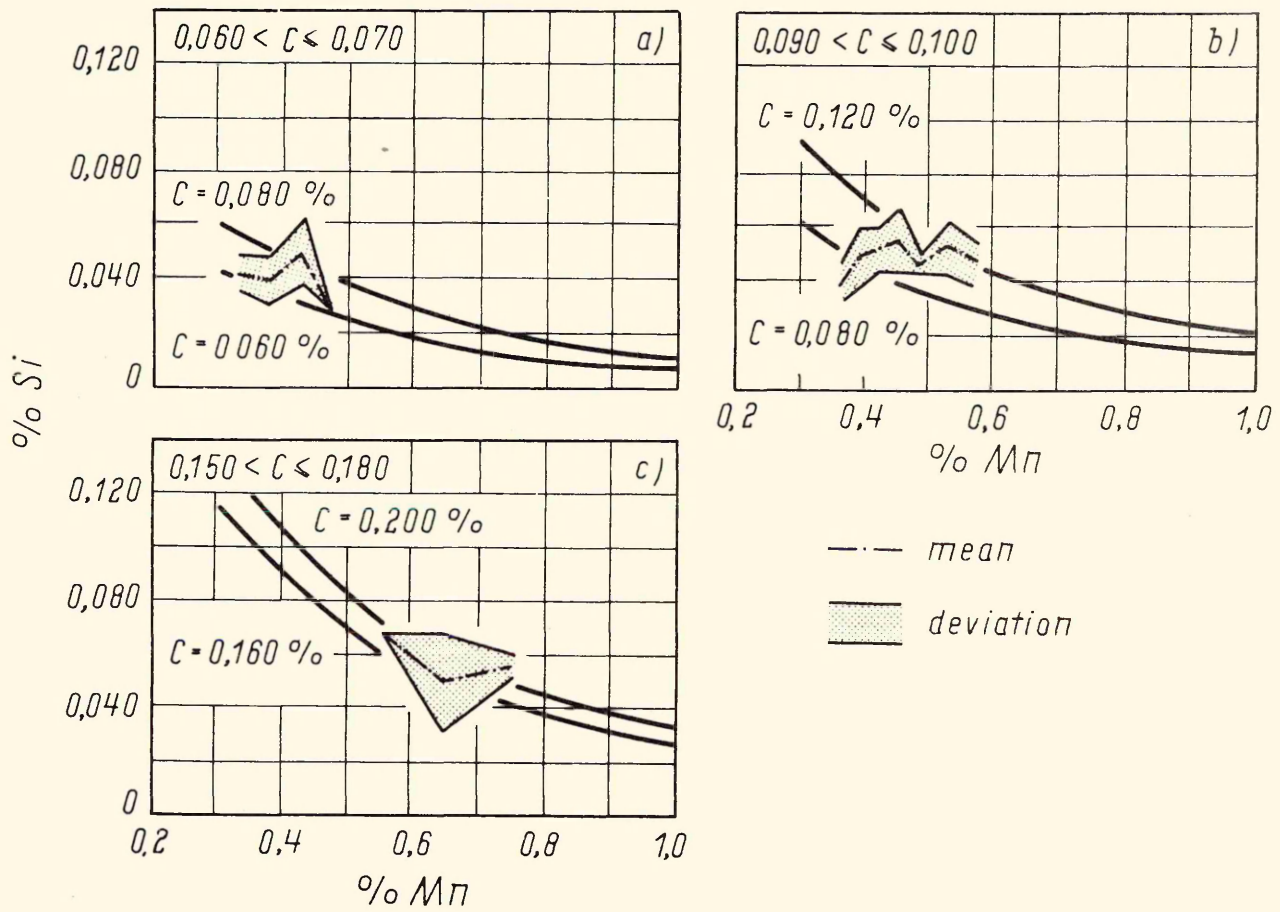
COMPARISON OF PREDICTED COMPOSITIONS OF BALANCED STEELS
WITH WORKS PRACTICE RESULTS (After Oeters et. al.[43])

Fig. 12
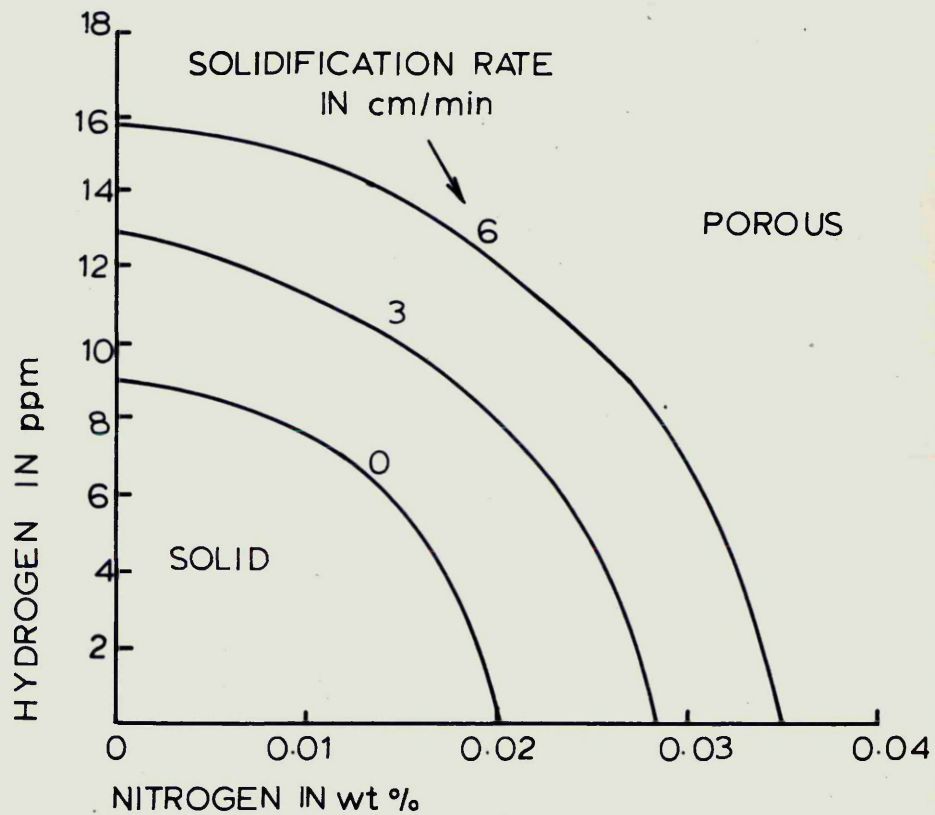
CRITICAL LEVELS OF HYDROGEN AND NITROGEN TO
PRODUCE POROUS INGOTS IN FULLY DEOXIDISED
STEEL (AFTER OETERS et.al.[44])

FIG.13.

o NILLES & SCIMAR, 0·5% Mn

●   "   "   1·0% Mn

———— TURKDOGAN'S PREDICTED LINES (TO LEFT OF LINES BLOWHOLES NOT FORMED : TO RIGHT OF LINES BLOWHOLES MAY FORM)
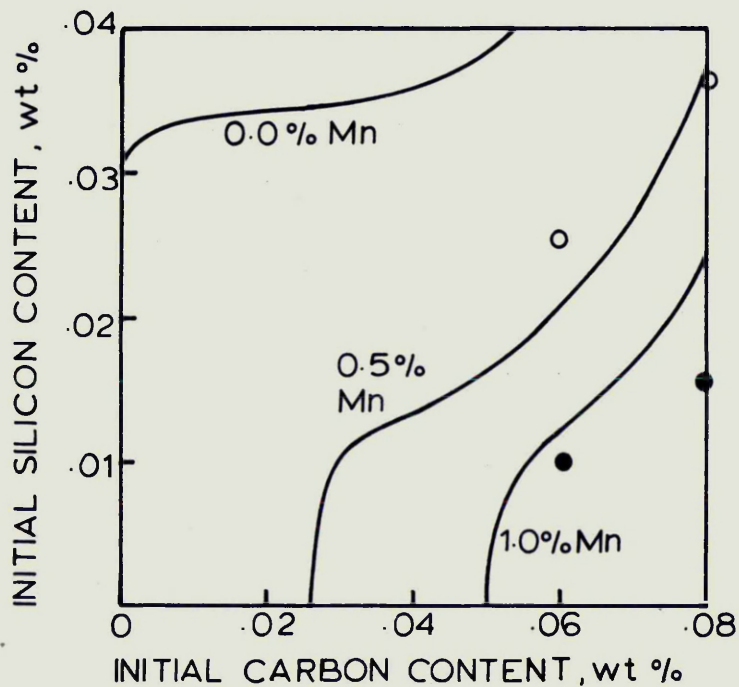
EFFECT OF MANGANESE CONTENT ON CRITICAL SILICON AND CARBON CONTENTS FOR FORMATION OF BLOWHOLES (OXYGEN= 0·010%, 1atm. CO ; FREEZING TEMP =1525°C : NO HYDROGEN OR NITROGEN) AFTER TURKDOGAN[46]

FIG.14 .
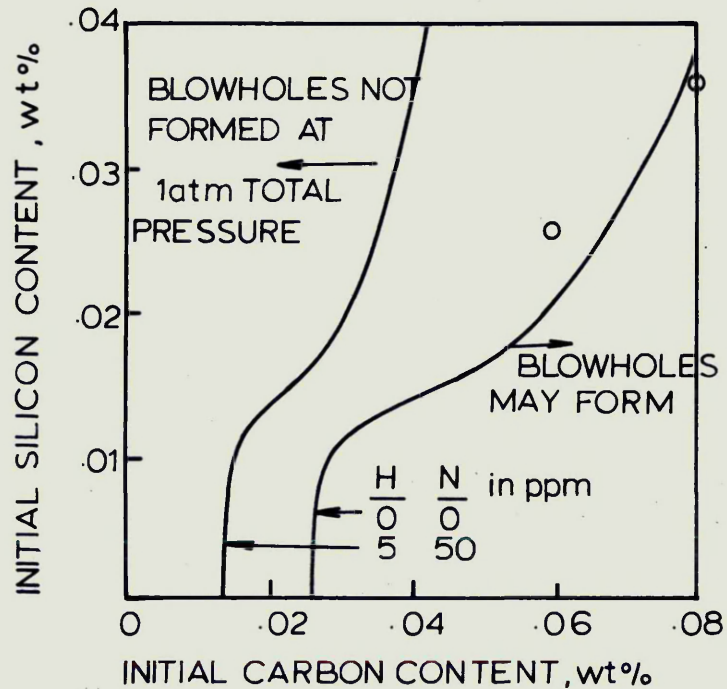
EFFECTS OF HYDROGEN AND NITROGEN IN STEEL ON CRITICAL SILICON AND CARBON CONTENTS FOR THE FORMATION OF BLOWHOLES (MANGANESE=0.5%; OXYGEN=0.010% ; FREEZING TEMP=1525°C; $P_{C_o}+P_{H_2}+P_{N_2}=$ 1 atm) AFTER TURKDOGAN [46]

FIG.15 .
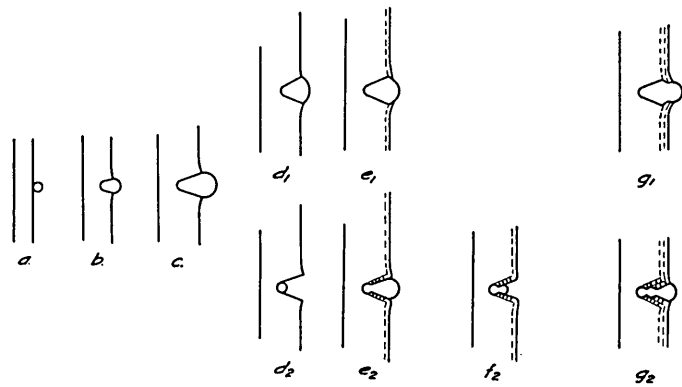
MODES OF BLOWHOLE GROWTH (After Hultgren & Phragmen[2])

Fig. 16
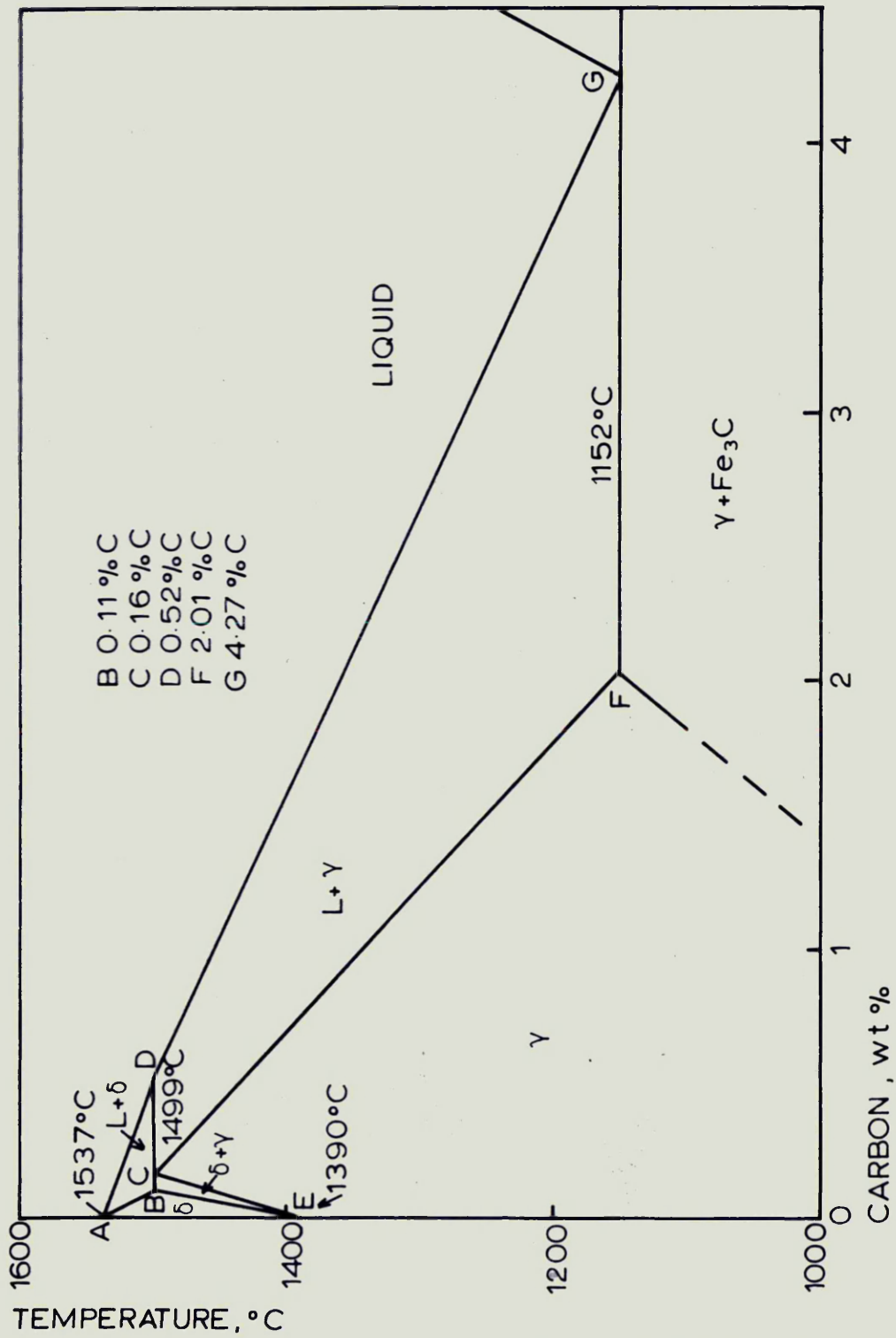
IRON-CARBON PHASE DIAGRAM (REF.102)

FIG.17

SILICA TUBING,
APPROX. 8mm. O.D

SOLID GLASS ROD

SEALED

29cm.

FILLER HOLE
5mm. DIAMETER

11/12cm

11cm.

SILICA TUBING
10mm I.D

EVACUATED
PYREX TUBING
8/10mm. I.D

SEALED

SEALED(WALL THICKNESS
THINNED DOWN)
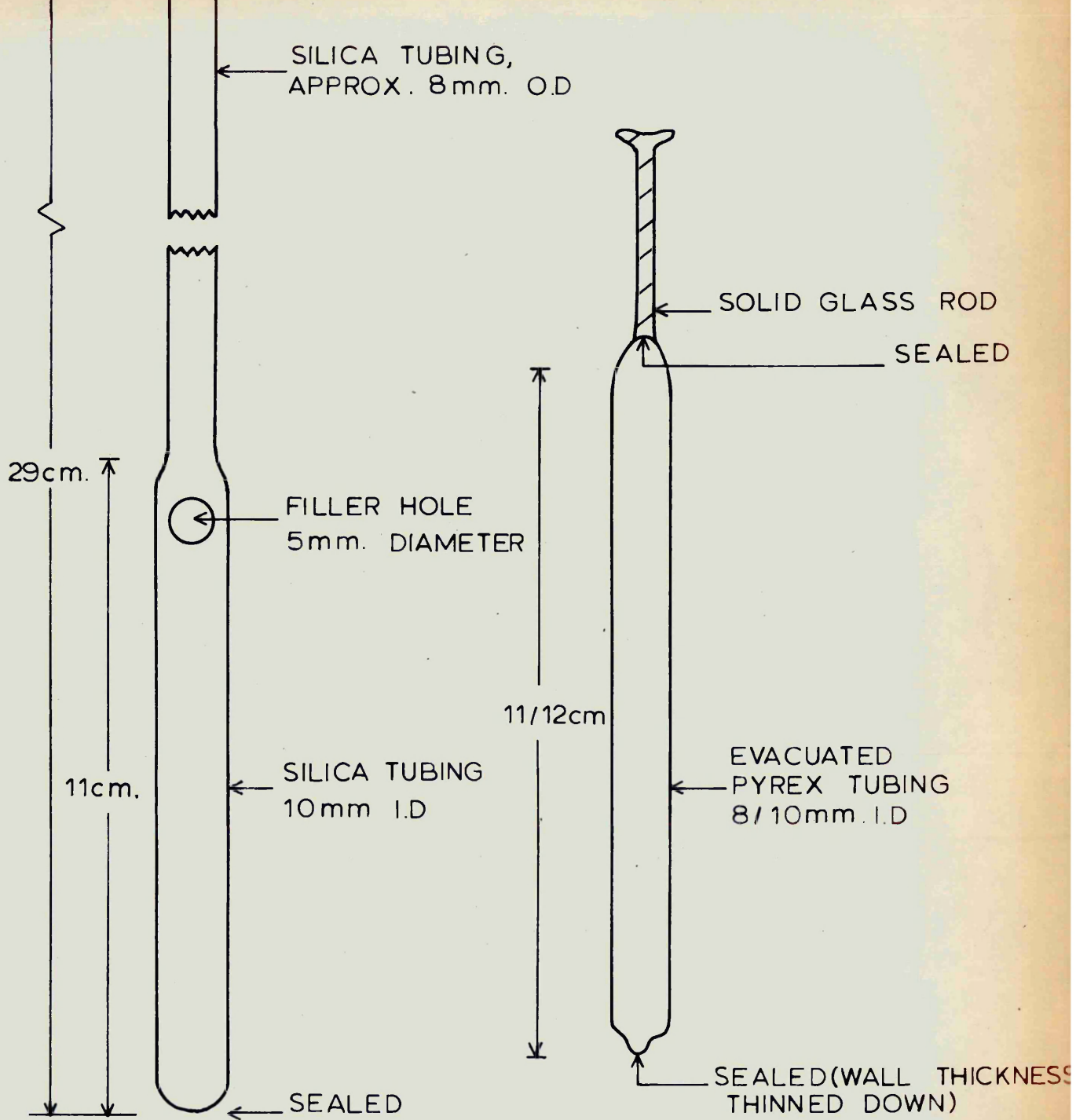
(a) GRAVITY-FILLING SILICA
TUBE

(b) EVACUATED PYREX TUBE

HYDROGEN SAMPLING TUBES
FIG.18 .

A	B	C	D
Solid	Borderline	Porous	Rimming
	Porosity	Rising top	
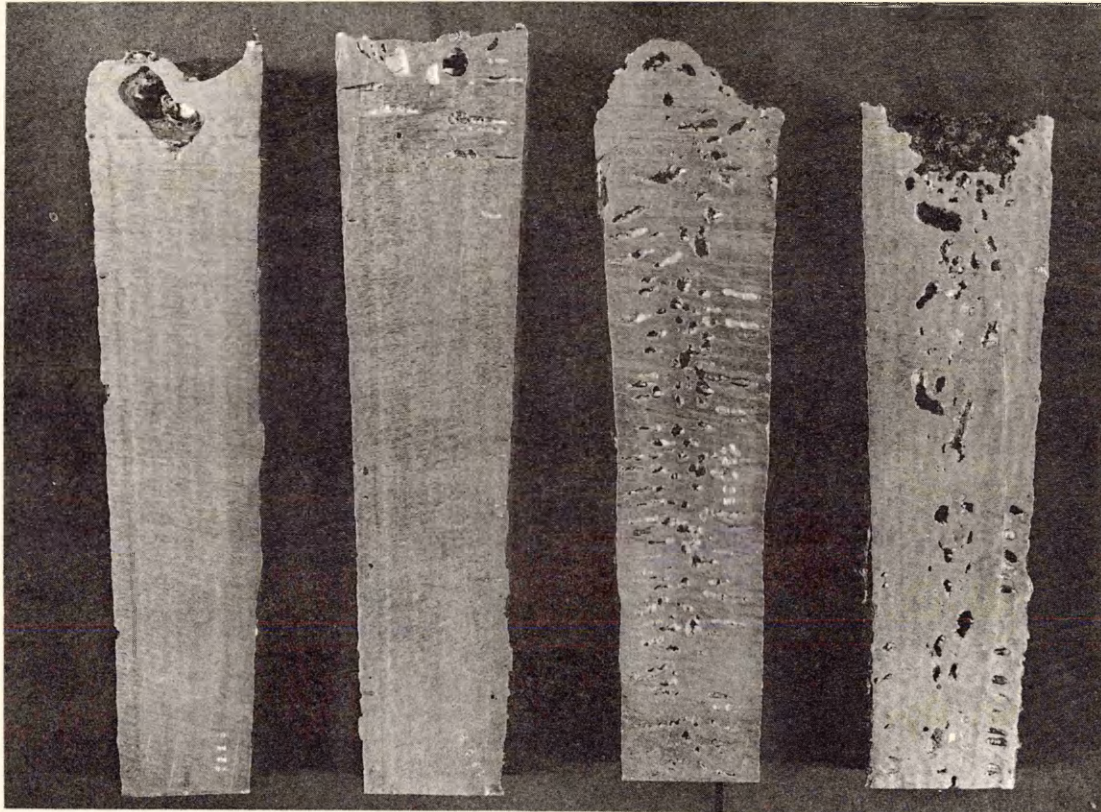
Mag. approx X $\frac{1}{3}$

EXPERIMENTAL INGOTS (281b) SHOWING VARYING DEGREES OF POROSITY

Fig. 19

NIL - .02 % Si

P

S

POROUS/SOLID BORDERLINE
SCATTER BAND

.02 - .05% Si

P

S

.05 - .10% Si

P

S

.10 - .20% Si

P

S

.20 - .30% Si

P

S

0   2   4   6   8   10
HYDROGEN CONTENT OF STEEL, m/100g
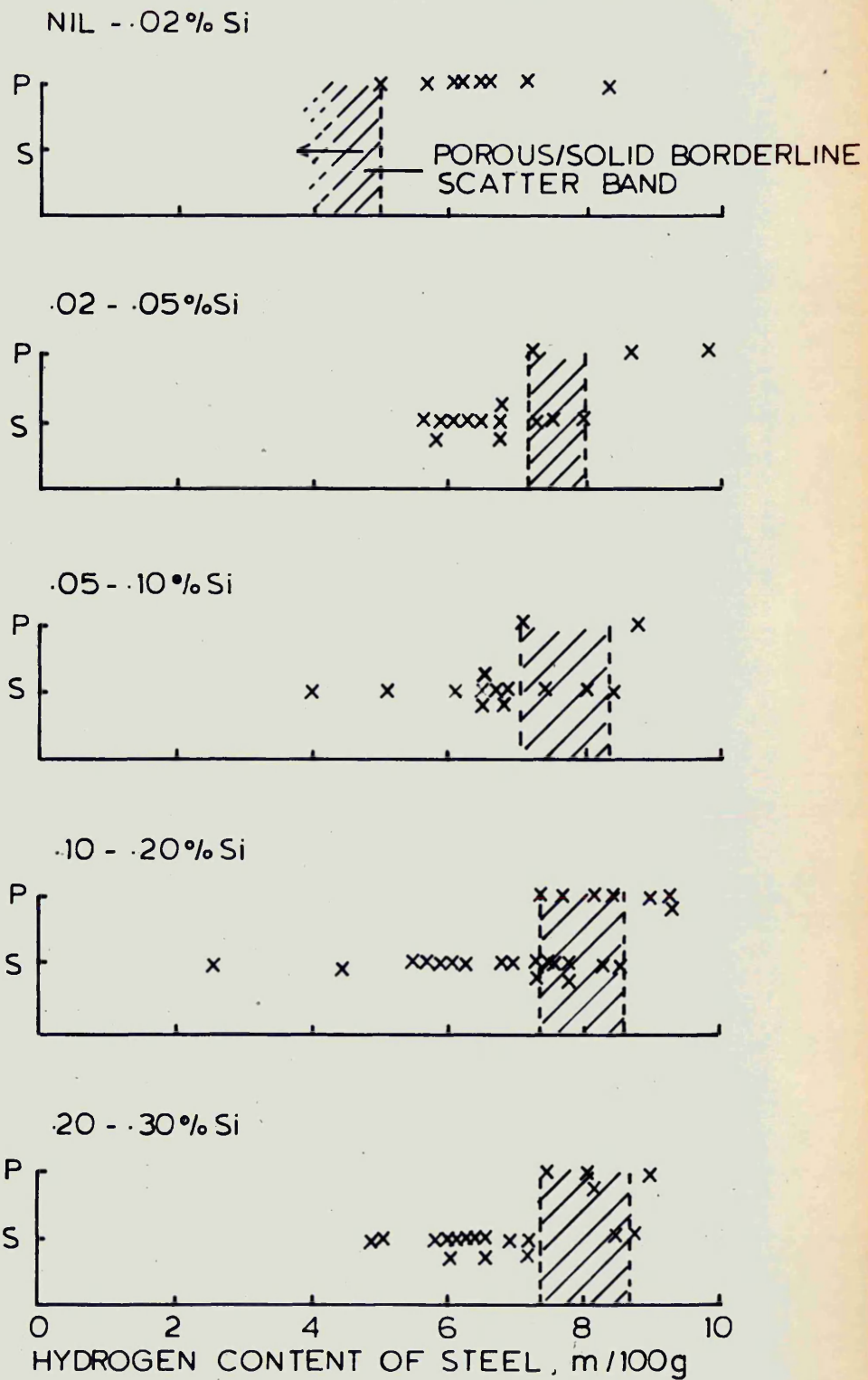
POROUS/SOLID BORDERLINES IN FREE CUTTING
STEEL INGOTS CONTAINING 0.10% CARBON, 1.0%
MANGANESE AND 0.008% NITROGEN

FIG. 20.

Y-axis: LOSS IN HYDROGEN CONTENT (ml/100g) BETWEEN FURNACE & (?)

X-axis: HYDROGEN CONTENT OF STEEL IN FURNACE, ml/100g (x)

0.2 /0.3 % S STEELS
(y = .38x - 1.5)

0.02 /0.03 % SULPHUR STEELS
(y = .52x - 3.1)
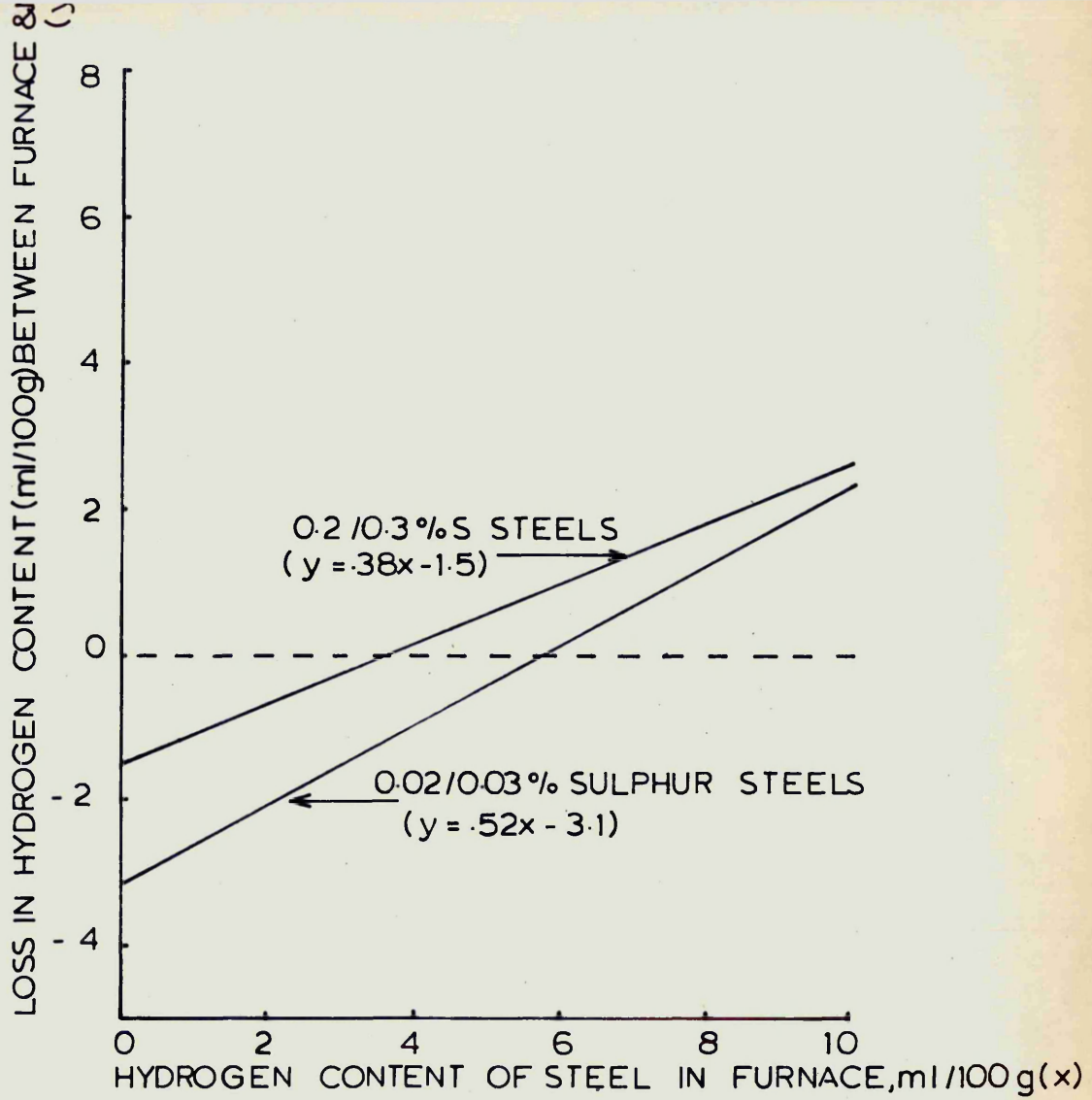
CHANGE IN HYDROGEN CONTENT BETWEEN FURNACE AND MOULD

FIG. 21
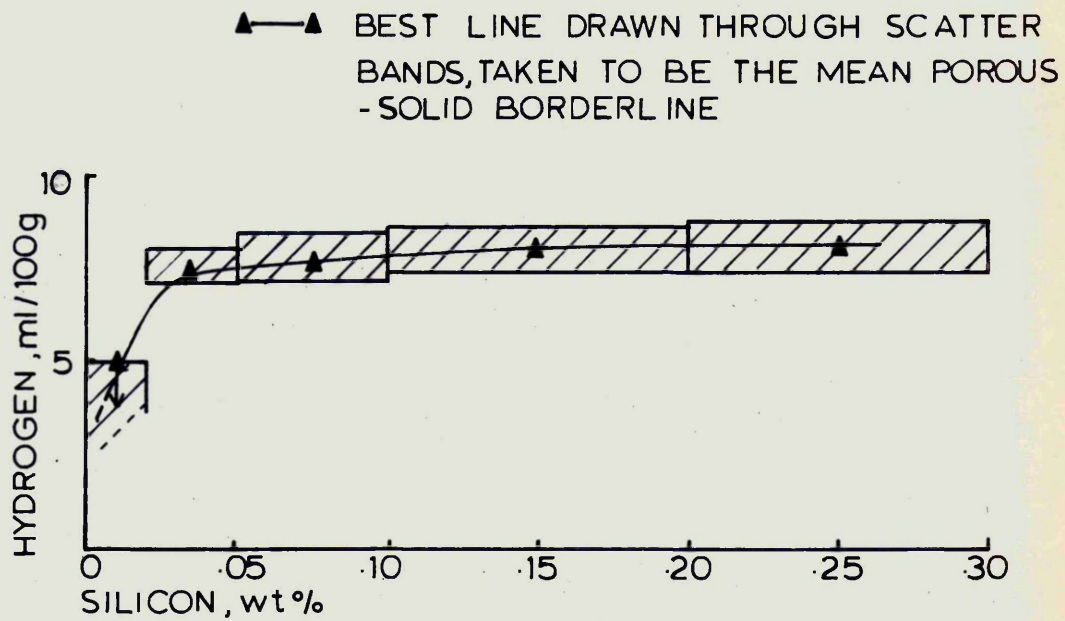
EFFECT OF SILICON ON HYDROGEN CONTENT AT
THE POROUS/SOLID BORDERLINE IN FREE CUTTING
STEELS CONTAINING 0.10% CARBON, 1.0% MANGANESE
AND 0.008% NITROGEN

FIG.22
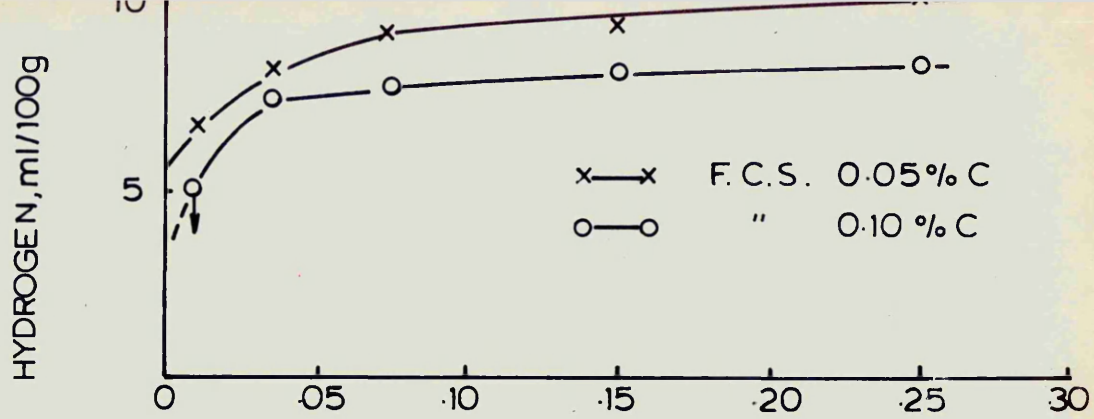
(b) 1.0%Mn; 0.008% N₂
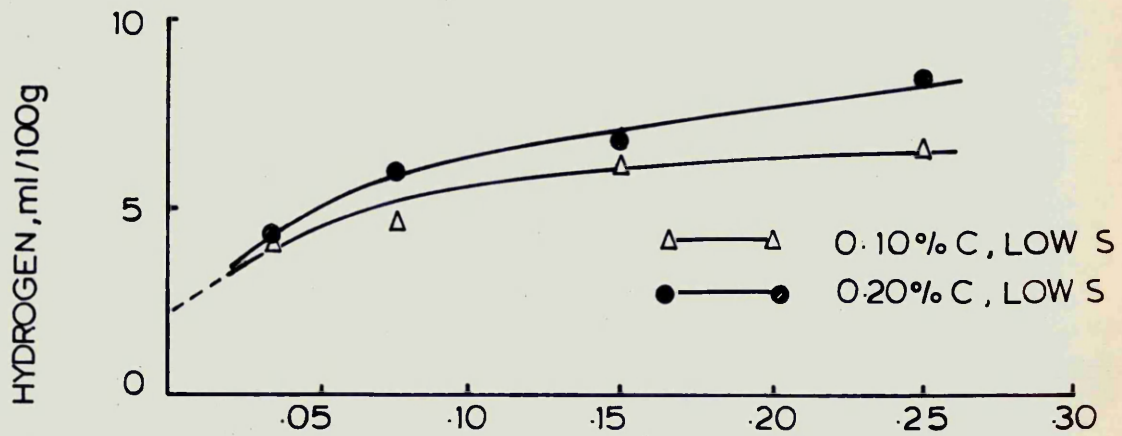
(c) 3.5 ppm H₂
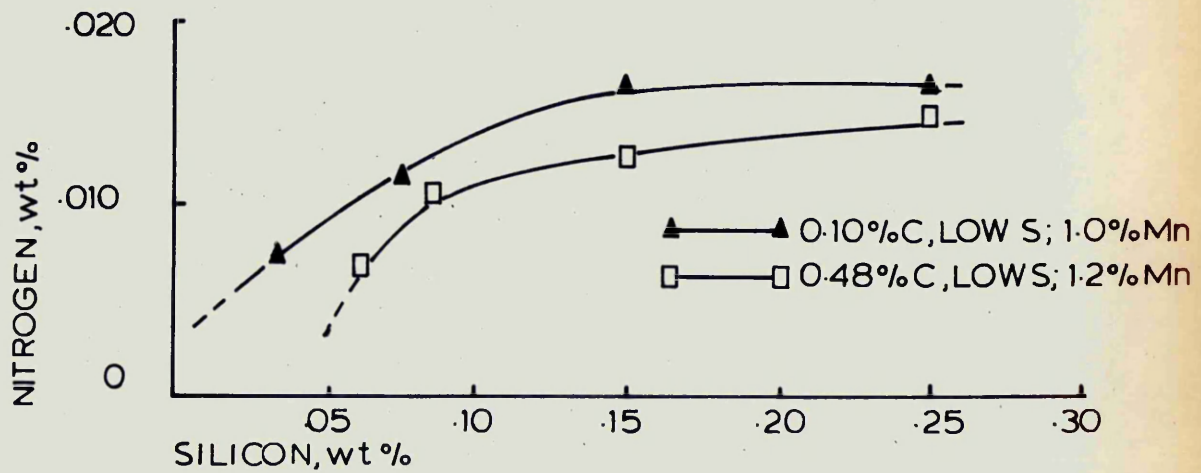
SILICON, wt %

EFFECT OF SILICON ON HYDROGEN AND NITROGEN
AT POROUS/SOLID BORDERLINES IN EXPERIMENTAL
STEEL INGOTS

FIG. 23.

(a) FREE CUTTING STEEL

THEORETICAL Si-O
EQUILIBRIUM CURVE
(1·0% Mn) AT 1600°C
(REF.46)
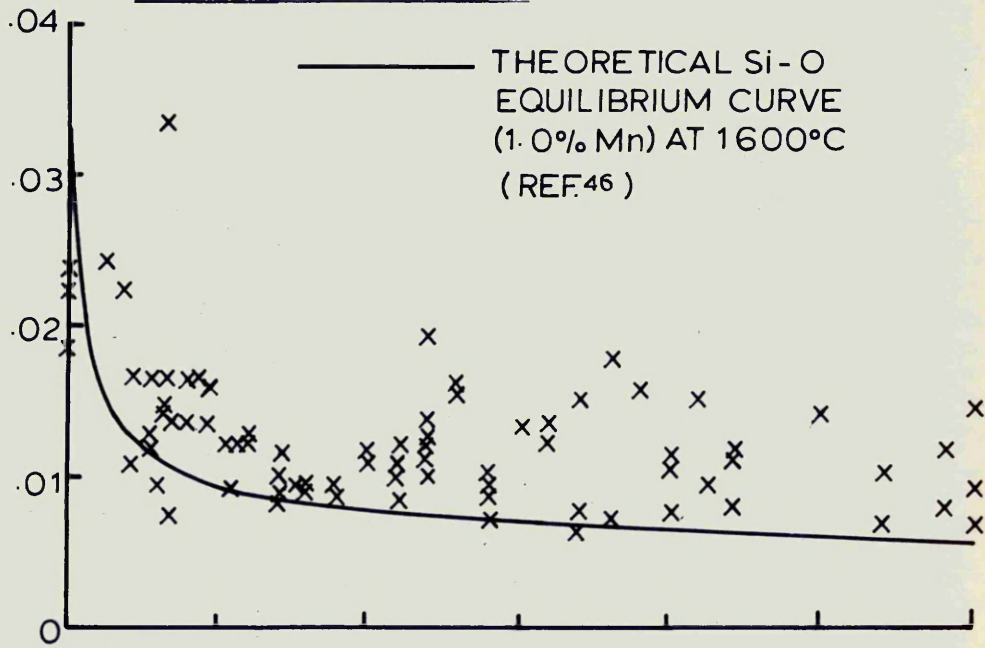
(b) LOW-SULPHUR STEEL

OXYGEN, wt %
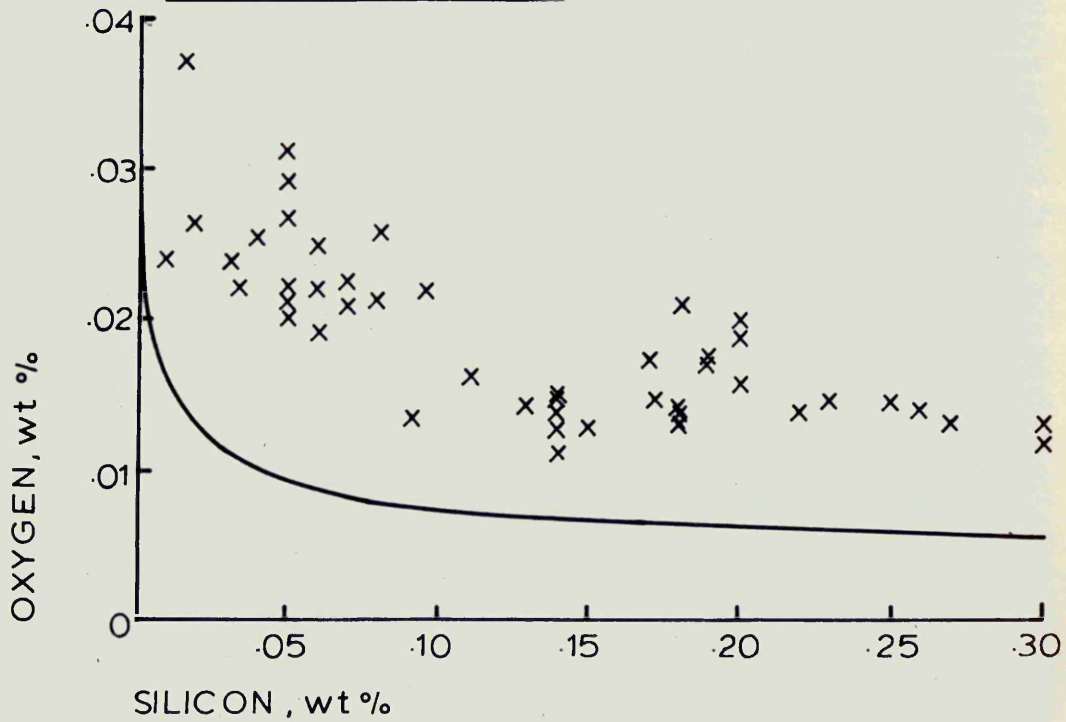
SILICON , wt %

SILICON-OXYGEN RELATIONSHIPS IN EXPERIMENTAL

0·1% CARBON, 1·0% MANGANESE STEELS

FIG.24.

(a) > 10 µ

(b) > 10 µ

(c) > 10 µ

(d) 4 - 10 µ

(e) < 4 µ
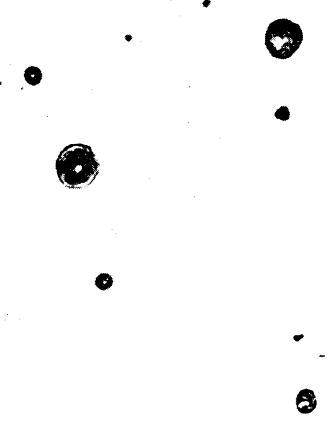
All magns. X 750

EXAMPLES OF INCLUSIONS FOUND IN OXYGEN SAMPLES

Fig. 25
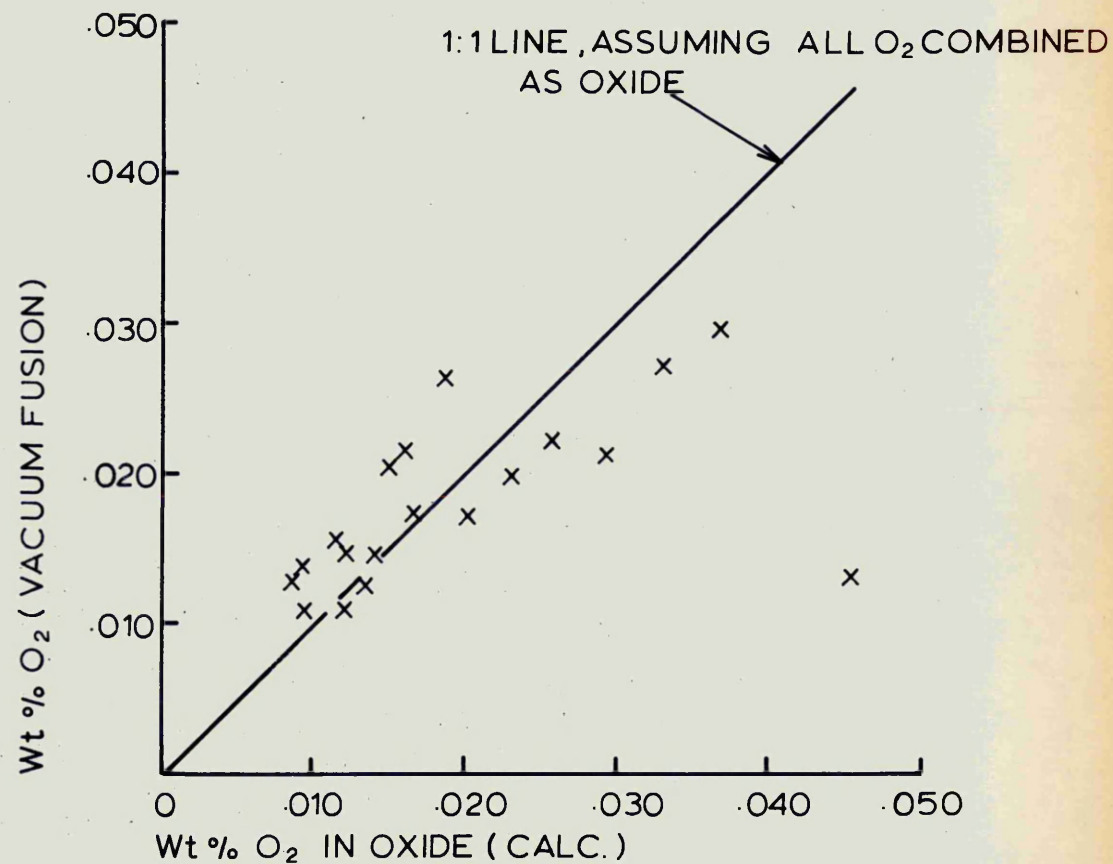
VACUUM FUSION OXYGEN FIGURES vs. CALCULATED
WEIGHT PERCENT OXYGEN IN OXIDES. (CALCULATED
FROM AREA PERCENT OXIDE, ASSUMING OXIDE
COMPOSITION $MnSiO_3$) RESULTS FOR 0.1 AND 0.2 %
CARBON STEELS

FIG. 26.
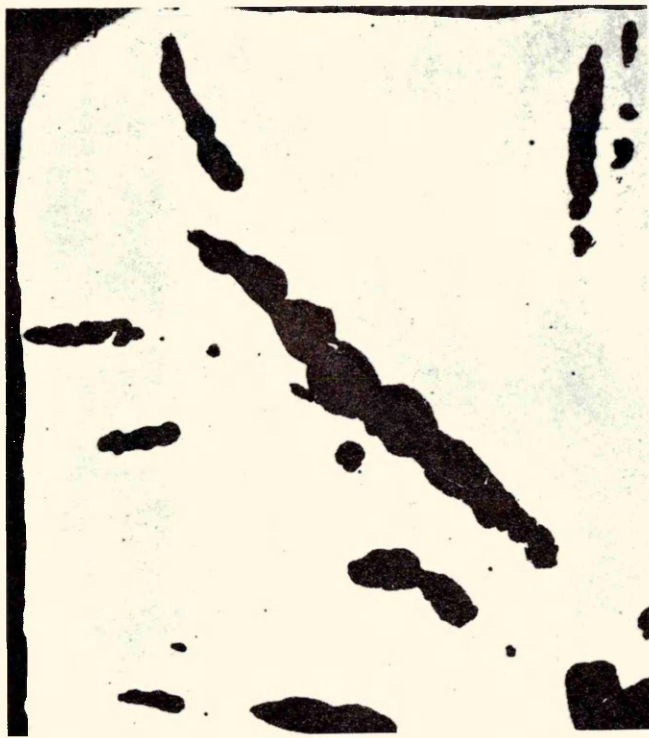
(a) 0·1% carbon free cutting steel
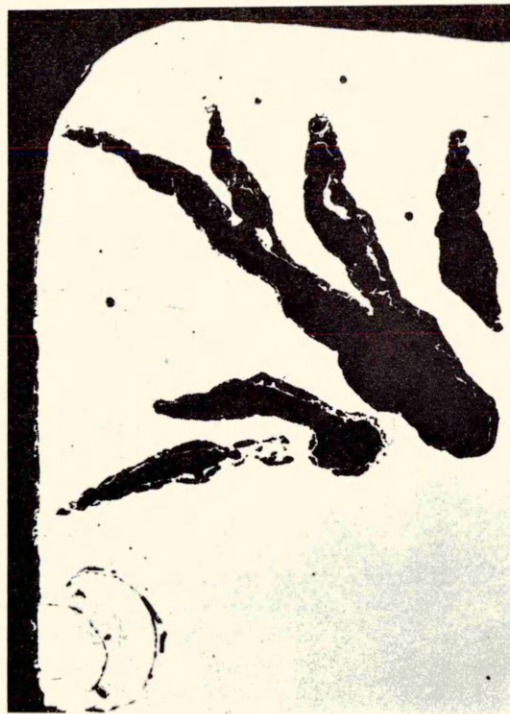
(h) Plain 0·1% carbon steel

BLOWHOLES IN EXPERIMENTAL INGOTS (UNETCHED SECTIONS, MAG. X 5)

Fig. 27
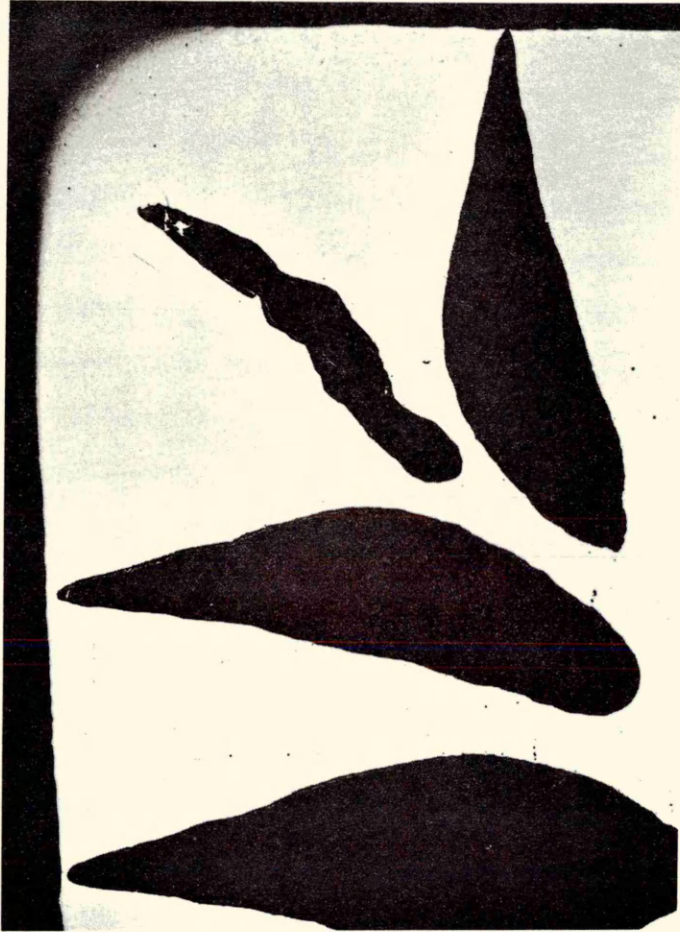
Unetched, Mag. X 5

BLOWHOLES IN EXPERIMENTAL 0·5% CARBON STEEL INGOT

Fig. 28

(a)

(b)

(c)

(d)
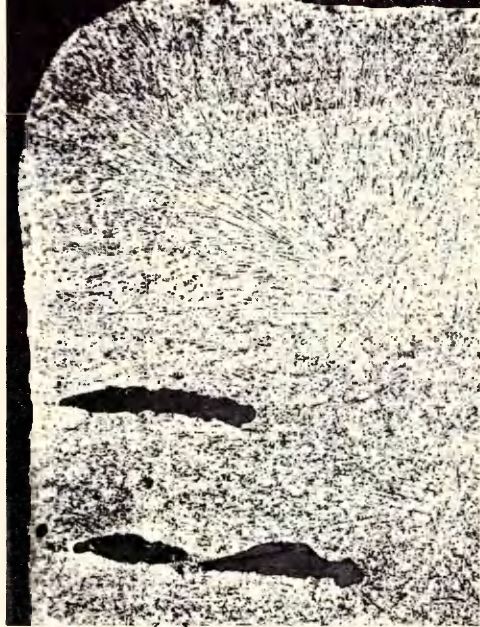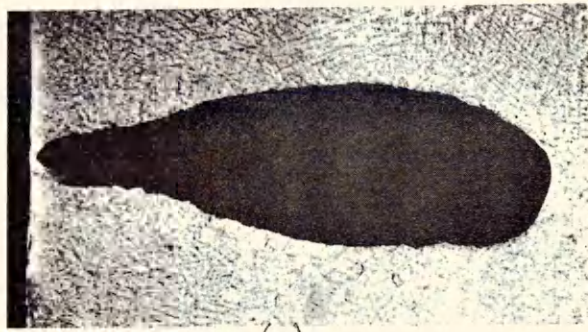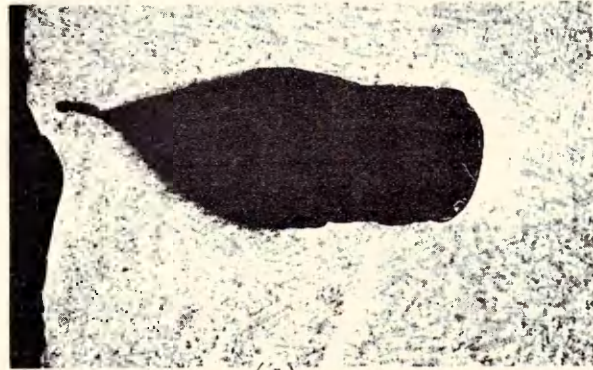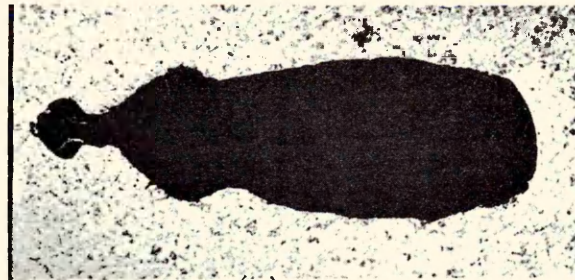
(e)

(a) and (b)   0·1% carbon

(c)   –   (e)   0·5% carbon

Oberhoffer etch,   Mag. X 7

BLOWHOLES IN EXPERIMENTAL INGOTS (ETCHED SECTIONS)

Fig. 29

PROXIMITY OF BLOWHOLES TO INGOT SURFACE
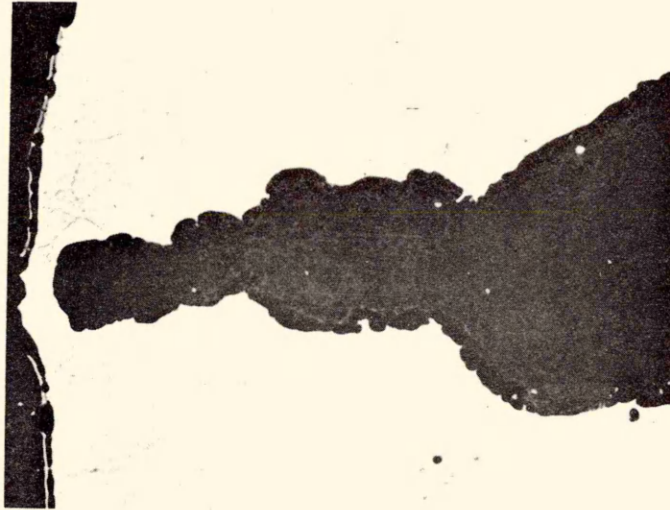
(a)
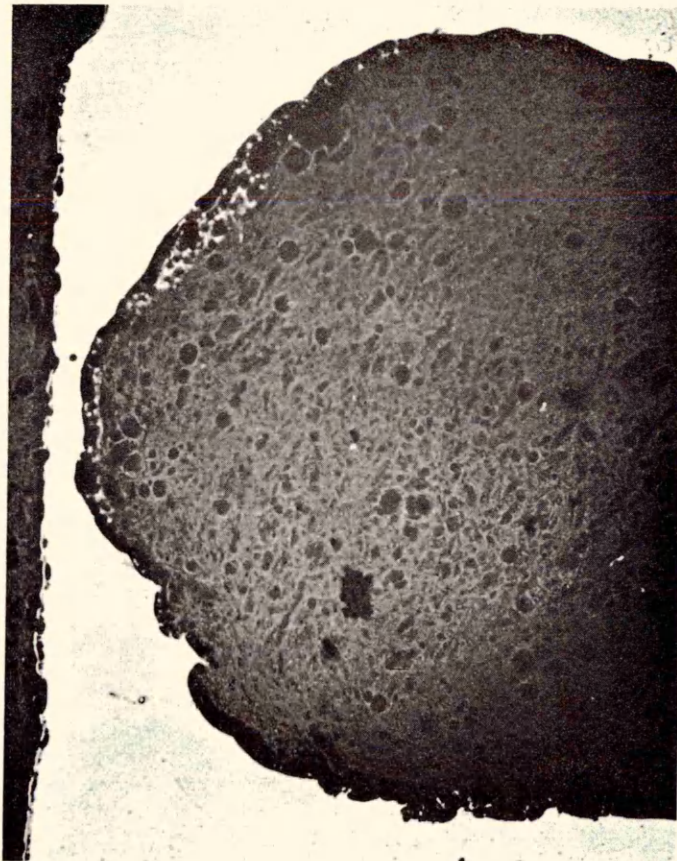
(b)

Mag. X 50

PROXIMITY OF BLOWHOLES TO INGOT SURFACE

Fig. 30
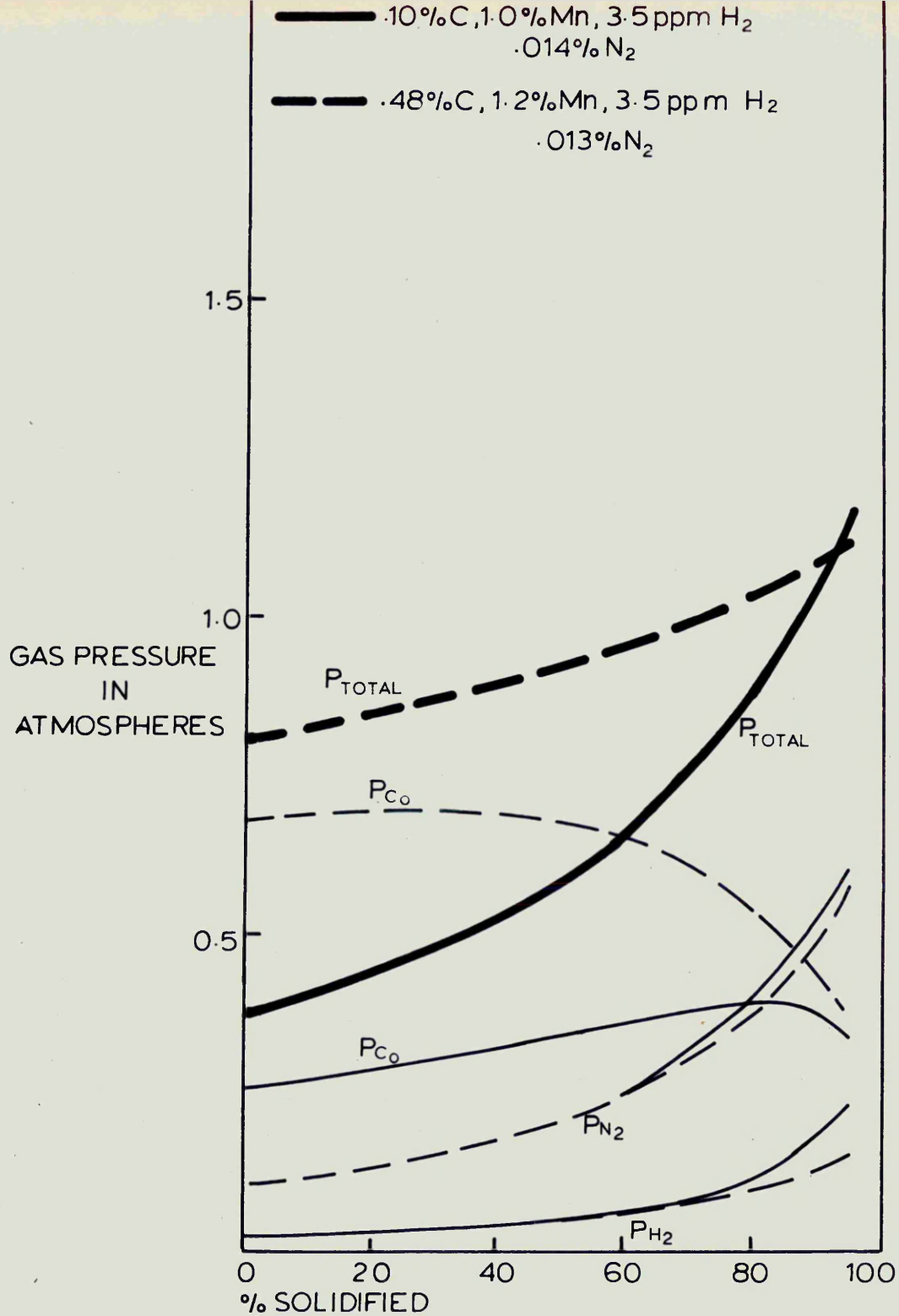
EXAMPLES OF THE CONTRIBUTIONS OF P_{Co}, P_{H_2}

AND P_{N_2} TO P_{TOTAL}

FIG. 31.

(a) ·05 C, 1·0 Mn, ·008 N₂ F.C.S. (b) ·10 C, 1·0 Mn, ·008 N₂ F.C.S.

Si	H
·03	7·3
·05	7·9
·10	8·5
·15	8·8
·25	9·1

Si	H
·03	6·6
·05	7·0
·10	7·3
·15	7·4
·25	7·5

P TOTAL IN ATOMSPHERES

% SOLIDIFIED
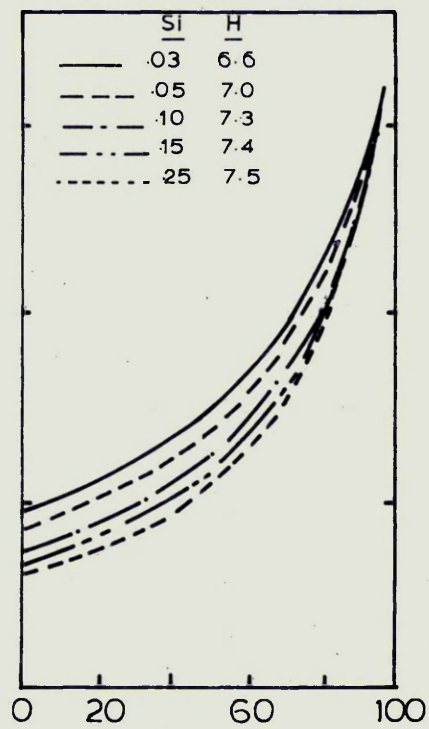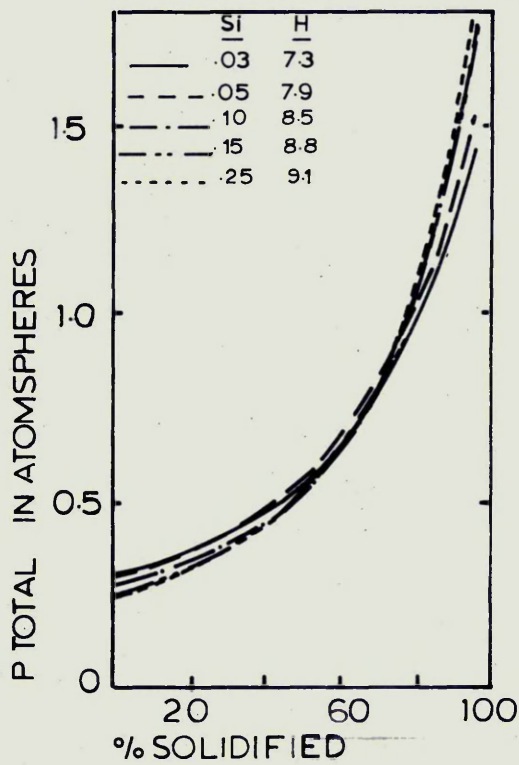
P_{TOTAL} VALUES FOR EXPERIMENTAL POROUS/SOLID BORDERLINE COMPOSITIONS IN FREE CUTTING STEEL

FIG. 32.

(a) ·10C, 1·0Mn, ·008N₂ PLAIN CARBON   (b) ·10C, 1·0Mn, 3·5ppm H₂ PLAIN CARBON
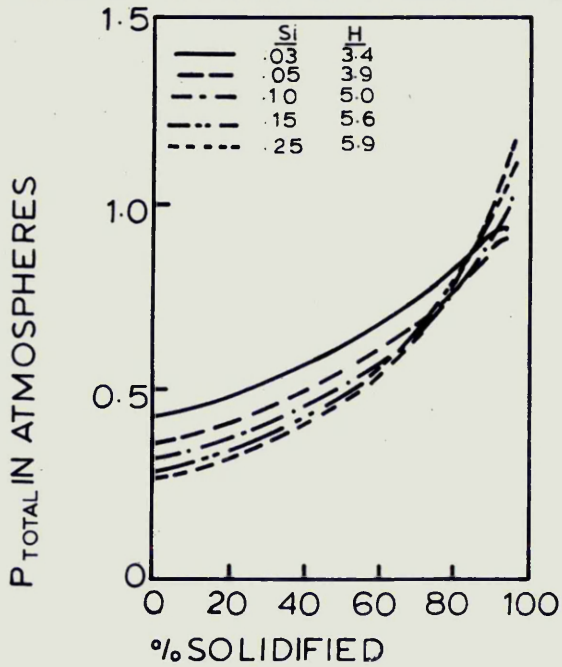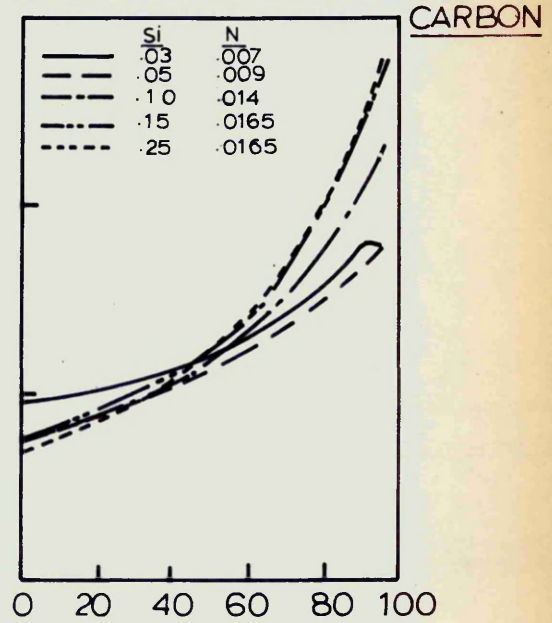
P_{TOTAL} VALUES FOR EXPERIMENTAL POROUS/SOLID

BORDERLINE COMPOSITIONS IN PLAIN 0·1% CARBON

STEELS

FIG. 33.

(a) $\cdot 20C$, $1\cdot0Mn$, $\cdot008N_2$ PLAIN CARBON (b) $\cdot48C$, $1\cdot2Mn$, $35ppm$ H_2 PLAIN CARBON
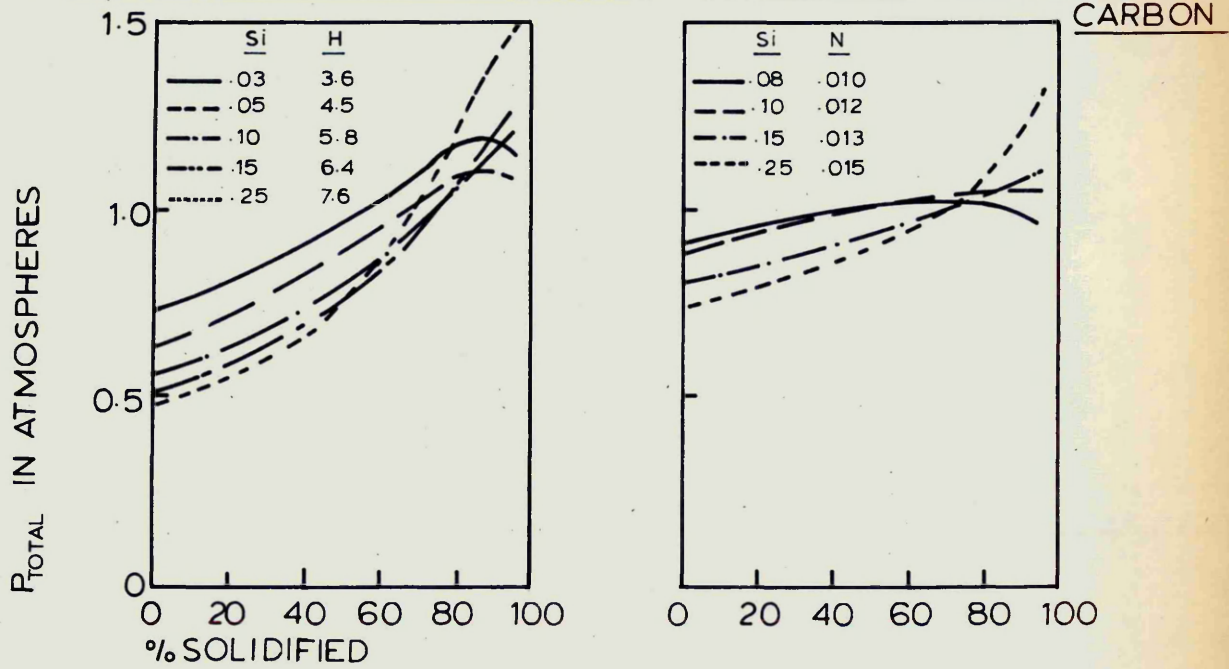
P_{TOTAL} VALUES FOR EXPERIMENTAL POROUS/SOLID BORDERLINE COMPOSITIONS IN PLAIN 0·2 AND 0·48% CARBON STEELS

FIG.34 .
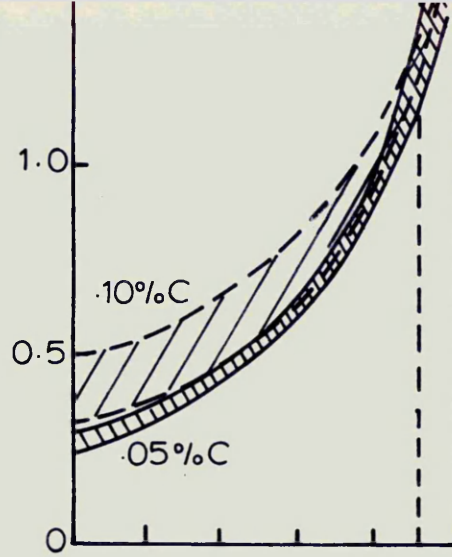
(a) FREE CUTTING STEELS
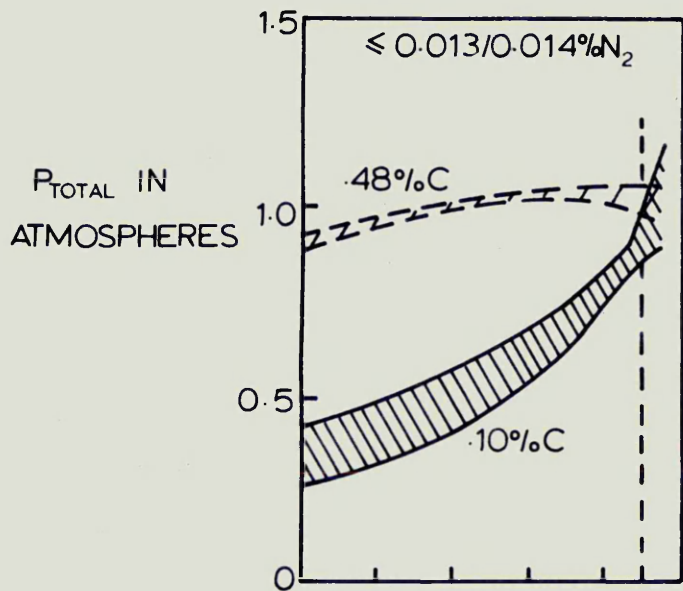
(b) LOW NITROGEN CARBON STEELS
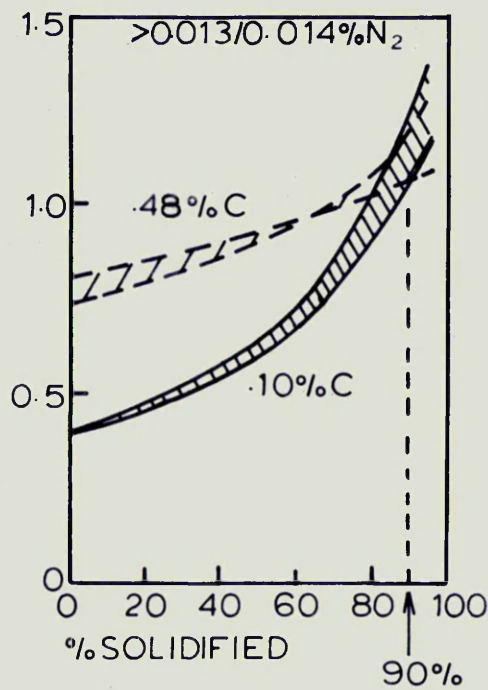
(c) HIGH NITROGEN CARBON STEELS

P_{TOTAL} SCATTER BANDS AND CONCEPT OF P_{TOTAL} (90%

SOLIDIFIED

FIG.35 .
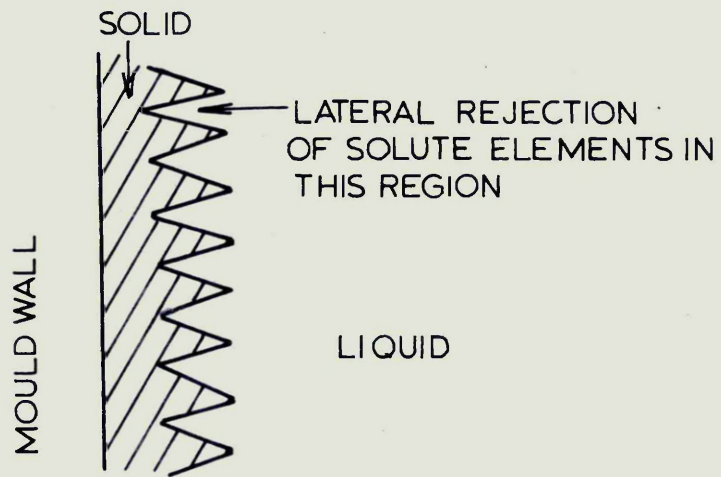
(a)
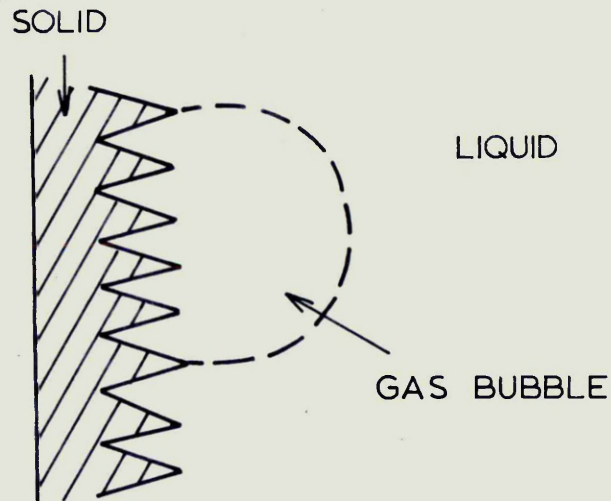
(b)

SCHEMATIC STRUCTURE AT SOLID/LIQUID INTERFACE

NEAR MOULD WALL AT TIME OF BLOWHOLE

NUCLEATION

FIG.36.
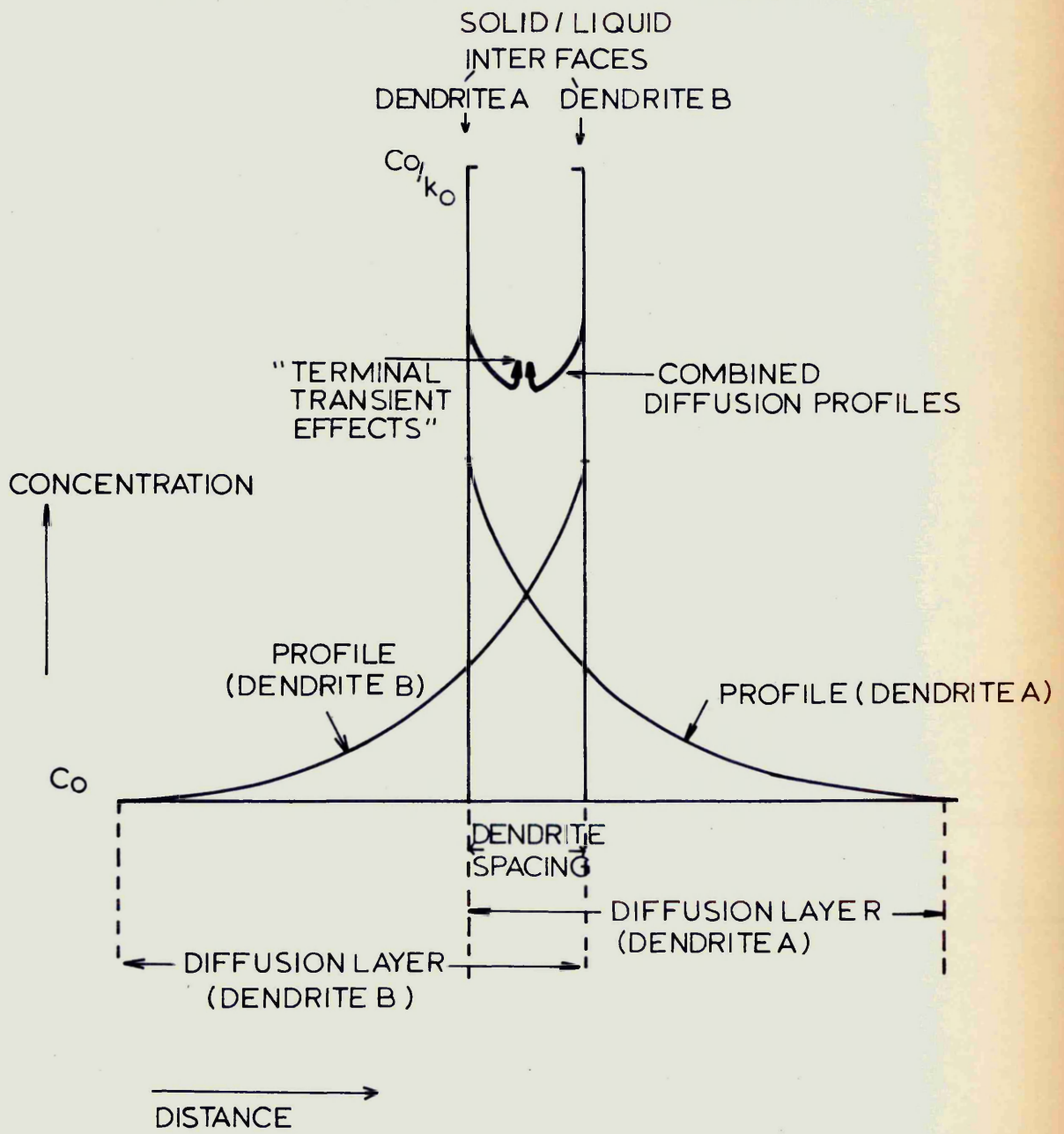
OVERLAPPING DIFFUSION PROFILES BETWEEN TWO
CLOSELY-SPACED DENDRITES

FIG. 37.

(a) 4 ppm H₂

(b) 8 ppm H₂

% SILICON

% MANGANESE
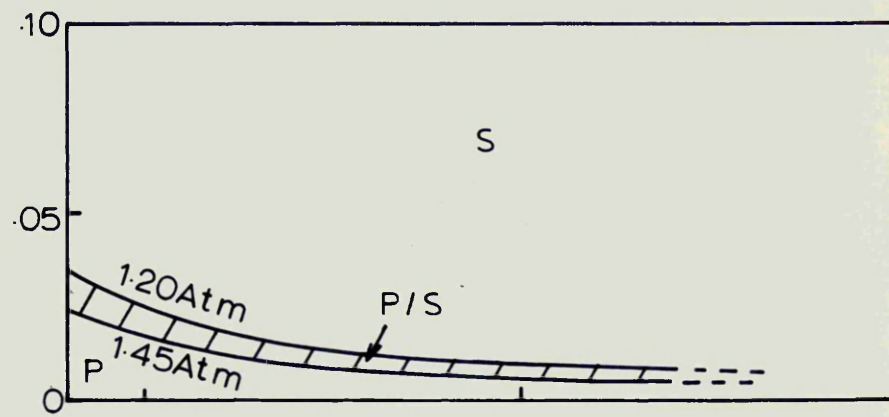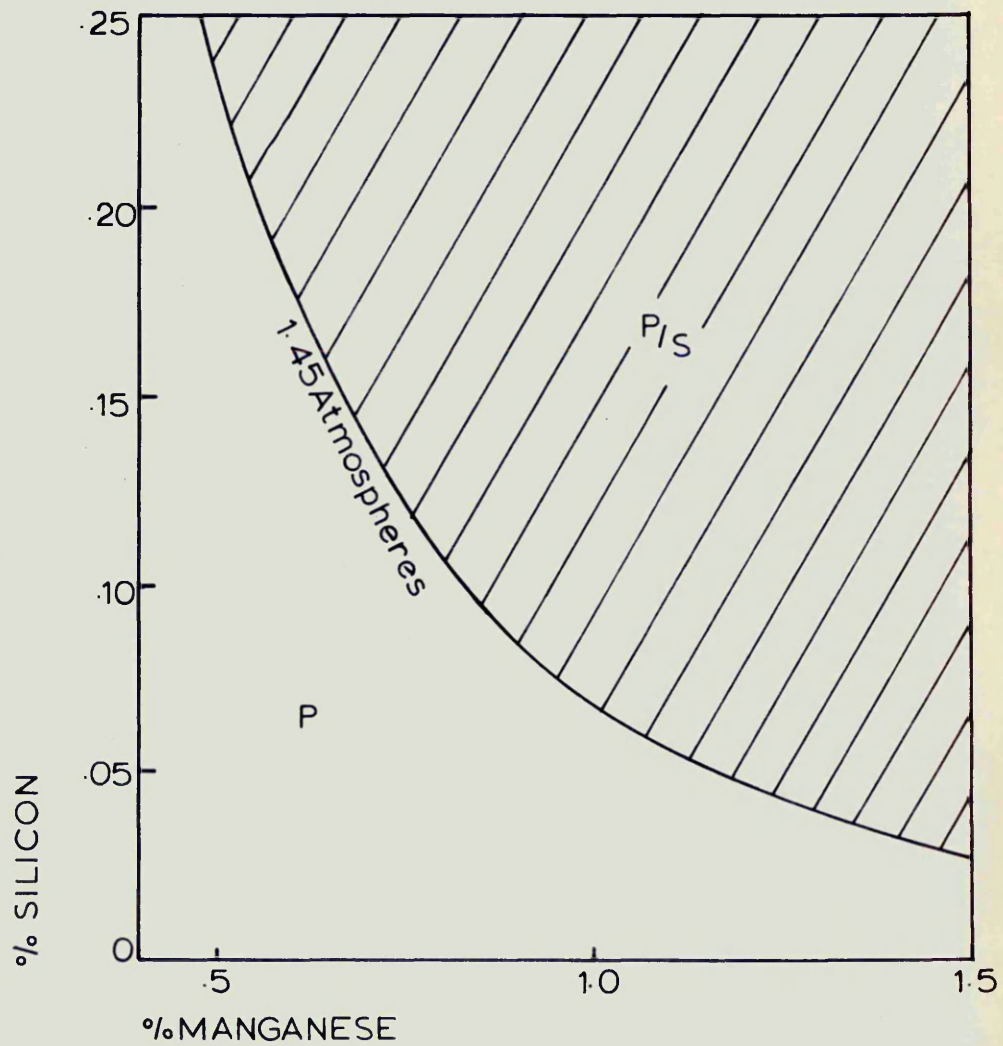
PREDICTED POROUS/SOLID COMPOSITIONS IN FREE

CUTTING STEELS (0·1% CARBON, 0·004 %NITROGEN)

FIG. 38.
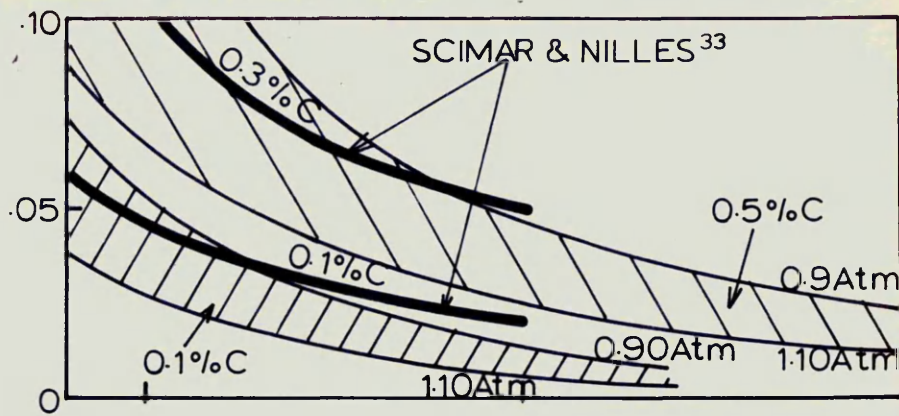
(b) 0.016% N₂
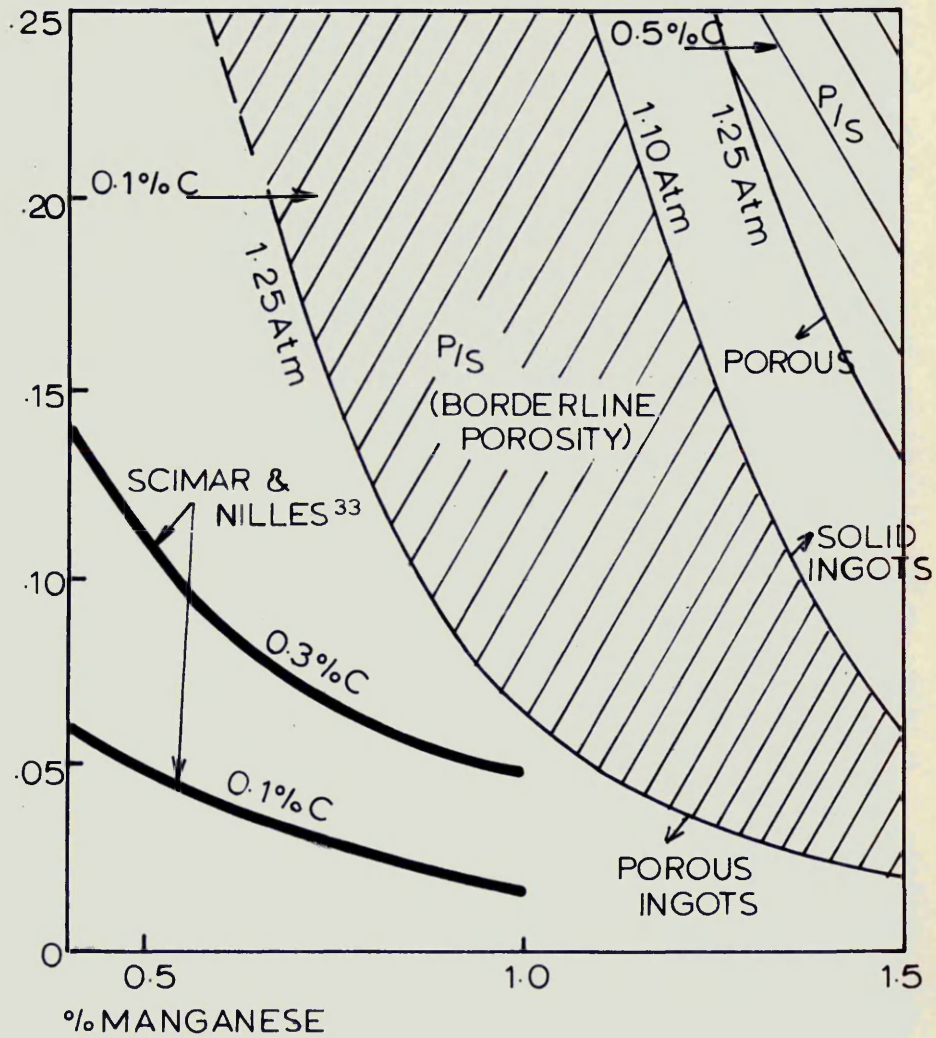
PREDICTED POROUS/SOLID BORDERLINE COMPOSITIONS IN PLAIN CARBON STEELS (0.1 AND 0.5% CARBON, 3ppm HYDROGEN)

FIG. 39.
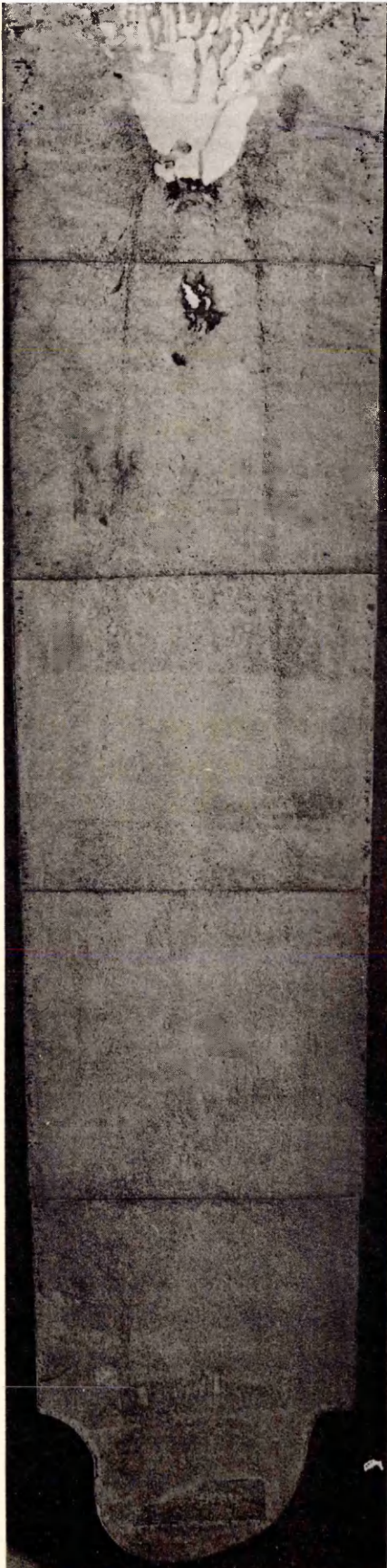
Analysis

    C   ·15%

  Mn 1·02%

  Si ·05%

  H 3·2ppm

  N ·010%

P_{Total} (90%)

1·09 Atmospheres

Mag. approx X 1/10

LADLE BALANCED INGOT ($3\frac{1}{2}$ TON, W.E.U.)

Fig. 40

COMMERCIAL INGOTS

• BALANCED
△ PIPED
x GASSY
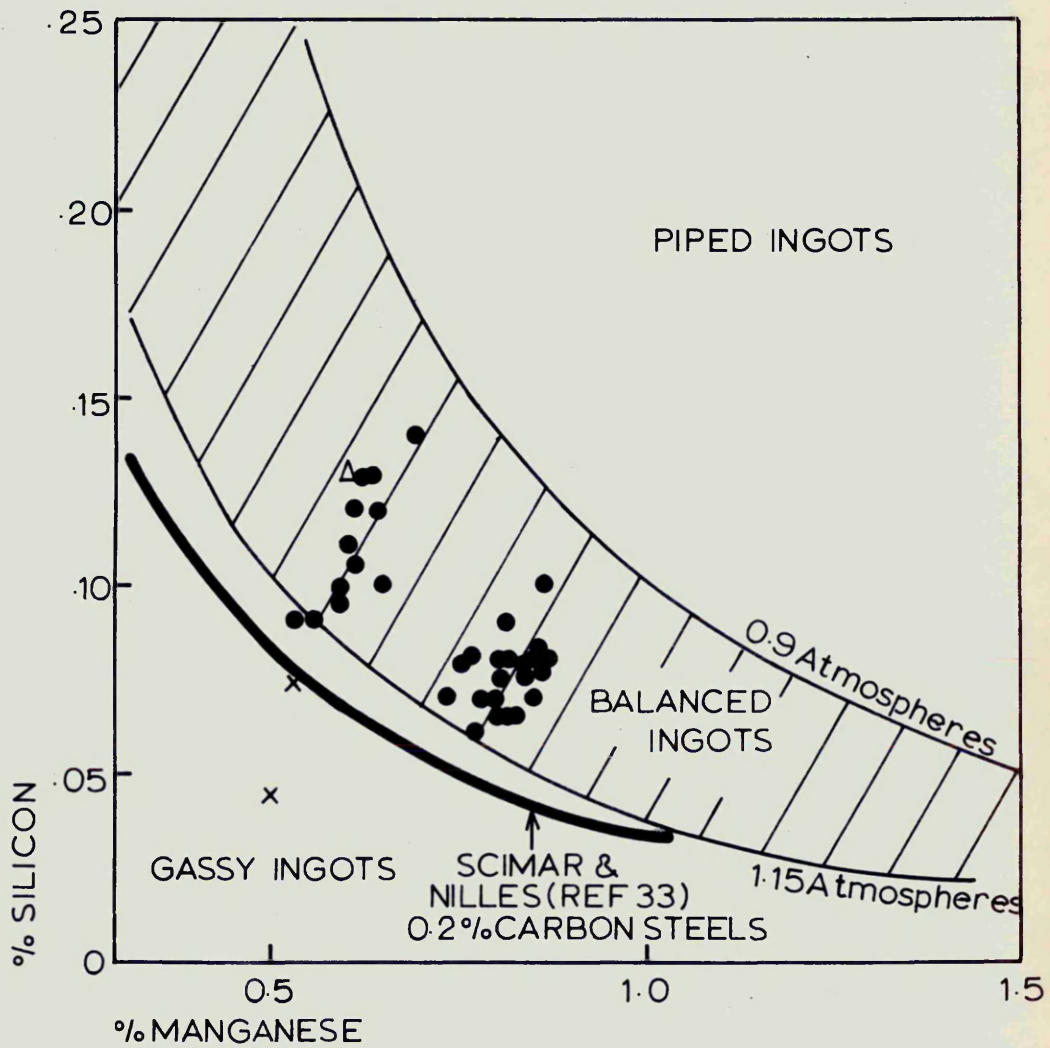
COMPARISON OF PREDICTED BALANCED STEEL
COMPOSITIONS WITH COMMERCIAL DATA ON 15 ton
INGOTS ($\cdot$2 /$\cdot$25%C; $\cdot$0035/$\cdot$0045%N$_2$; 4$\frac{1}{2}$/5$\frac{1}{2}$ppmH$_2$)

FIG. 41.
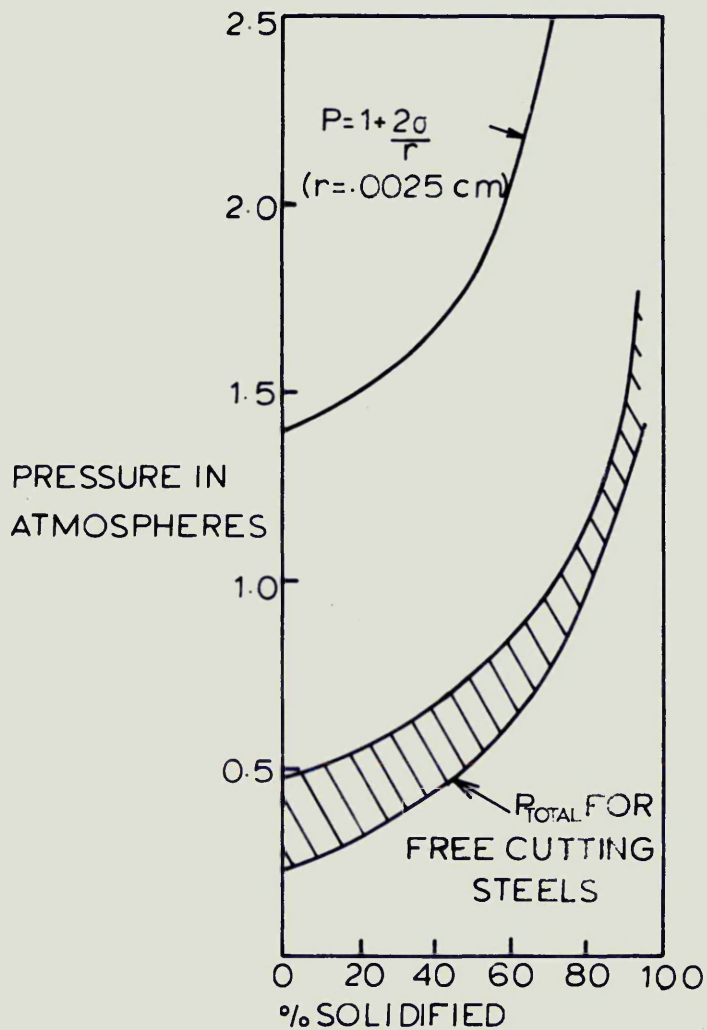
COMPARISON OF P_{TOTAL} FOR POROUS/SOLID
BORDERLINE FREE CUTTING STEELS WITH
GAS PRESSURE REQUIRED TO OVERCOME
$P_A + P_F + 2\sigma_r$ (P_A =1atmosphere P_F =0; σ =500
dynes/cm)

FIG. 42.

A.1 Basis of Computer Programme

A.1.1 Solute Enrichment Equations

Combining equations (4) and (8) and Tables VIII and IX the expressions for calculating solute enrichment in the liquid C_L, during solidification are as follows:-

	Solidification to δ		Solidification to γ	
Carbon	$C_L = \dfrac{C_0}{1-0.8g}$	.. (A1)	$C_L = \dfrac{C_0}{1-0.64g}$	.. (A2)
Oxygen	$C_L = \dfrac{C_0}{1-0.946g}$	.. (A3)	$C_L = \dfrac{C_0}{1-0.98g}$	.. (A4)
Hydrogen	$C_L = \dfrac{C_0}{1-0.73g}$	.. (A5)	$C_L = \dfrac{C_0}{1-0.55g}$	.. (A6)
Nitrogen	$C_L = \dfrac{C_0}{1-0.62g}$	.. (A7)	$C_L = \dfrac{C_0}{1-0.46g}$	.. (A8)
Manganese	$C_L = \dfrac{C_0}{(1-g)^{0.32}}$	.. (A9)	$C_L = \dfrac{C_0}{(1-g)^{0.05}}$	.. (A10)
Silicon	$C_L = \dfrac{C_0}{(1-g)^{0.40}}$	.. (A11)	$C_L = \dfrac{C_0}{(1-g)^{0.50}}$	.. (A12)

where C_0 = initial uniform concentration.

g = fraction of system solidified.

Solidification is assumed to occur in 5% incremental stages. At each stage of the solidification, say g^1, the concentration of solute is obtained from the concentration at the previous stage, $(g^1 - 0.05)$, say g. Hence if $C_L^{\ 1}$ is the concentration of solute in the liquid at

g^1 and C_L the concentration at g, C_L^1 is given by:-

$$C_L^1 = C_L \left[\frac{1-(1-k_o)g}{1-(1-k_o)g^1} \right] \quad .. \quad .. \quad .. \quad .. \quad .. \quad (A13)$$

for carbon, oxygen, hydrogen and nitrogen and by:-

$$C_L^1 = C_L \left[\frac{(1-g)^{1-k_o}}{(1-g^1)^{1-k_o}} \right] \quad .. \quad .. \quad .. \quad .. \quad .. \quad (A14)$$

for silicon and manganese.

The values of k_o are programmed to change from k^δ to k^γ (the equilibrium distribution coefficients of the various elements between liquid iron and δ- and γ-iron respectively) when the carbon concentration in the interdendrite liquid exceeds 0.5%.

A.1.2 Equilibrium Deoxidation Data

Including interaction effects, the equilibrium constant for the reaction, $\underline{C} + \underline{C} = CO(g)$, see equation 19, becomes

$$K_{CO} = \frac{P_{CO}}{\left[f_C . wt.\%C \right] \left[f_O . wt.\%O \right]} \quad .. \quad .. \quad .. \quad .. \quad (A15)$$

where f_C and f_O are calculated from:

$$\log_{10} f_C = e_C^C \left[wt.\%C \right] + e_C^O \left[wt.\%O \right] + e_C^{Mn} \left[wt.\%Mn \right] +$$
$$+ e_C^{Si} \left[wt.\%Si \right] \quad .. \quad .. \quad .. \quad (A16)$$

$$\log_{10} f_O = e_O^C \left[wt.\%C \right] + etc. \quad .. \quad .. \quad .. \quad .. \quad (A17)$$

($e_C^C = + 0.22$; $e_C^{Mn} = - 0.012$; $e_C^{Si} = + 0.07$; $e_C^O = -0.31$

$e_O^C = - 0.41$; $e_O^{Mn} = - 0.021$; $e_O^{Si} = - 0.16$; $e_O^O = - 0.20$)

It is assumed that the temperature dependence of K_{CO} remains unaltered when interaction effects are

considered and K_{CO} may be obtained from the expression:

$$\log_{10} K_{CO} = \frac{1168}{T} + 2.07 \quad \cdots \quad \cdots \quad \cdots \quad \cdots \quad (A18)$$

which appeared in the original method. T is in degrees absolute and the expression is valid only up to 1.0% carbon.

For combined deoxidation with manganese and silicon, Turkdogan considered the following reaction:

$$\underline{Si} + 2MnO(S) = 2\underline{Mn} + SiO_2(S) \quad \cdots \quad \cdots \quad \cdots \quad (A19)$$
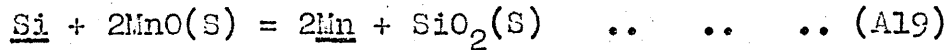
The equilibrium constant for this reaction is:

$$K_{Mn-Si} = \frac{[\%Mn]^2 a_{SiO_2}}{[\%Si](a_{MnO})^2} \quad \cdots \quad \cdots \quad \cdots \quad \cdots \quad \cdots \quad (A20)$$

where K_{Mn-Si} is given by:

$$\log_{10} K_{Mn-Si} = \frac{510}{T} + 1.77 \quad \cdots \quad \cdots \quad \cdots \quad \cdots \quad (A21)$$

Turkdogan derived equation A21 from other published data, a_{SiO_2} and a_{MnO} are activities of oxides in the molten deoxidation product $MnO.SiO_2$ with respect to the solid oxides. Manganese and silicon concentrations are in weight percent.

Fig. (A1) shows the activity of MnO in various $MnO.SiO_2$ melts, given in a log-log plot. The plot of $\log a_{MnO}$ vs. $\log {}^{a}SiO_2/(a_{MnO})^2$ is considered to approximate to a straight line, for the present purposes, and is expressed as:

$$a_{MnO} = b_4 \left[\frac{a_{SiO_2}}{(a_{MnO})^2} \right]^{b_3} \quad \cdots \quad \cdots \quad \cdots \quad \cdots \quad (A22)$$

where $b_3 = -0.2915$ and $b_4 = \exp.(2.7309 - 0.001919T)$.

In order to calculate the dissolved oxygen in equilibrium with manganese and silicon, Turkdogan considered a further reaction involving FeO and MnO. For liquid metal and solid MnO.FeO phase, the binary oxide solution can be taken as ideal and it is possible to obtain the following expression:

$$K_{Mn-O} = \frac{N_{MnO}}{\%Mn \; \%O} \qquad \text{(for solid oxide)} \quad .. \quad .. \quad (A23)$$

where $\log_{10} K_{Mn-O} = \frac{14950}{T} - 6.68 \qquad .. \quad .. \quad .. \quad .. \quad (A24)$

Equation A23 is true only for FeO-MnO mixtures. However K_{Mn-O} is applicable to any other solid or liquid oxide or silicate containing, MnO, providing a_{MnO} (with respect to solid MnO) is used instead of N_{MnO} in equation A21. a_{MnO} is the activity of MnO in the oxide or silicate system considered.

The sequence of steps involved in calculating the dissolved oxygen is as follows:

(i)   Compute $a_{SiO_2}/(a_{MnO})^2$ for known manganese and silicon concentrations, see equations A20 and A21.

(ii) Obtain a_{MnO} from equation A22.

(iii) Insert a_{MnO} in place of N_{MnO} in equation A23 to obtain the oxygen concentration (having first evaluated A24)

Having carried out the above procedure, and knowing the carbon content of the liquid steel, P_{CO}

can be calculated from equations A15 to A18.

The reactions which occur during solidification while the solute concentrations in the liquid are changing must now be examined.

A.1.3 Deoxidation by Manganese and Silicon During Solidification

Consistent with Turkdogan, it is assumed that heterogeneous nucleation of an oxide phase at the solid/liquid interface can take place with negligible supersaturation.

Consider, at a particular stage of solidification, g^1, that the liquid phase contains C_O^1 percent oxygen, C_{Si}^1 percent silicon, and C_{Mn}^1 percent manganese, in equilibrium with $MnO.SiO_2$. On further solidification at g^{11}, concentrations of solutes, calculated from equations A13 and A14 will be C_O^{11}, C_{Si}^{11} and C_{Mn}^{11} respectively. Since the new concentrations are above those for Mn-Si-O equilibrium, reaction will take place producing more $MnO.SiO_2$. The mass balance of solutes is given by:-

$$(C_O^{11} - C_O) = \frac{32}{28.09} (C_{Si}^{11} - C_{Si}) + \frac{16}{54.94} (C_{Mn}^{11} - C_{Mn}) \quad .. \text{ (A25)}$$

where C_O, C_{Si} and C_{Mn} represent the equilibrium concentrations after deoxidation at g^{11}. If the composition of silicate formed is given by N_{MnO}/N_{SiO_2}, stoichiometric requirements give:

$$(C_{Mn}^{11} - C_{Mn}) = \frac{54.94}{28.09} \cdot \frac{N_{MnO}}{N_{SiO_2}} (C_{Si}^{11} - C_{Si}) \quad .. \quad .. \quad .. \text{ (A26)}$$

The relationship between a_{MnO} and N_{MnO}/N_{SiO_2} is given in fig. A1(b). The lines are assumed to be straight and given by:-

$$\frac{N_{MnO}}{N_{SiO_2}} = b_1 + b_2 \cdot a_{MnO} \quad .. \quad .. \quad .. \quad .. \quad .. \quad (A27)$$

where $b_1 = 0.5$ and $b_2 = -4.3165 + 0.003716T$.

C_O, C_{Si} and C_{Mn} are obtained by solving the six simultaneous equations A20, A22, A23, A25-27. For this a method of successive approximations is used. P_{CO} is now calculable at g^{11} at the temperature concerned, the concentration of carbon having been obtained from equation A13. The above process is then repeated for each increment of the solidification process.

The above method deviates slightly from Turkdogan's. First of all at high manganese levels he ignored slight changes in manganese content due to reaction (i.e. $C_{Mn}^{11} \simeq C_{Mn}$). These changes were accounted for in the present method. Secondly, in plotting the change in oxygen content in the inter-dendrite liquid during freezing, Turkdogan assumed various oxygen contents at nil percent solidified, irrespective of the initial manganese and silicon concentrations. He then derived an expression showing the critical stage of solidification for the onset of deoxidation reactions. His curves, therefore, showed an initial oxygen enrichment with no deoxidation taking place, followed by a residual

oxygen determined by the manganese and silicon.
In the present method, it is assumed that the
residual oxygen content is determined by manganese
and silicon throughout the whole range of solidifica-
tion. It is felt that this is more appropriate to
air melting since the initial residual oxygen content
of the steel prior to solidification will be determined
by the initial concentration of deoxidants in the
steel.

A.1.4 Hydrogen and Nitrogen Partial Pressures

Including interaction effects, the equilibrium
constants for dissolution of hydrogen and nitrogen
in liquid steel become:

$$K_H = \frac{f_H \cdot [ppmH]}{(P_{H_2})^{\frac{1}{2}}} \qquad .. \quad .. \quad .. \quad .. \quad .. \quad (A28)$$

and

$$K_N = \frac{f_N \cdot [wt.\%N]}{(P_{N_2})^{\frac{1}{2}}} \qquad .. \quad .. \quad .. \quad .. \quad .. \quad (A29)$$

where $\log f_H = e_H^C [wt.\%C] + e_H^{Mn} [wt.\%Mn] + e_H^{Si} [wt.\%Si]$ (A30)

$$\log f_N = e_N^C [wt.\%C] + etc. \qquad .. \quad .. \quad .. \quad (A31)$$

The temperature dependence of K_H and K_N is as
follows:

$$\log_{10} K_H = -\frac{1637}{T} + 2.316 \qquad .. \quad .. \quad .. \quad .. \quad (A32)$$

$$\log K_N = -\frac{188.1}{T} + 1.246 \qquad .. \quad .. \quad .. \quad .. \quad (A33)$$

The calculation of P_{H_2} and P_{N_2} is fairly straightforward. Following the calculation of the hydrogen and nitrogen concentrations, using equation A13 at a particular stage of solidification, and knowing the carbon, manganese and silicon concentrations at the same stage of solidification, (see earlier), the gas pressures are obtained from equations A28-33.

A.1.5 <u>Effect of Varying the Liquidus Temperature</u>

Before any of the reactions can be evaluated, the equilibrium constants must be calculated for the temperature, T, in question. The liquidus temperature is assumed to be determined solely by the carbon content of the steel. The liquidus curves in the iron-carbon phase diagram, see fig. 17, are assumed linear and it is possible to express the liquidus temperature as follows:

(i) Solidification to δ-iron ($\leq 0.5\%$ carbon)

$$T^{\circ}K = 1810 - \frac{\Delta T}{\Delta(\%C)} \cdot (\%C) \quad .. \quad .. \quad .. \quad .. \quad (A34)$$

where ΔT = change in temperature.

$\Delta(\%C)$ = change in carbon content to produce ΔT.

Hence $T^{\circ}K = 1810 - \frac{(1810-1772)}{(0.52-0)} \cdot (\%C)$

$\therefore T^{\circ}K = 1810 - 73(\%C) \quad .. \quad .. \quad .. \quad .. \quad (A35)$

(ii) For solidification to γ-iron ($> 0.5\%$ carbon)

$$T^{\circ}K = 1772 - \frac{(1772-1425)}{(4.27-0.52)} \cdot (\%C-0.52)$$

$\therefore T^{\circ}K = 1819 - 91.3(\%C) \quad .. \quad .. \quad .. \quad .. \quad (A36)$

The computer programme may be operated in two ways:

(a)   T is determined by the initial carbon content and remains constant throughout solidification.

(b)   T changes throughout solidification as carbon varies. Should the carbon content exceed 0.5%, then equation A35 is replaced by A36. Though this part of the programme has been considered last, the procedure cannot begin until T is known.

A.2   Effects of Modifications on gas pressure calculations

A.2.1 Carbon Monoxide Partial Pressure, P_{CO}

Before considering the effects of the modifications on P_{CO}, the effect of changing silicon content, particularly at low silicon levels will be demonstrated, see fig. A2. It will be noted that the calculated P_{CO} changes extremely rapidly when the silicon content of the steel is varied in the range nil to 0.03%. Beyond this level the change in P_{CO} becomes less marked as silicon varies.

A.2.1.1 Interaction effects

Examples of interaction effects on P_{CO} are given in figs. A3-5. Carbon levels considered are 0.10% (fig. 3), 0.20% (fig. 4) and 0.50% (fig. 5) at a constant manganese level of 1.0%. Only 0.10% silicon is considered at 0.20 and 0.50% carbon, but at 0.10% carbon, three levels of silicon are dealt with. It is found that the interaction

coefficients lowering f_C and f_O to values less than unity, see Tables IV and V, are dominant. Consequently, the net effect of introducing the coefficients into the calculations is to lower the product $f_C \cdot f_O$, and hence P_{CO}. The magnitude of these changes is found to increase with:

(i) increasing carbon content for fixed manganese and silicon levels and at a particular stage of solidification.

(ii) increasing % solidified for a particular initial composition.

(iii) increasing silicon content for fixed carbon and manganese levels at a particular stage of solidification. (Though not shown, a similar result is obtained if the manganese is increased at constant carbon, silicon and % solidified).

Because of the greater initial values of P_{CO} (i.e. before interaction) at the higher carbon levels, the magnitude of the change in P_{CO} at these levels is much higher than at low carbon levels. In fig. A3 it is evident that the changes in P_{CO} at 0.03% silicon caused by interaction are larger than at 0.10 and 0.25% silicon. This is only because, initially, P_{CO} at 0.03% silicon is higher than at 0.10 and 0.25%. The percentage change in P_{CO} increases with increasing silicon content according to point (iii) above.

The gas pressures in figs. A3 to A5 were calculated at constant temperatures, each temperature being determined by the initial carbon content of the steel under consideration according to equations A35 and A36. For 0.10, 0.20 and 0.50% carbon, the temperatures were 1530, 1522 and 1500°C respectively.

A.2.1.2 Effect of δ to γ change

None of the P_{CO} curves in fig. A3 and A5 show the effects of exceeding 0.5% carbon during solidification. For 0.10% carbon, the primary solidification phase was δ at all stages of solidification, while for 0.50% carbon, the primary phase was γ at all times. The effects of phase change during the solidification process are, however, shown clearly in figs. A4 and A6, where P_{CO} curves for a 0.20% carbon steel are considered. The carbon level exceeds 0.5% at approximately 75% solidified, causing the normally smooth curves to 'kink'. In fig. A6 the pressures were calculated ignoring interaction effects. It is seen that allowing the distribution coefficients to change during the course of solidification produces a decrease in P_{CO}, causing the curves to level off from about 75% solidified onwards. In fig. A6 pressure curves were drawn primarily to demonstrate the interaction effects mentioned earlier, but show clearly that P_{CO} levels off when solidification to γ begins.

A.2.1.3 Effect of Varying Solidification Temperature

Constant and varying temperature calculations are compared in figs. A7 to A9. In the case of constant temperature calculations, the solidification temperature is determined by the initial carbon content of the steel (i.e. at nil% solidified) and remains fixed. For varying temperature calculations, the reaction temperature is governed at each stage of solidification by the carbon content of the enriched interdendritic liquid. In all cases interaction effects are included.

The values of P_{CO} obtained by varying the solidification temperature are lower than at constant temperature. The difference in P_{CO} increases during solidification as the carbon concentrates in the interdendritic liquid. Also, the effect of varying temperature becomes more pronounced as the initial carbon content of the steel increases. Carbon levels considered are again 0.10, 0.20 and 0.50%, at 1.0% manganese. The δ to γ change in the 0.20% carbon steels does not appear to affect the trend in results. At 0.20 and 0.50% carbon only 0.10% silicon is considered, but at 0.10% carbon, 0.03, 0.25% silicon are also again dealt with. The magnitude of the drop in P_{CO}, resulting from varying temperature, increases with decreasing silicon. However it is found that the percentage drop in P_{CO} remains constant, as is to be expected since the temperature effects are governed solely by the carbon content of the steel.

It was shown in Turkdogan's paper [46] that a reduction in temperature reduces the oxygen in solution.

(See also section A.1.2 of the Appendix). Since the liquidus temperature decreases with increasing carbon content, it is obvious that allowing the temperature to change in this way will result in a reduction in the dissolved oxygen, and hence P_{CO}.

The changes in P_{CO}, resulting from varying the solidification temperature, are smaller than those caused by interaction effects.

A.2.2 <u>Hydrogen and Nitrogen Partial Pressures, P_{H_2} and P_{N_2}</u>

Before considering the effects of modifications on P_{H_2} and P_{N_2}, it is pertinent to demonstrate the variation in these gas pressures during solidification using the data supplied by Turkdogan [46]. This is done in figs. A10 and 11, for 3, 5 and 7 ppm hydrogen and 0.004, 0.008, 0.012 and 0.016% nitrogen. Curves for both δ and γ solidification are shown and it is evident that gas pressures developed during solidification to δ are greater than those during solidification to γ

In order to simplify the diagrams showing the effects of interaction, etc., only single levels of hydrogen and nitrogen were considered. To demonstrate the effects most clearly, fairly high levels of the two gases, (with respect to the levels obtained in the majority of modern steel-making practices for plain carbon steels) were chosen, viz. 7 ppm hydrogen and 0.016% nitrogen. At lower concentrations than these, the effects of interaction, etc., will be less pronounced.

A.2.21 Interaction effects

Examples of interaction effects are shown in figs. A12-17 for the three carbon levels 0.10, 0.20 and 0.50%, constant 1.0% manganese and 0.10% silicon. For hydrogen the net effect of interaction is to increase P_{H_2} at each of the chosen compositions and at both the beginning and end of solidification. This is because the positive interaction terms for carbon and silicon, see Tables VI and VII, are found to be larger than the negative terms for manganese, and hence f_H exceeds unity. For a particular composition the change in P_{H_2} resulting from interaction increases progressively during solidification, due mainly to the fact that carbon concentrates at a faster rate than manganese in the interdendritic liquid. In the case of nitrogen, in the 0.10% carbon steels, the negative term for manganese was found just to outweigh the positive terms for carbon and silicon during the very early stages of solidification, and f_N was just less than unity. However the drop in P_{N_2} this produces is too small to show in fig. A13. As solidification in the 0.10% carbon steel progresses, f_N exceeds unity and P_{N_2} is higher than when no interaction is considered, but the change in P_{N_2} is small. With increasing carbon content, the increases in gas pressures become more marked. The effects of increasing manganese and silicon on P_{H_2} and P_{N_2} are shown only qualitatively in figs. A12-A17, where the pressures were calculated at

constant temperature, each temperature being determined by
the carbon content of the steel at nil% solidified.

A.2.2.2 Effect of δ to γ change

The effects of changing from δ to γ during solidifica-
tion on P_{H_2} and P_{N_2} are shown in figs. A14 and A15. The
phase change occurs at approximately 70% solidified, where-
upon the gas pressures begin to increase less rapidly than
at earlier stages of solidification, in accordance with the
change in distribution coefficients, see figs. A10 and A11.
The differences in pressure so produced increase as
solidification progresses following the phase change.
However, as shown in figs. A14 and A15, interaction effects
may offset these differences.

A.2.2.3 Effect of Varying Solidification Temperature

Constant and varying temperature calculations are
compared in figs. A18-23. Interaction effects are
included in all the calculations. As before, three carbon
levels 0.10, 0.20 and 0.50% are considered, at constant
1.0% manganese and 0.10% silicon.

Equations A32 and A33 show that the solubilities
of hydrogen and nitrogen decrease with decreasing
temperature. Consequently as the carbon content of the
steel increases, P_{H_2} and P_{N_2} must decrease for given
hydrogen and nitrogen concentrations. The effect on
P_{N_2} is small even in the 0.50% carbon steel, where the
change in solidification temperature during solidification
is some 75°C. The effect on P_{H_2} is slightly more pronounced

than on P_{N_2}, but the changes are less than those produced by interaction and the δ to γ phase change. Changes produced by varying the solidification temperature supplement those produced by interaction but offset those resulting from the δ to γ transition.

A.2.3 Combined effects of Modifications on Gas Pressures

Since the original purpose of the theoretical work was to calculate the total pressure of gases in the steel, P_{Total} $(= P_{CO} + P_{H_2} + P_{N_2})$, the combined effect of interaction, etc. on this pressure will be demonstrated together with the effects on P_{CO}, etc. The results are shown in figs. A24-A26.

It was shown that interaction, varying temperature and the δ to γ change all reduce P_{CO}. These effects, added together result in a marked decrease in P_{CO}, which becomes more pronounced as the initial carbon content of the steel increases and as solidification proceeds. In the 0.10 and 0.50% carbon steels, figs. A24 and A26, the net effect of modifications on P_{H_2} and P_{N_2} is an increase in pressure which becomes more pronounced with increasing carbon and as solidification proceeds. In the 0.20% carbon steels, fig. A25, P_{N_2} is greater after modifications than before them, but the difference is reduced to some extent during the later stages of solidification by the effects of the δ to γ change. For P_{H_2}, the effect of the phase change is large enough, late in solidification, to cause the pressures, calculated after modifications, to fall just

below those obtained without the modifications. The
pressure curves for P_{H_2} in fig. A25 in fact cross at
90% solidified.

The outcome of the effects described above is a
reduction in P_{Total}. At 0.1% carbon the change in P_{Total}
is fairly small, since the decrease in P_{CO} is almost
matched by increases in P_{H_2} and P_{N_2}, which take effect
particularly during the later stages of solidification.
At 0.20% carbon, the reduction in P_{Total} is more marked
than at 0.10%, in particular during the later stages of
solidification after the phase change. The reduction
in P_{Total} is even more marked at 0.50% carbon, than it is
at 0.20% carbon except at 95% solidified. Here, the
effect of the $\delta - \gamma$ change in the 0.20% carbon steels causes
the drop in P_{Total} to exceed that in the 0.5% carbon
steels.
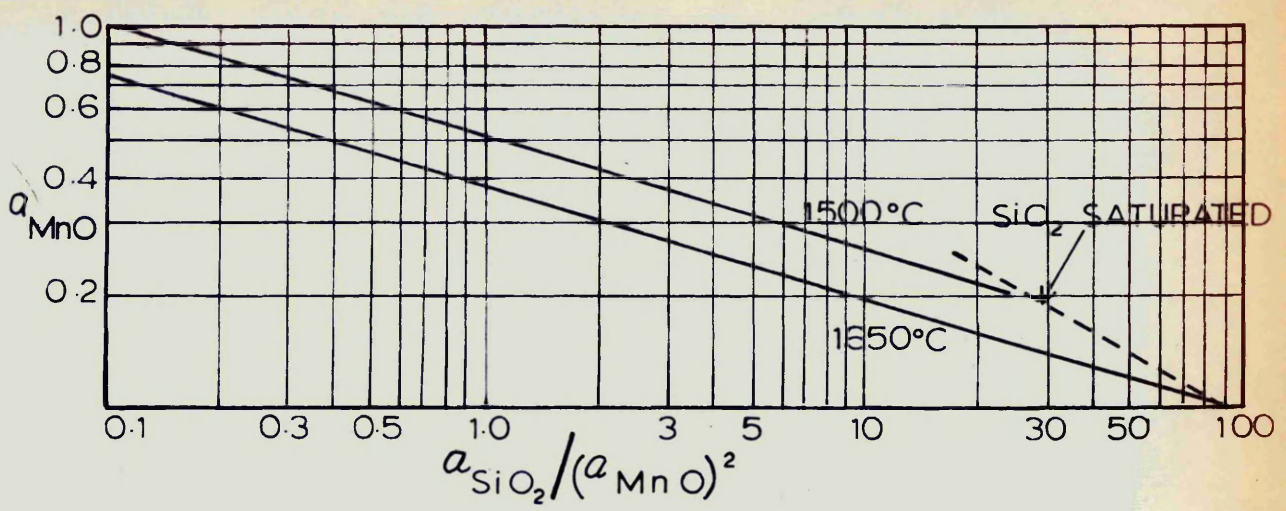
(b.)
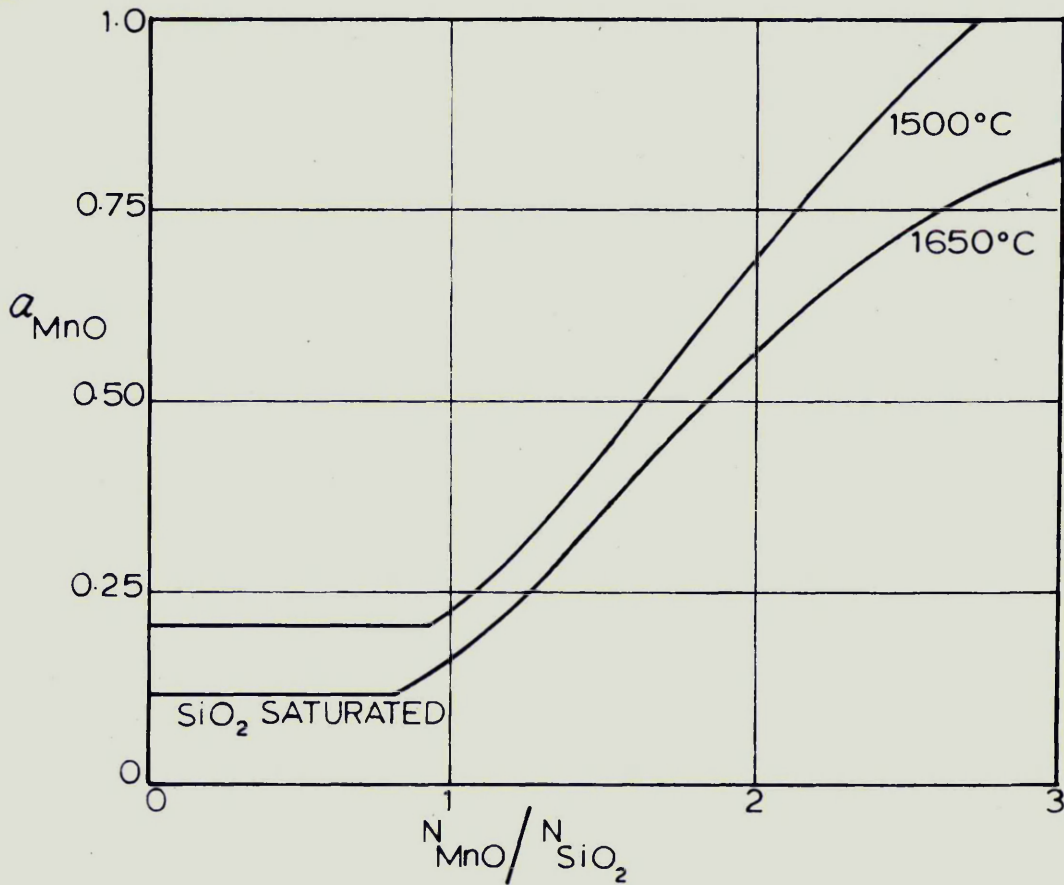
ACTIVITY RELATIONS FOR MOLTEN MnO-SiO$_2$ SYSTEM
WITH RESPECT TO SOLID OXIDES AS STANDARD STATES
FIG. A1
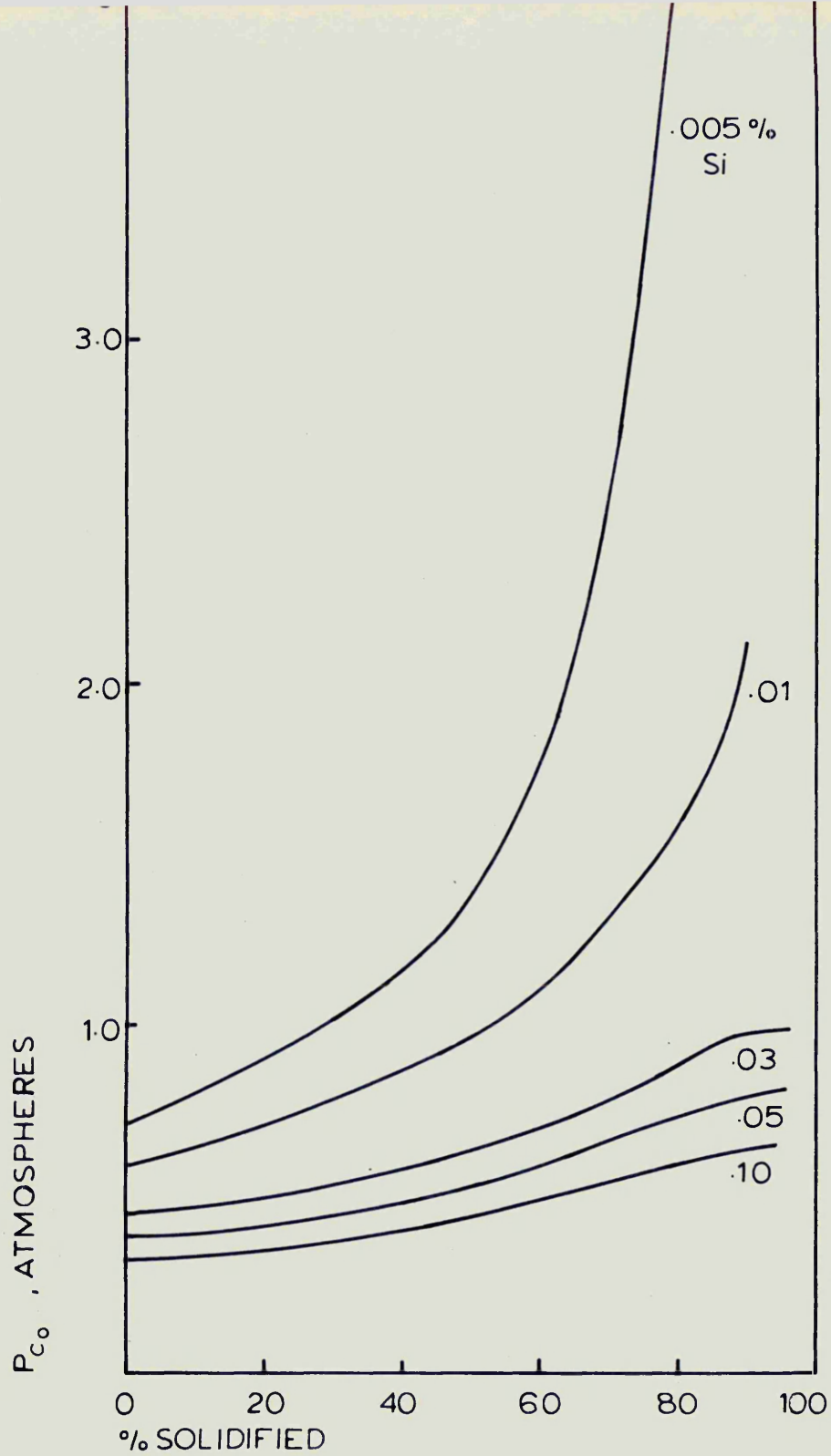
EFFECT OF VARYING SILICON ON P_{Co} AT 0.10%
CARBON AND 1.0% MANGANESE AT 1525°C (NO
MODIFICATIONS MADE TO THEORY)

FIG. A2.
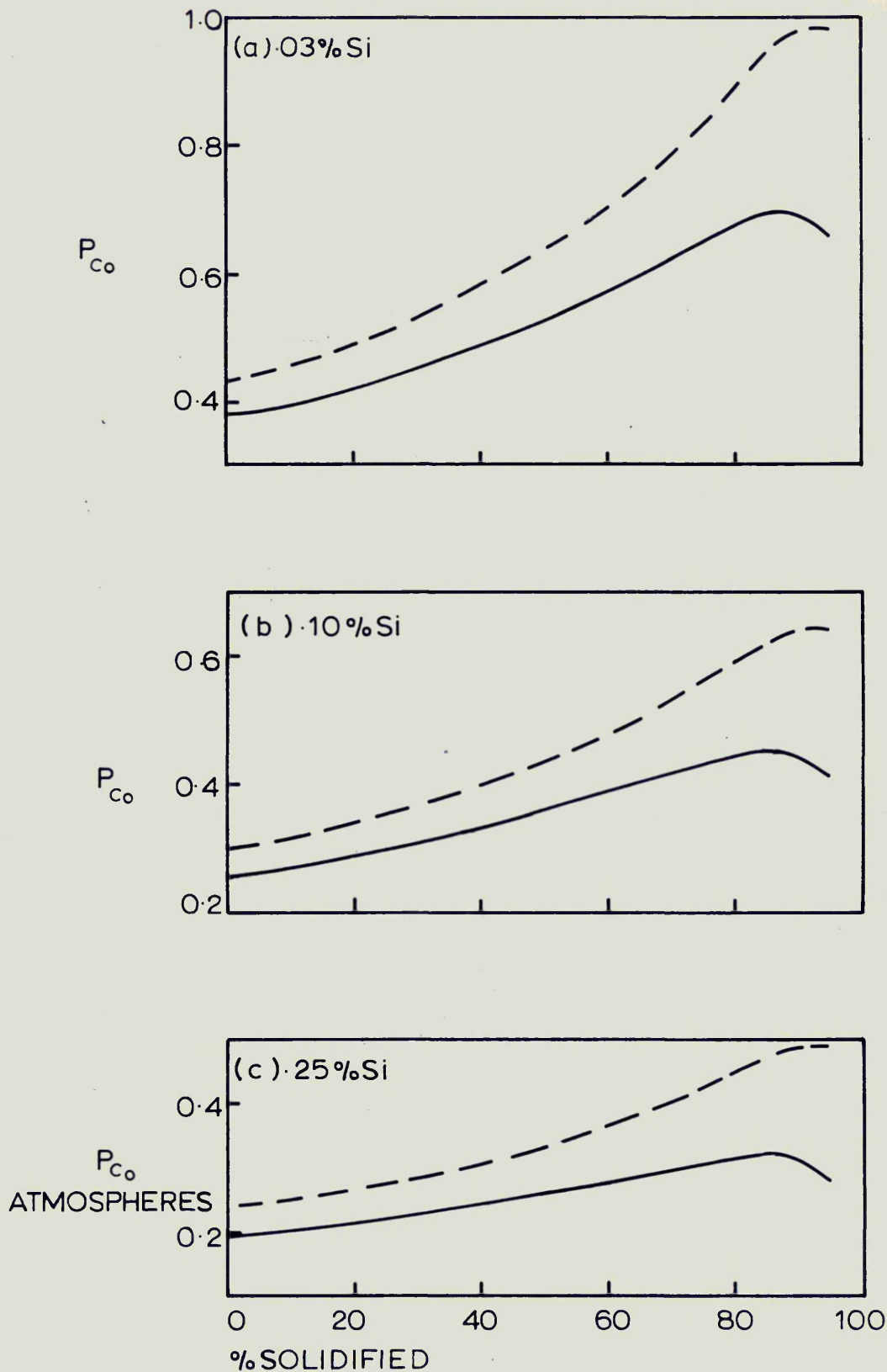
EFFECT OF INTERACTION COEFFICIENTS e_c^x AND e_o^x

$(x = C, Mn, Si, O)$ ON P_{CO} IN STEEL CONTAINING $1.0\% C$

AND $1.0\% Mn$

FIG. A3.
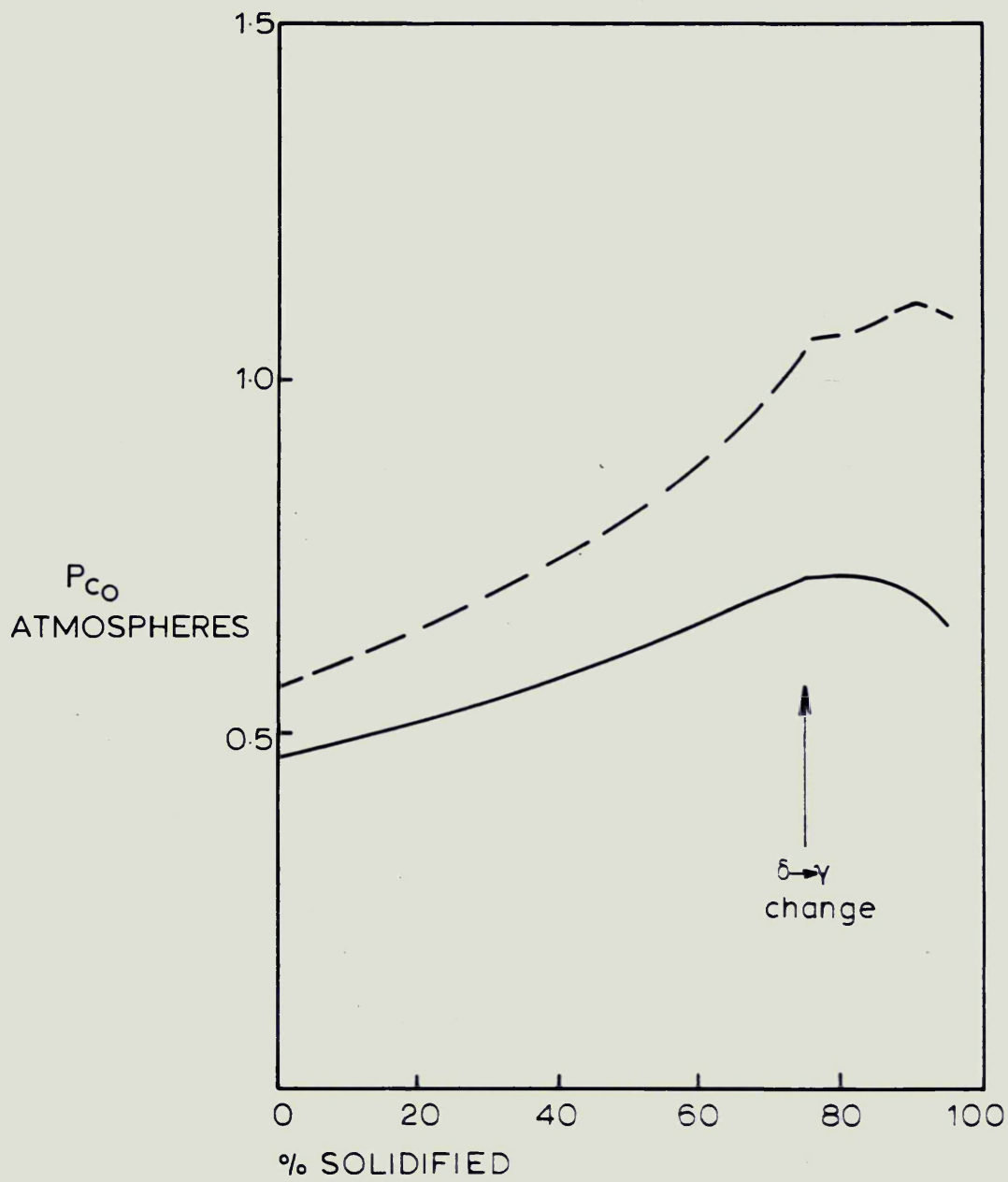
EFFECT OF INTERACTION COEFFICIENTS e_C^x AND e_O^x

$(x = C, Mn, Si, O)$ ON P_{CO} IN STEEL CONTAINING $\cdot 20\% C, 1\cdot 0\% Mn$

AND $\cdot 10\% Si$

FIG. A4.
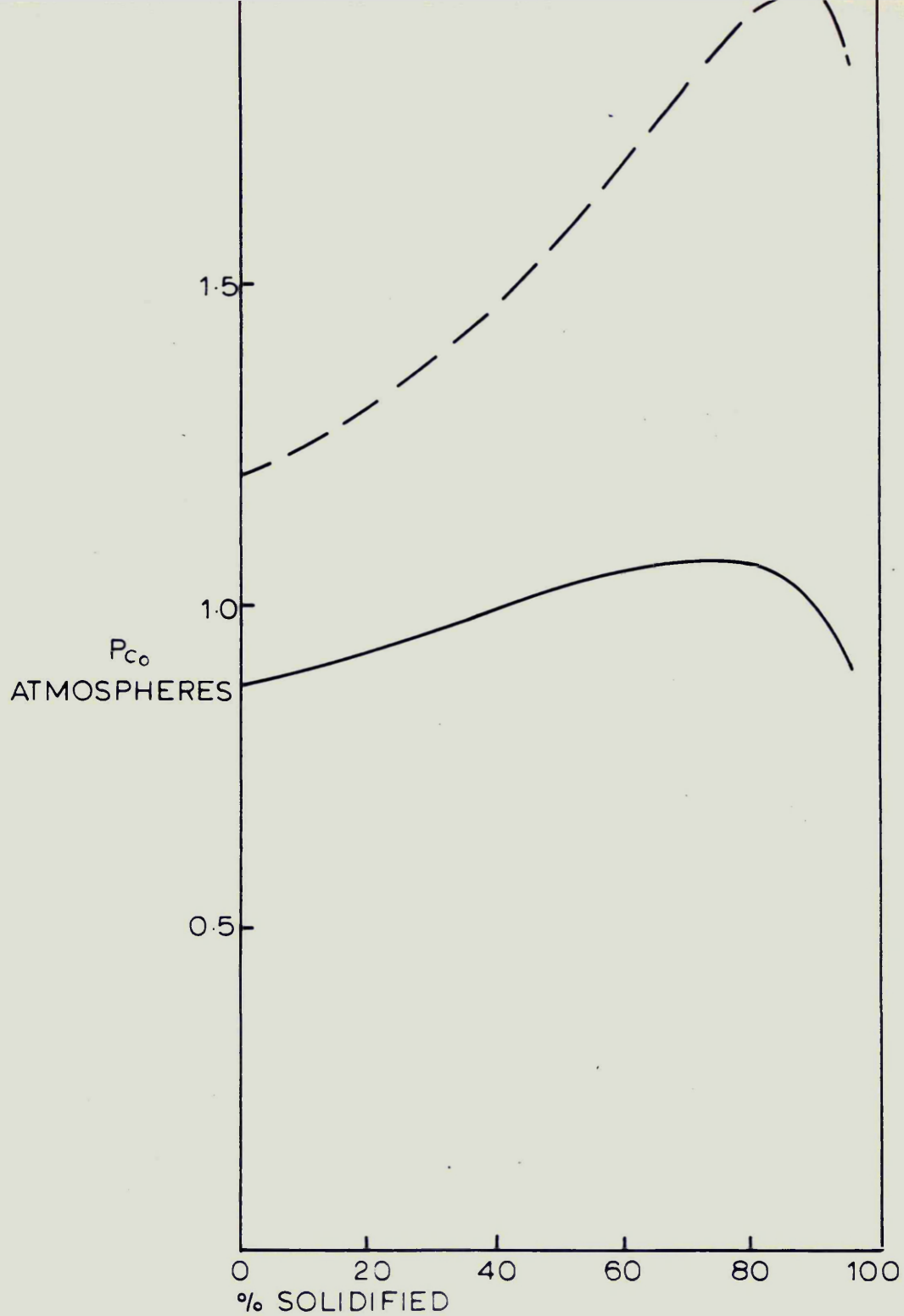
EFFECT OF INTERACTION COEFFICIENTS e_C^x AND e_O^x

$(x=C, Mn, Si, O)$ ON P_{CO} IN STEEL CONTAINING $.50\% C$, $1.0\% Mn$

AND $.10\% Si$

FIG. A5.
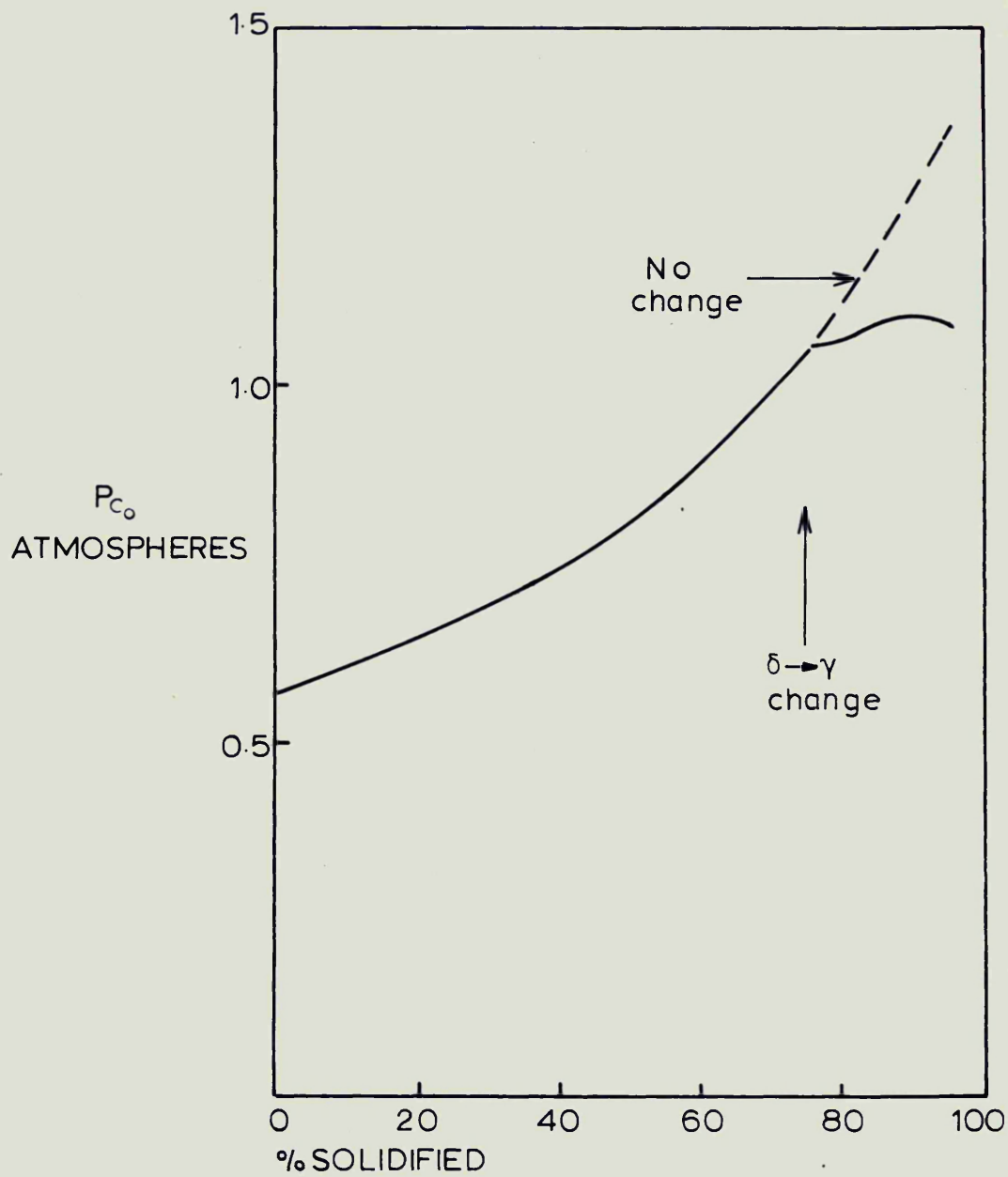
EFFECT OF $\delta \rightarrow \gamma$ CHANGE ON P_{Co} IN STEEL CONTAINING
.20% C, 1.0% Mn, .10% Si SOLIDIFYING AT A CONSTANT
TEMPERATURE OF 1522°C (NO INTERACTION)

FIG. A6.
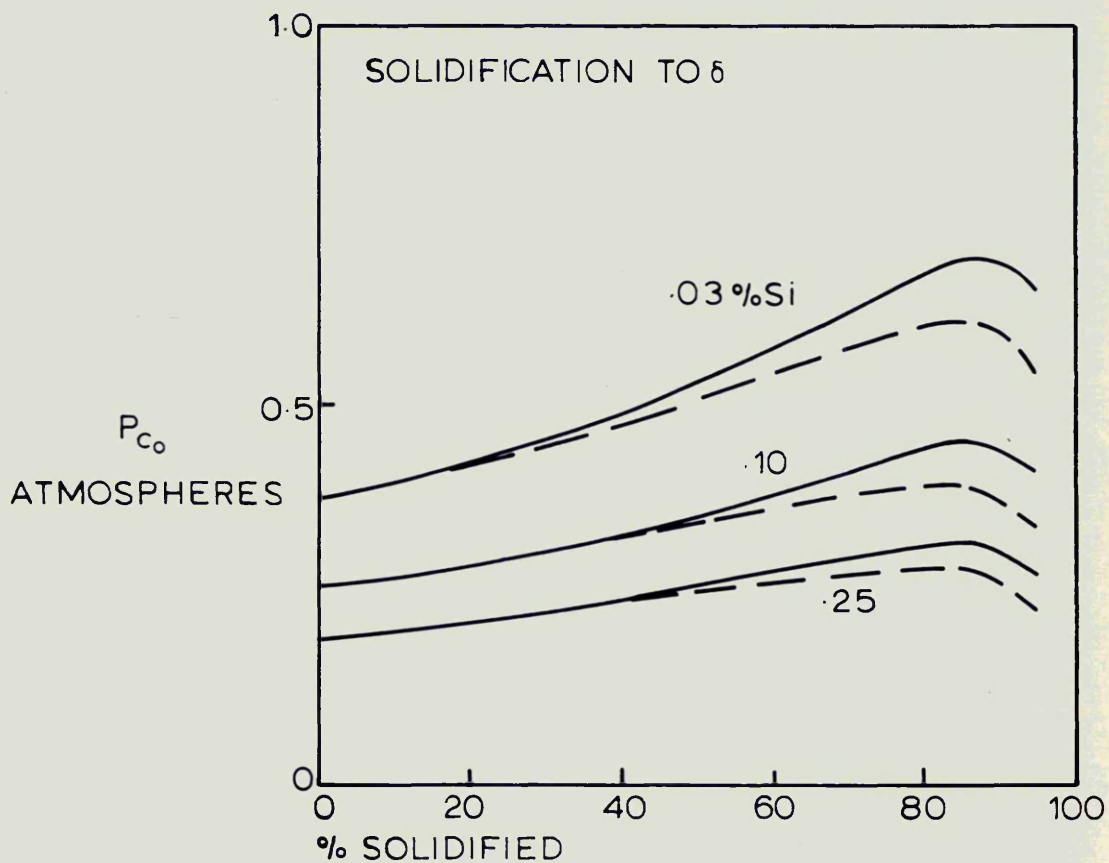
COMPARISON OF CONSTANT AND VARYING TEMPERATURE
CALCULATIONS OF P_{Co} IN STEELS CONTAINING ·10%C AND
1·0 % Mn (INCLUDING INTERACTION EFFECTS)

FIG. A7.
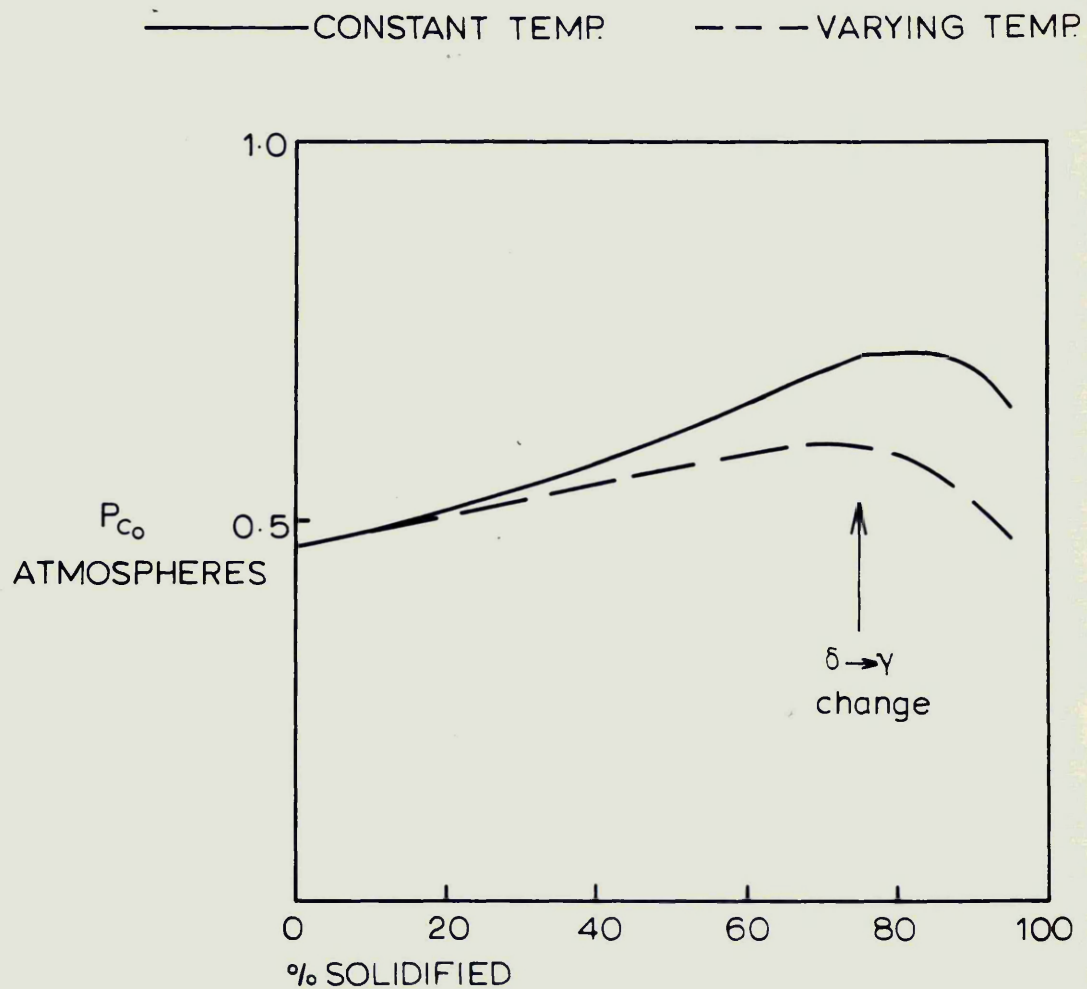
COMPARISON OF CONSTANT AND VARYING TEMPERATURE CALCULATIONS OF P_{Co} IN STEELS CONTAINING ·20%C, 1·0%Mn AND ·10% Si (INCLUDING INTERACTION EFFECTS)

FIG. A8.

CONSTANT TEMP. — — — — VARYING TEMP.
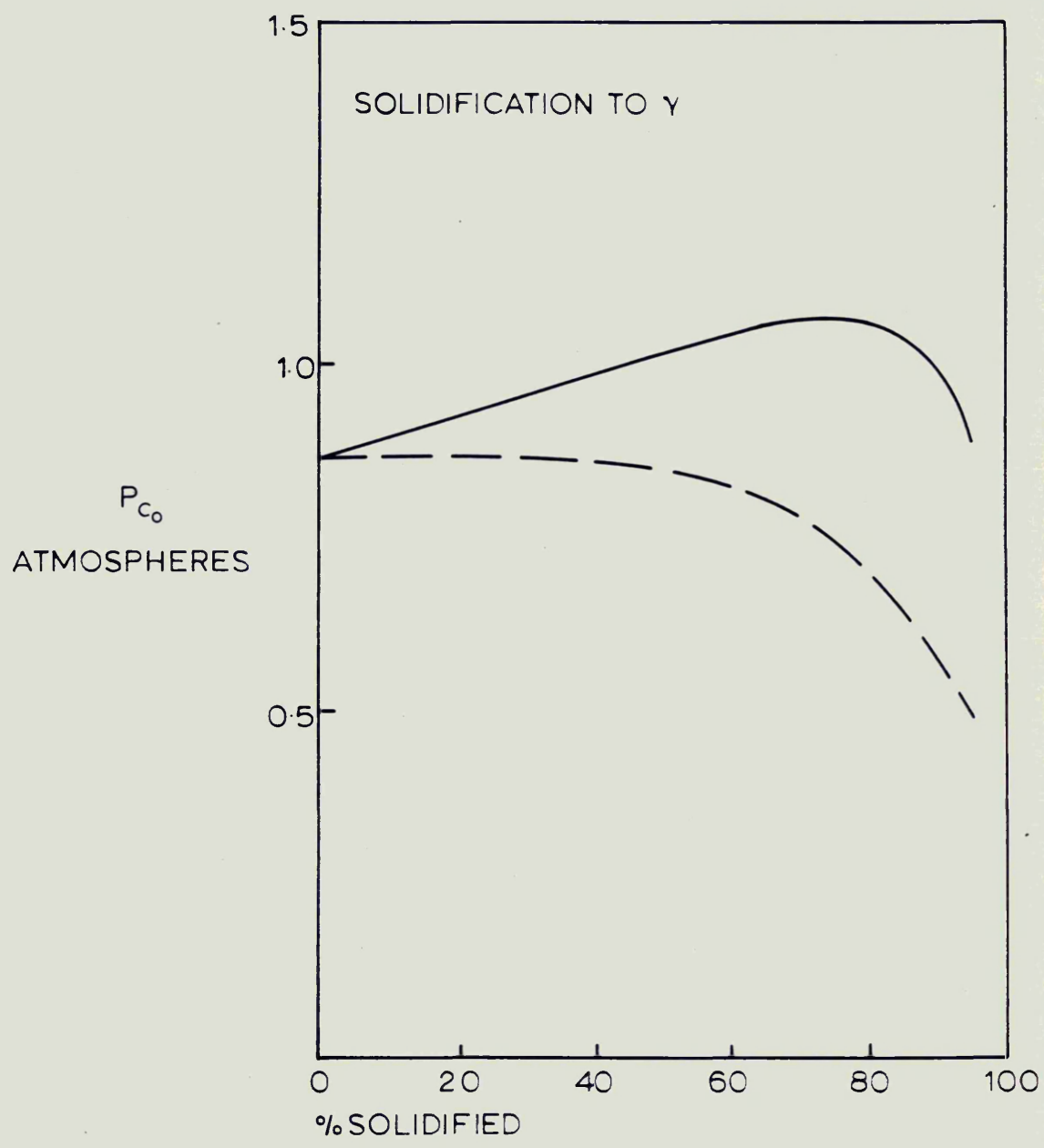
SOLIDIFICATION TO γ

P_{C_O}
ATMOSPHERES

% SOLIDIFIED

COMPARISON OF CONSTANT AND VARYING TEMPERATURE
CALCULATIONS OF P_{C_O} IN STEELS CONTAINING 50%C,
1·0%Mn AND ·10 % Si (INCLUDING INTERACTION EFFECTS)

FIG. A9.
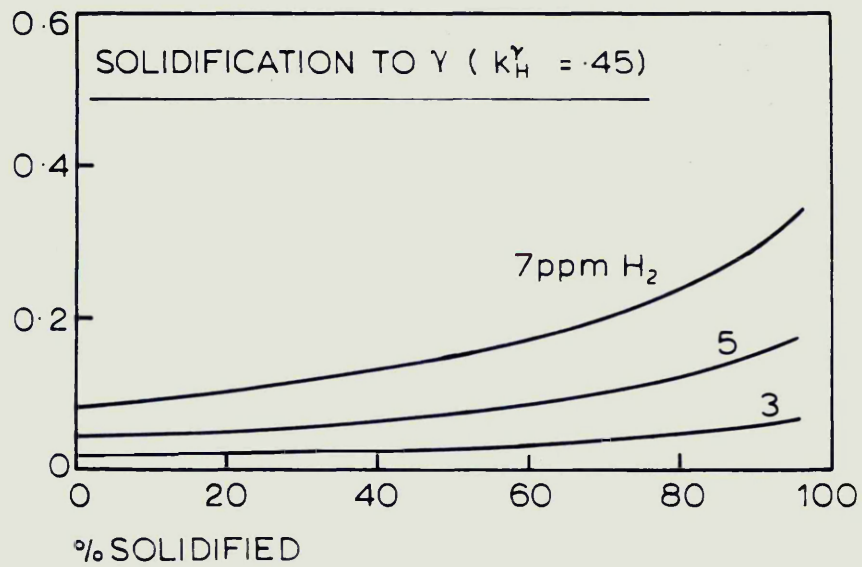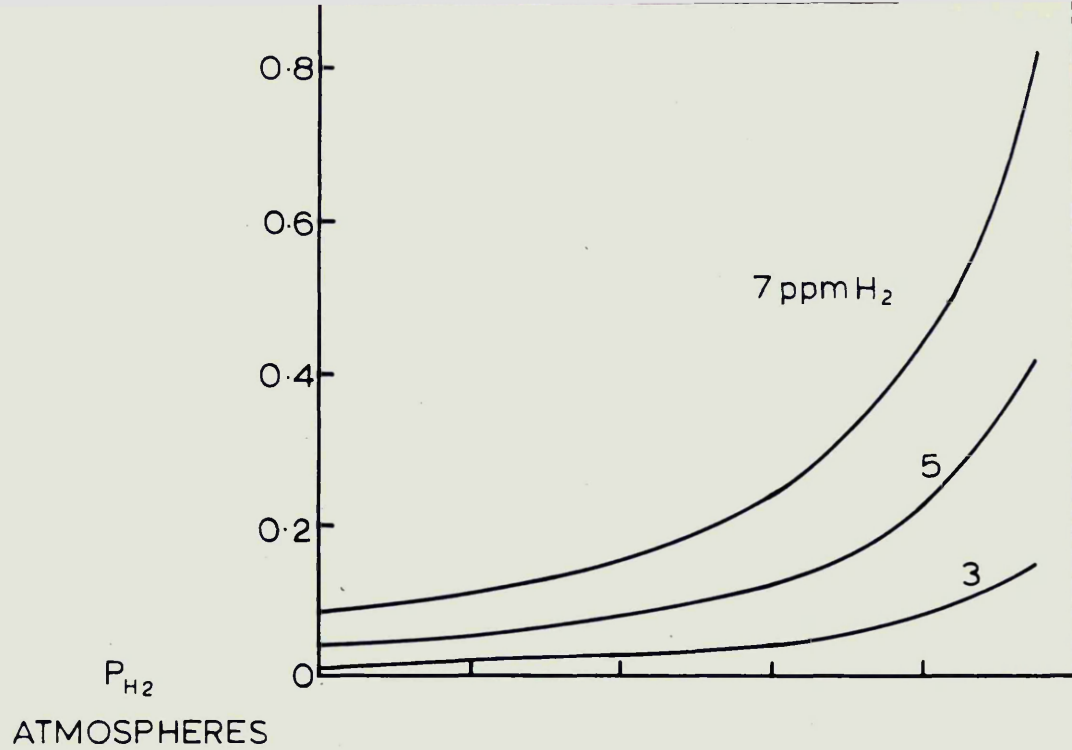
P_{H_2} IN STEELS SOLIDIFYING TO δ AND γ AT A CONSTANT TEMPERATURE OF 1525°C (NO INTERACTION)

FIG. A10.
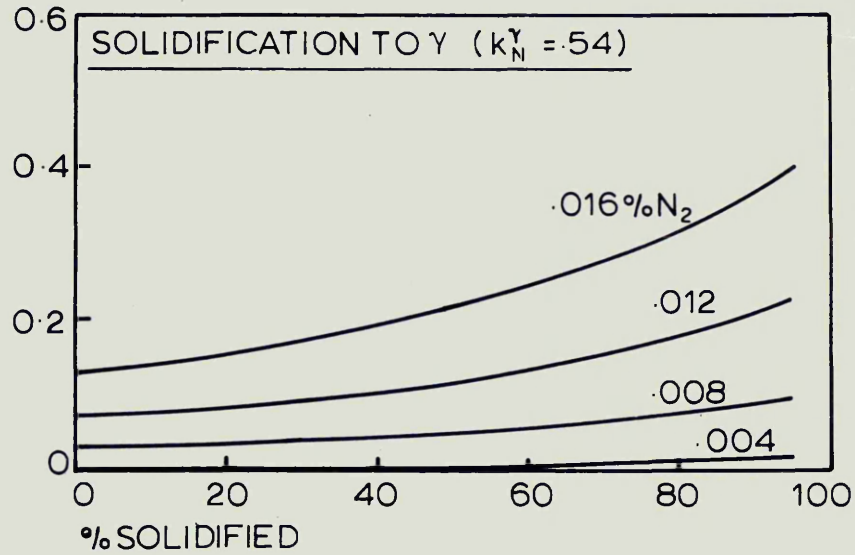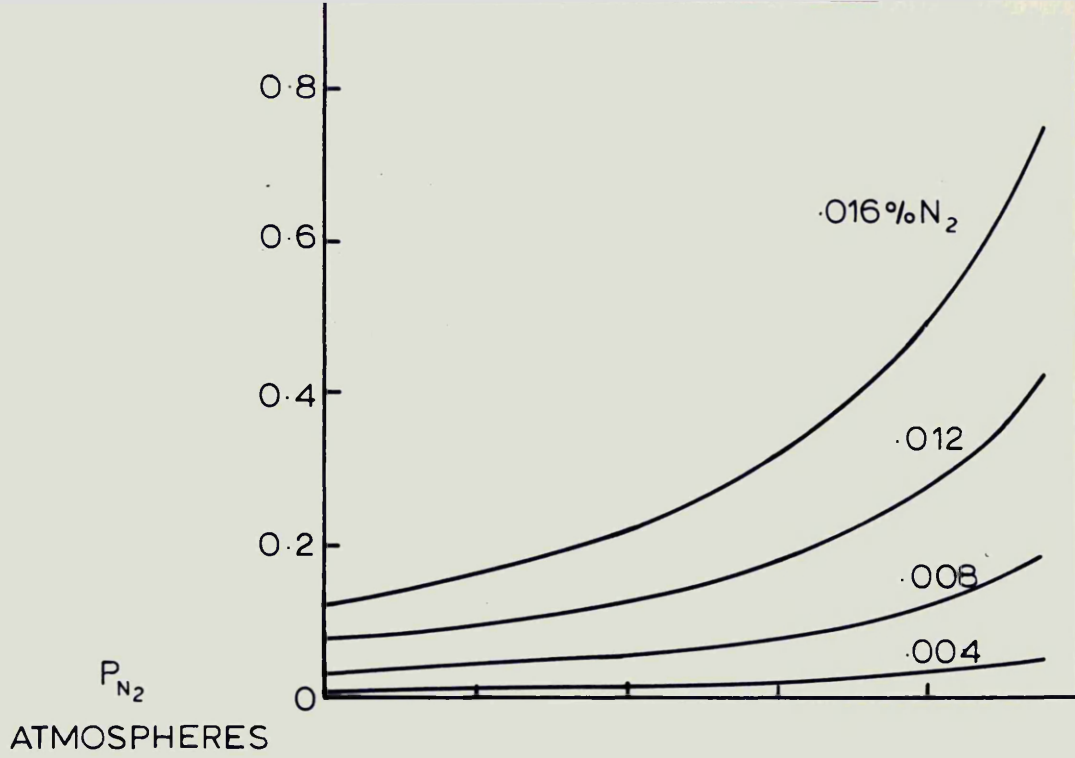
P_{N_2} IN STEELS SOLIDIFYING TO δ AND γ AT A CONSTANT TEMPERATURE OF 1525°C (NO INTERACTION)

FIG. A11.
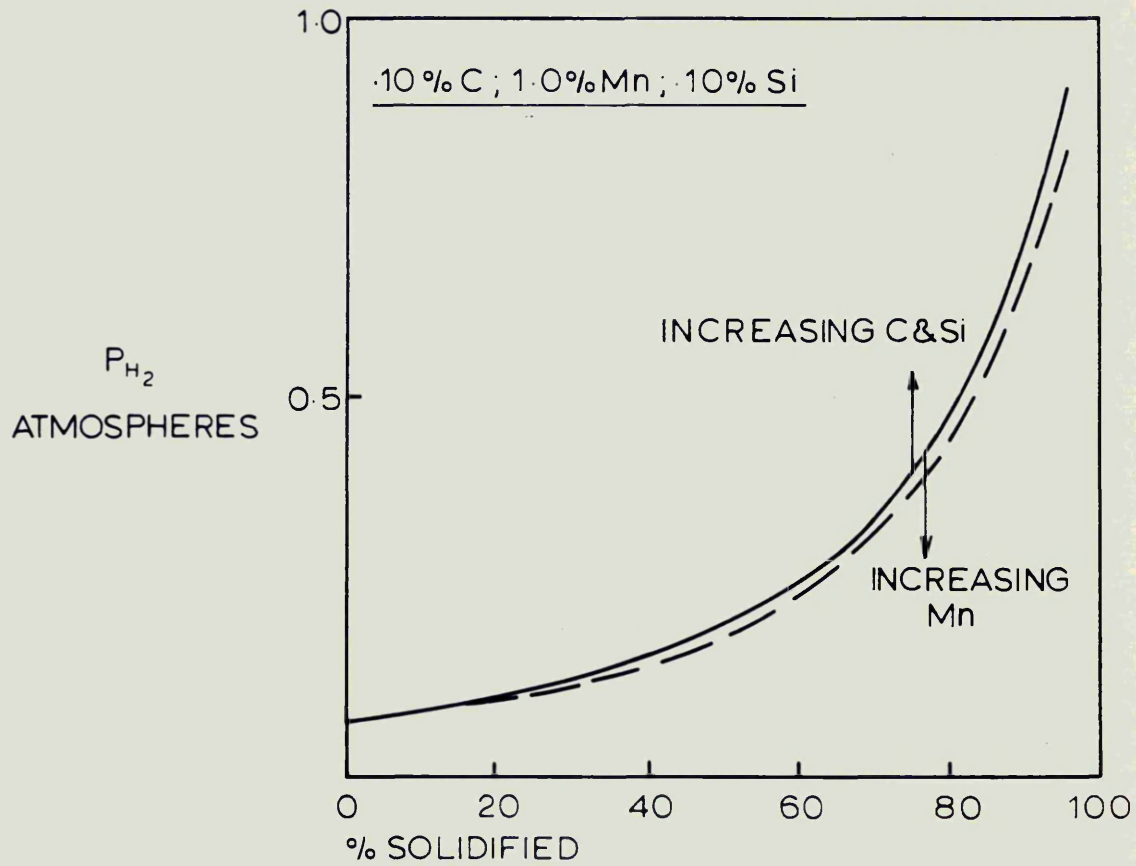
EFFECT OF C+Mn+Si INTERACTION ON P_{H_2} IN A STEEL

CONTAINING 7ppm, H_2 SOLIDIFYING TO δ AT A CONSTANT

TEMPERATURE OF 1530°C

FIG. A12
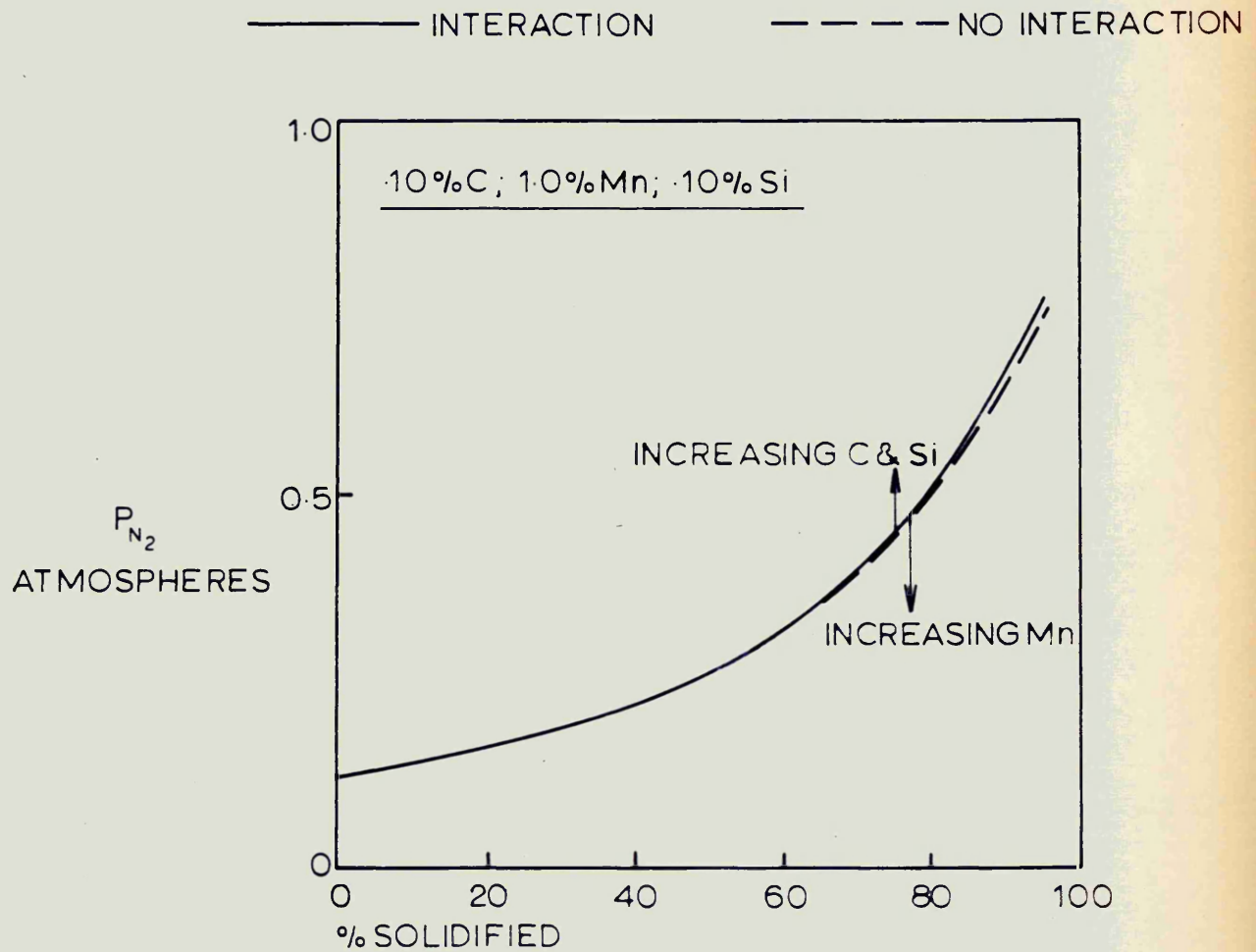
EFFECT OF C+Mn+Si INTERACTION ON P_{N_2} IN A STEEL

CONTAINING ·016 %N_2, SOLIDIFYING TO δ AT A CONSTANT

TEMPERATURE OF 1530°C

FIG. A13.

INTERACTION
-----NO INTERACTION } INCLUDING δ →γ
—·— " " NO δ→γ CHANGE
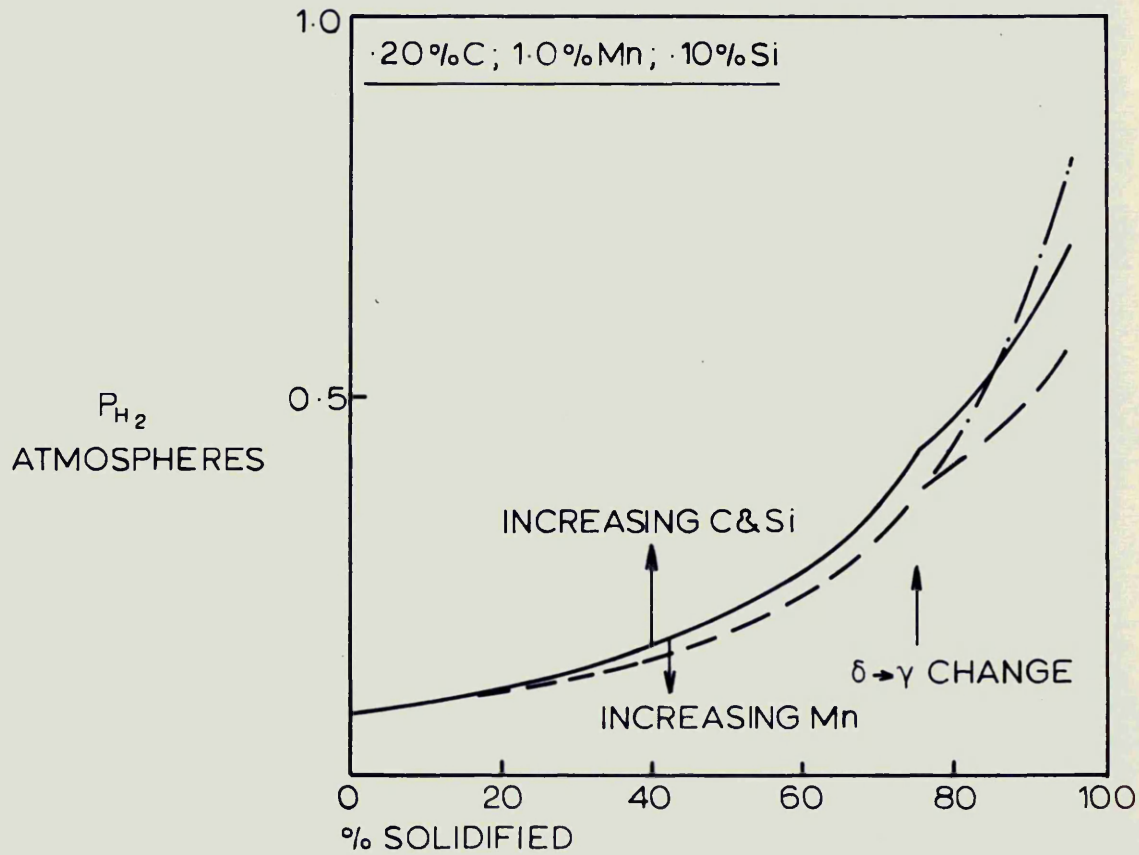
EFFECT OF C+Mn+Si INTERACTION ON P_{H_2} IN A STEEL

CONTAINING ·7 ppm H_2 AT A CONSTANT SOLIDIFICATION

TEMPERATURE 1522°C (INCLUDING δ→γ CHANGE)
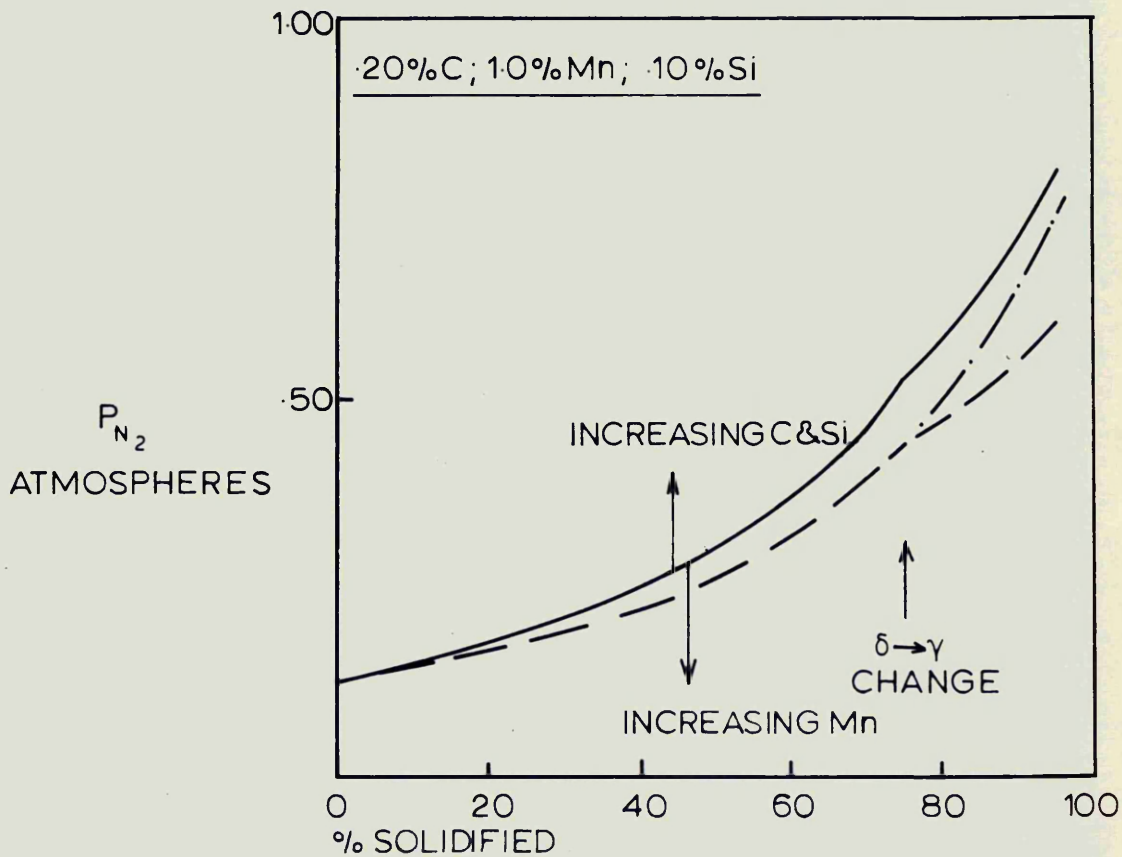
FIG. A14

EFFECT OF C+Mn+Si INTERACTION ON P_{N_2} IN A STEEL
CONTAINING ·016%N_2 AT A CONSTANT SOLIDIFICATION
TEMPERATURE OF 1522°C (INCLUDING δ→γ CHANGE)
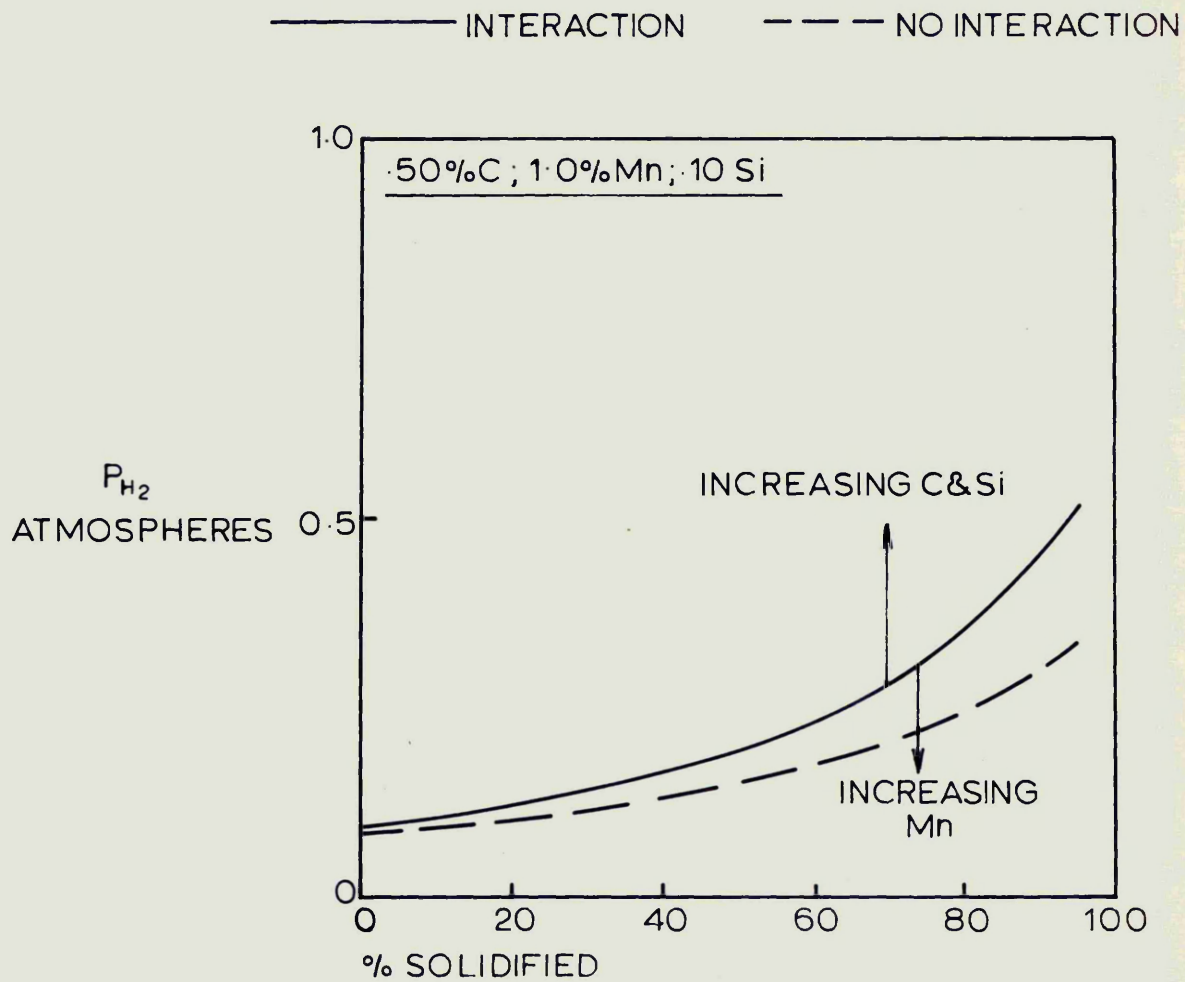
FIG. A15

EFFECT OF C+Mn+Si INTERACTION ON P_{H_2} IN A STEEL
CONTAINING 7ppm H_2 SOLIDIFYING TO Y AT A CONSTANT
TEMPERATURE OF 1500°C

FIG. A16.
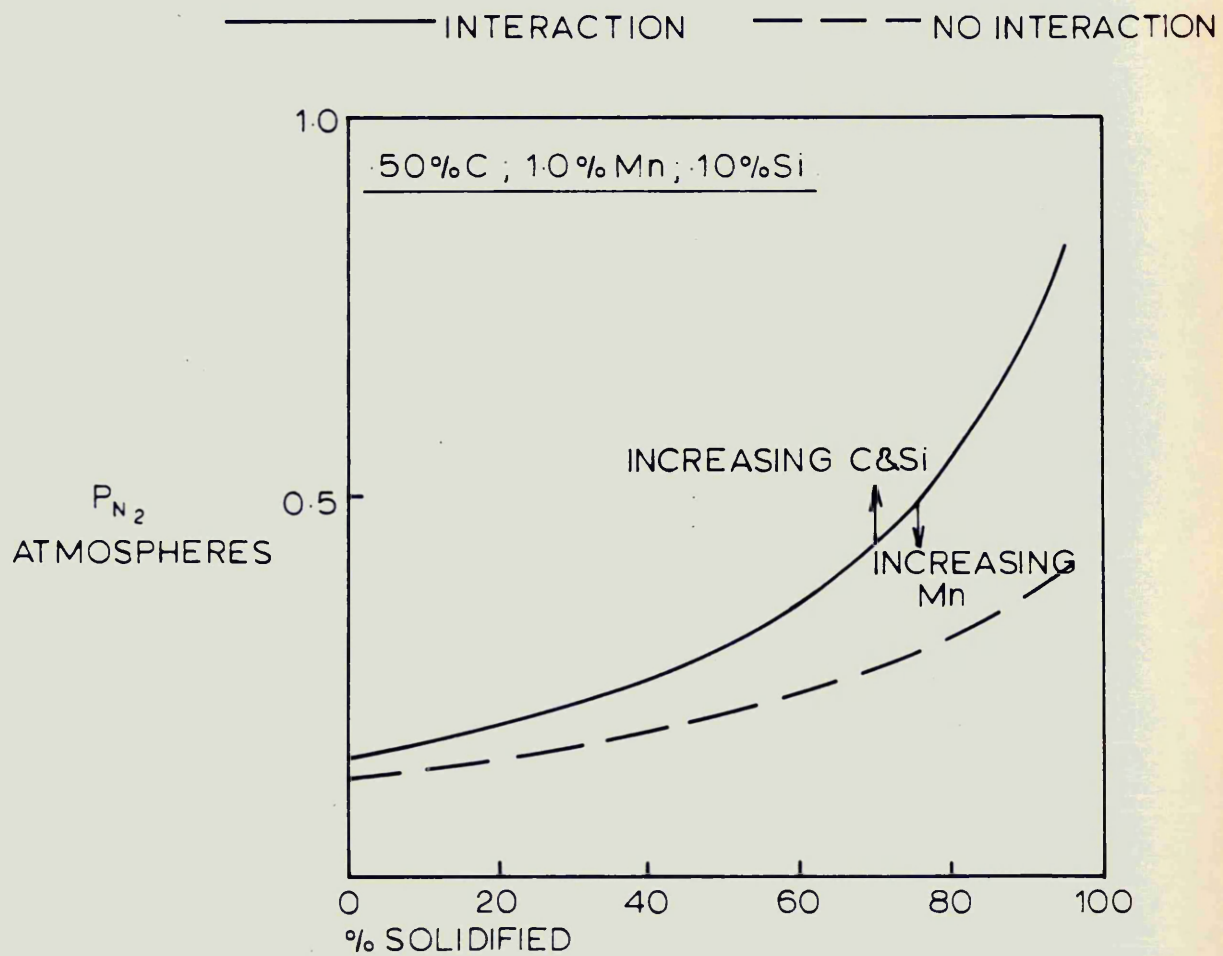
EFFECT OF C+Mn+Si INTERACTION ON P_{N_2} IN A STEEL CONTAINING ·016% N_2, SOLIDIFYING TO γ AT A CONSTANT TEMPERATURE OF 1500°C

FIG. A17.

COMPARISON OF CONSTANT AND VARYING TEMPERATURE CALCULATIONS OF P_{H_2} IN A STEEL CONTAINING 7ppm H_2 SOLIDIFYING TO δ (INCLUDING INTERACTION EFFECTS)
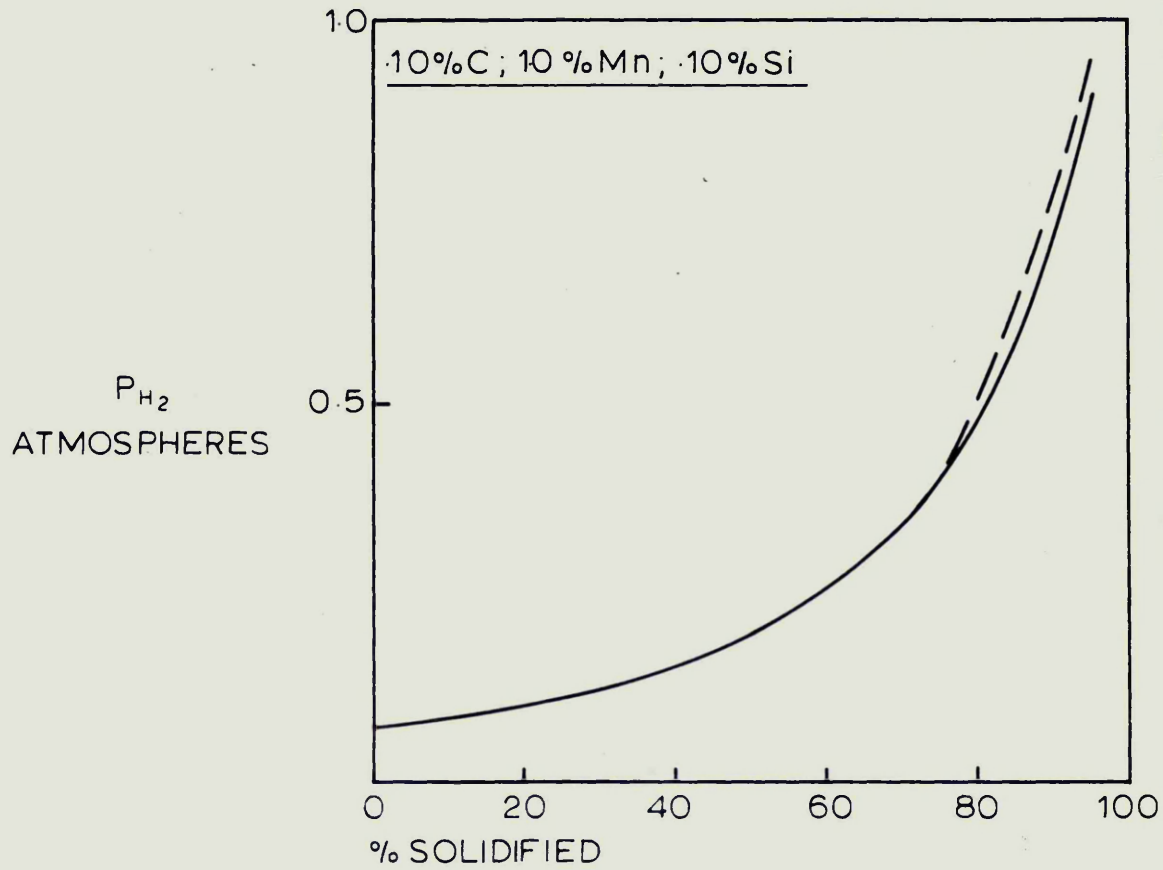
FIG. A18.
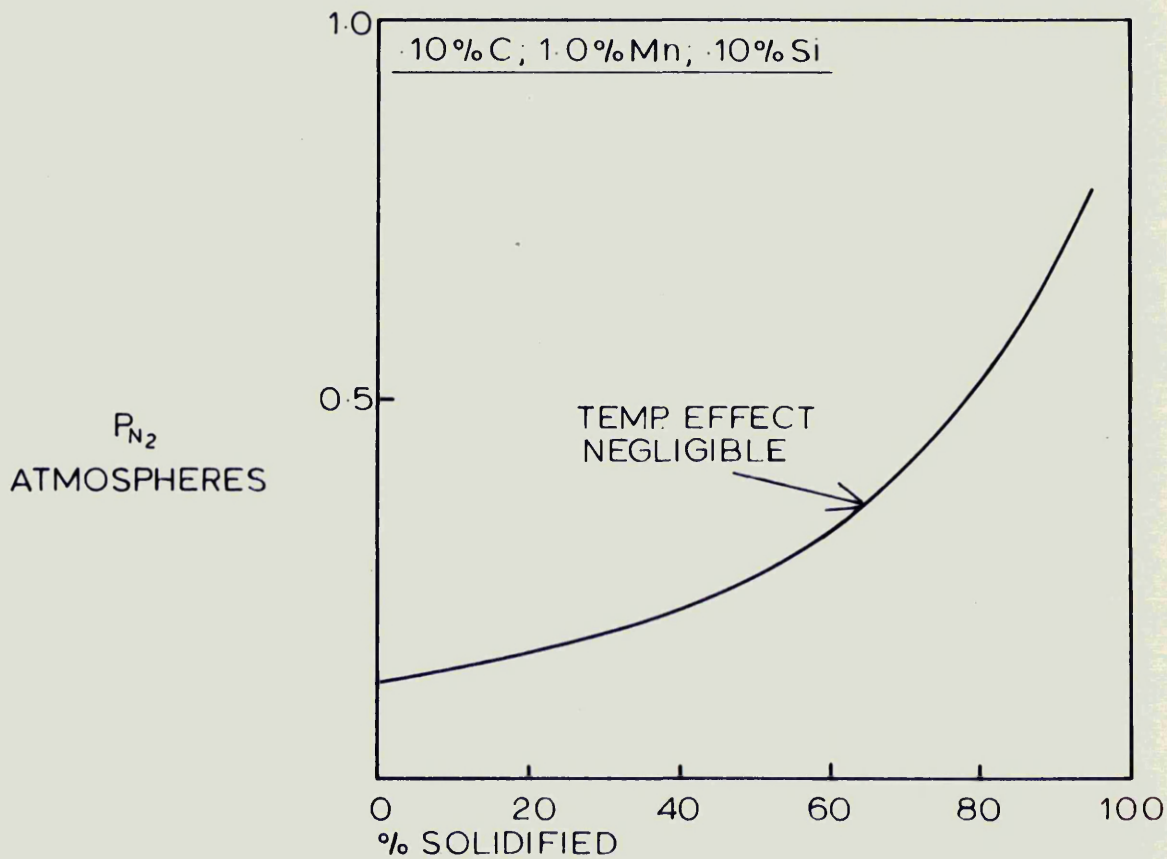
COMPARISON OF CONSTANT AND VARYING TEMPERATURE
CALCULATIONS OF P_{N_2} IN A STEEL CONTAINING $\cdot 016\% N_2$,
SOLIDIFYING TO δ (INCLUDING INTERACTION EFFECTS)

FIG.A19.

COMPARISON OF CONSTANT AND VARYING TEMPERATURE CALCULATIONS OF P_{H_2} IN A STEEL CONTAINING 7ppm H_2, UNDERGOING $\delta \rightarrow \gamma$ CHANGE DURING SOLIDIFICATION (INCLUDING INTERACTION EFFECTS)

FIG. A20

CONSTANT TEMP. — — — VARYING TEMP.

P_{N_2}
ATMOSPHERES

COMPARISON OF CONSTANT AND VARYING TEMPERATURE
CALCULATIONS OF P_{N_2} IN A STEEL CONTAING ·016% N_2 .
UNDERGOING δ→γ CHANGE DURING SOLIDIFICATION
(INCLUDING INTERACTION EFFECTS)
FIG.A21.
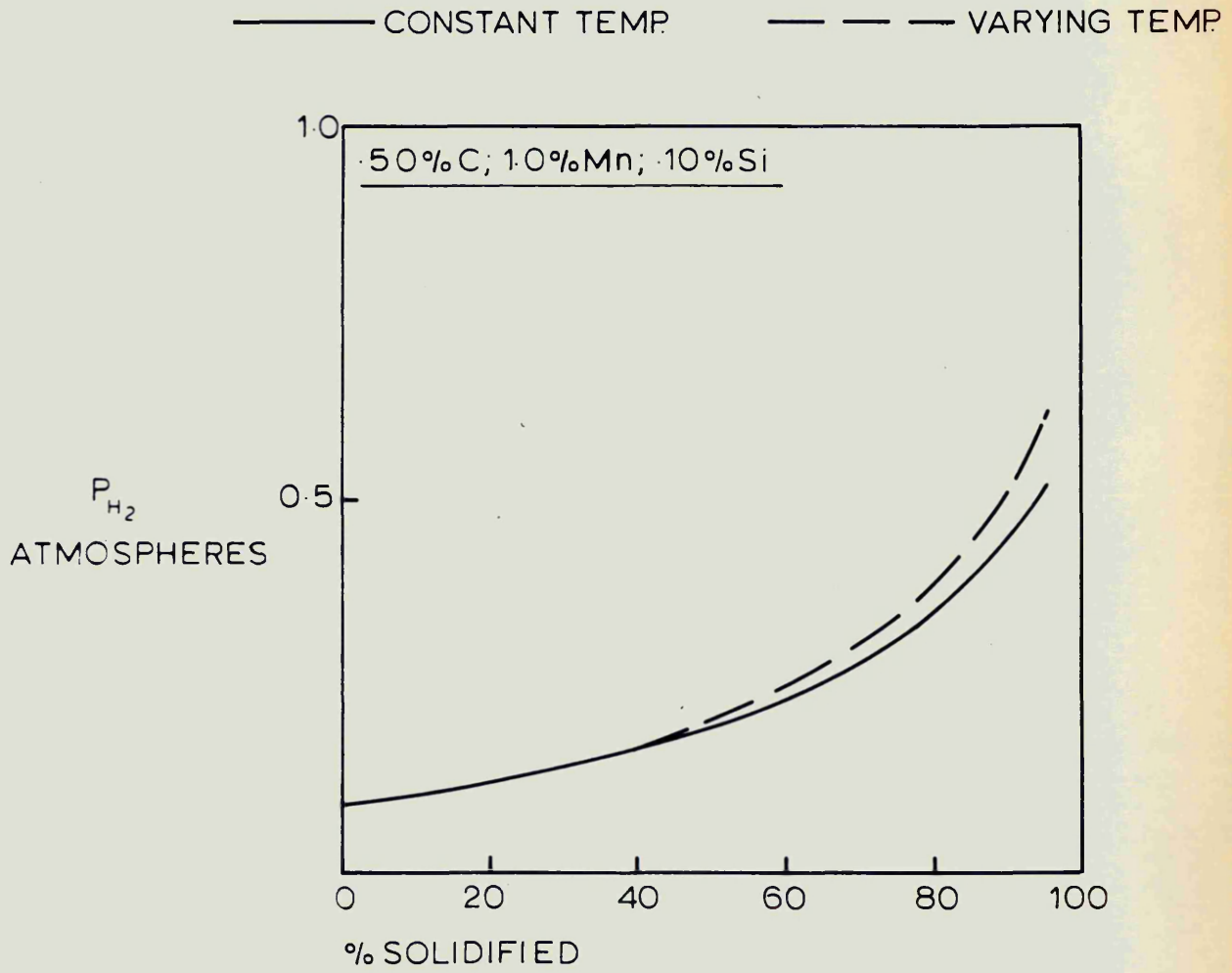
COMPARISON OF CONSTANT AND VARYING TEMPERATURE
CALCULATIONS OF P_{H_2} IN A STEEL CONTAINING 7ppm H_2
SOLIDIFYING TO γ (INCLUDING INTERACTION EFFECTS)

FIG.A22.

COMPARISON OF CONSTANT AND VARYING TEMPERATURE
CALCULATIONS OF P_{N_2} IN A STEEL CONTAINING ·016% N_2
SOLIDIFYING TO γ (INCLUDING INTERACTION EFFECTS)
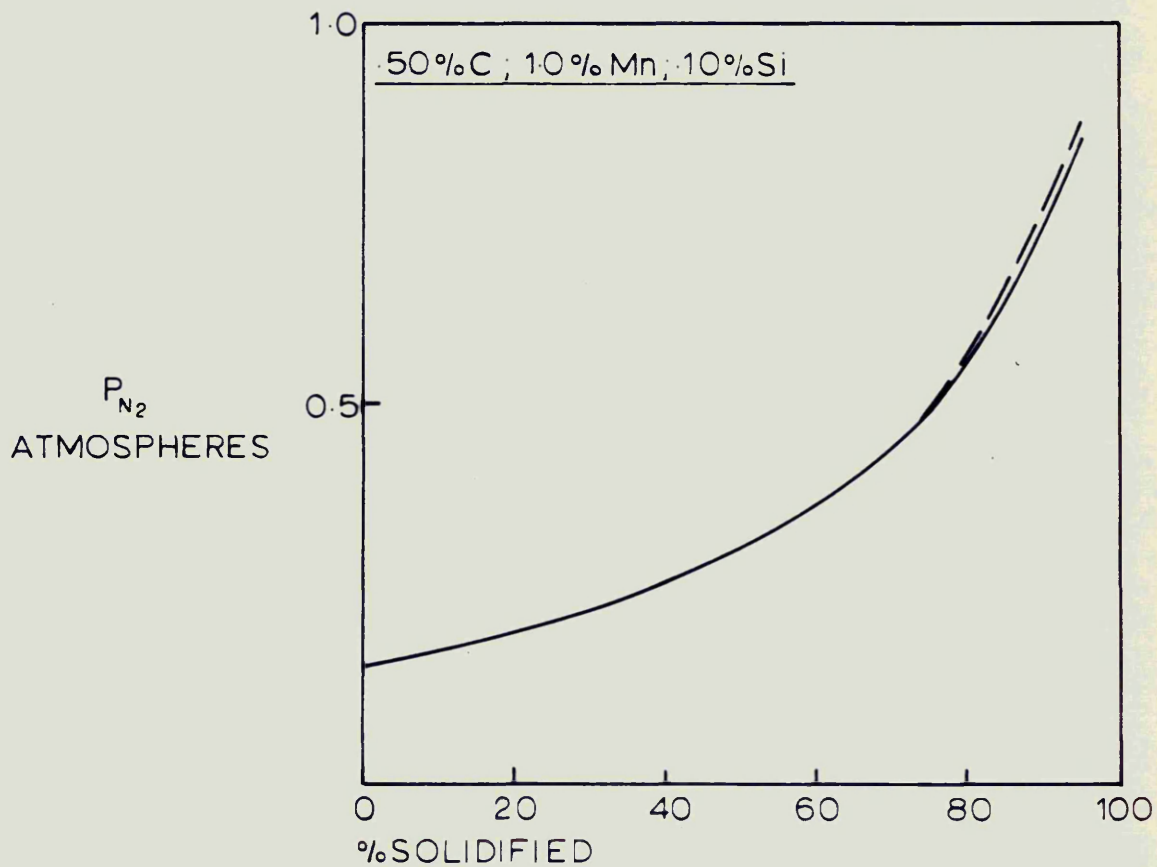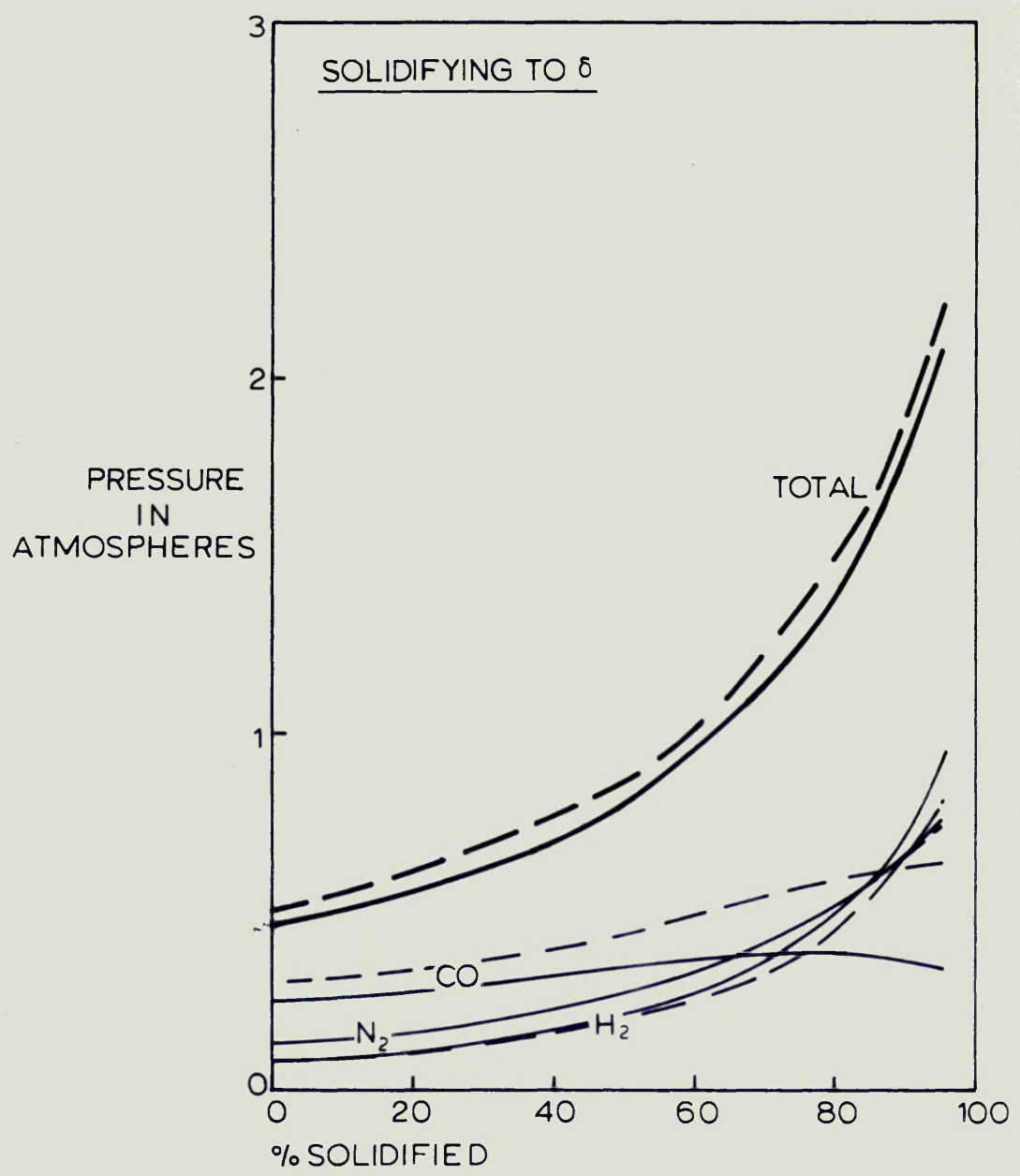
FIG. A23.

NET EFFECT OF COMPUTER PROGRAMME MODIFICATIONS
ON GAS PRESSURES IN A STEEL CONTAINING ·10%C,1·0%Mn
·10Si , ·016%N₂ AND 7ppm H₂

FIG.A24.
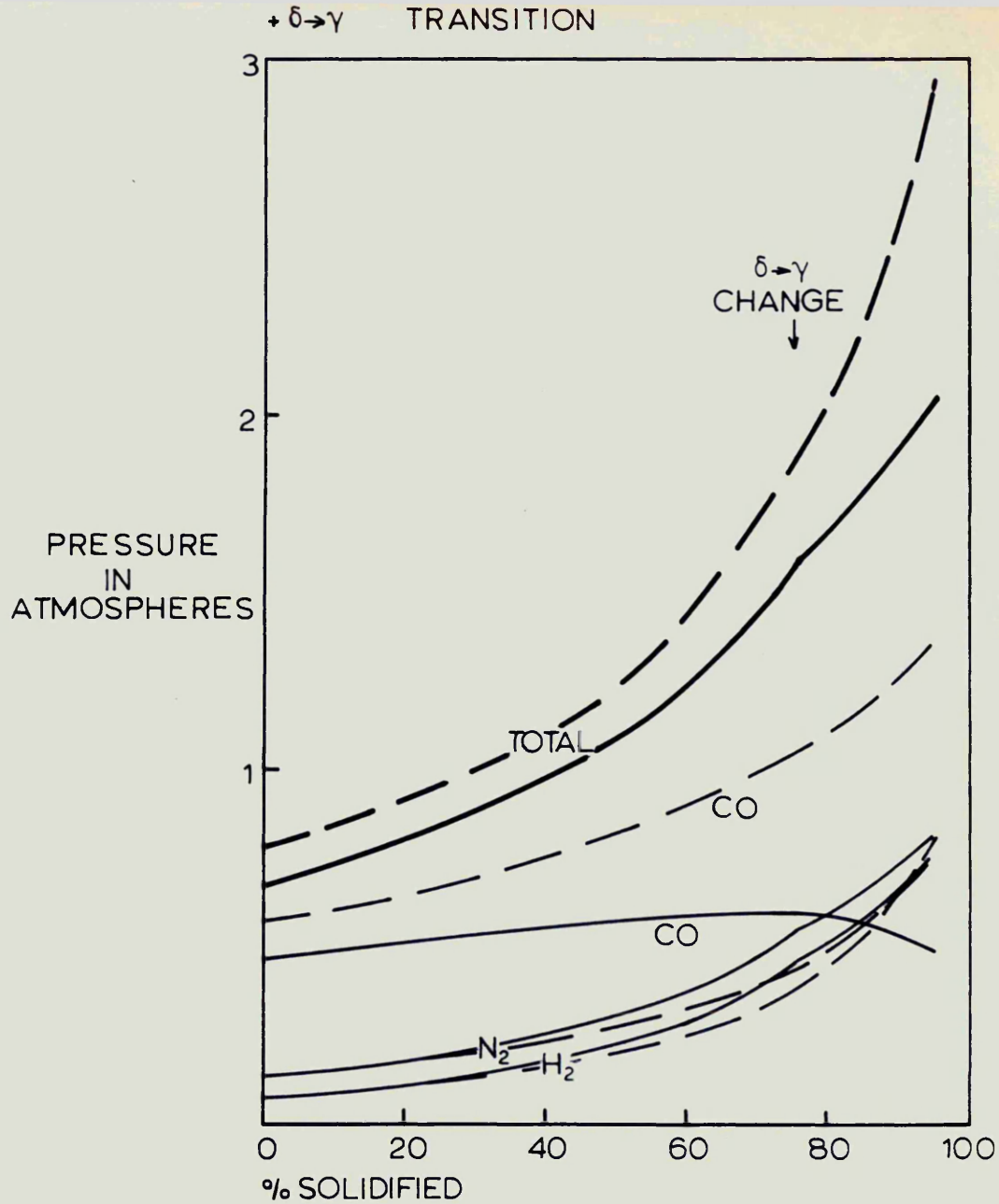
NET EFFECT OF COMPUTER PROGRAMME MODIFICATIONS
ON GAS PRESSURES IN A STEEL CONTAINING ·20%C,1·0%Mn
·10%Si ,·016%N₂ AND 7ppm H₂

FIG.A25.
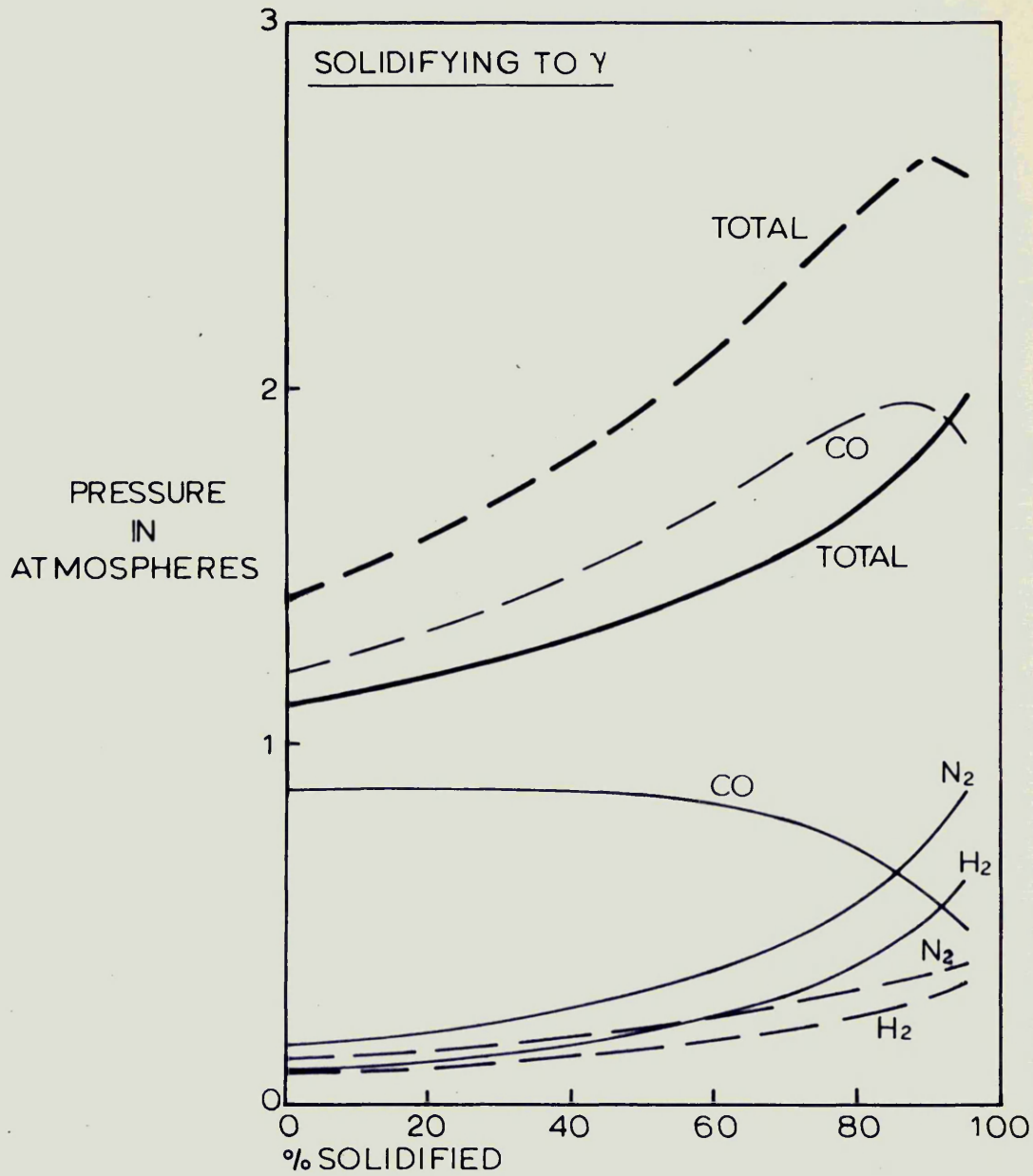
NET EFFECT OF COMPUTER PROGRAMME MODIFICATIONS
ON GAS PRESSURES IN A STEEL CONTAINING ·50%C, 1·0%Mn,
·10% Si , ·016 %N₂ AND 7ppm H₂

FIG. A26